NTNU
Innovation and Creativity

Steady-state and dynamic converter modeling in system analysis

Thomas Skånøy

Master of Science in Energy and Environment
Submission date: June 2007
Supervisor: Olav B Fosso, ELKRAFT

Norwegian University of Science and Technology
Department of Electrical Power Engineering

Problem Description

Mid-Norway has a significant power deficit. This deficit will increase in the years to come unless new production capacity with high utilization time is installed. An increased utilization of the transmission system increases the probability of collapse when the system is exposed to line disconnections. Load modelling is then an important issue when determining the probability of voltage collapse due to various system faults.

There are several large industrial loads in this area and modelling of such loads may be crucial for the system performance. One of these loads is the Ormen Lange where large motors are supplied by a converter station based on power electronics. Traditionally these loads are included as a PQ-model. Such a model can be made conservative due power consumption, but it is not possible to uncover the impact such systems may have on dynamic performance.

This work will address alternative load models to illustrate the necessity to go for more detailed models in the dynamic analysis also for such loads. The work should try to use the existing models within PSS/E to illustrate the performance by using such models compared to the traditional PQ-loads. One possibility is to use an HVDC-link to emulate the converter station. It is important to address assumptions, simplifications and data requirements in the dynamic modelling as well as discussing the performance of the model. For the load flow and dynamic analysis the tool should be PSS/E with Mid-Norway as basis. The Nordic power model given by Statnett should be used in the simulations.

Assignment given: 15. January 2007
Supervisor: Olav B Fosso, ELKRAFT

Preface

The master thesis “Steady-state and dynamic converter modeling in system analysis” is written at the Department of Electrical Power Engineering at the Norwegian University of Science and Technology (NTNU).

I would like to thank Leif Warland at Sintef Energy Research for guidance in the use of computer tool program Power System Simulator for Engineering (PSS/E). Further, I would like to thank Kjetil Uhlen at Sintef Energy Research for technical inputs. Finally, I would like to thank my subject teacher Professor Olav Bjarte Fosso for guidance throughout the semester.

Trondheim, June 12, 2007

Thomas Skånøy

Abstract

This master thesis was executed at the Department of Electrical Power Engineering at the Norwegian University of Science and Technology (NTNU). The thesis was initiated to establish and evaluate an alternative model representation of the facility at Ormen Lange. Traditionally, a PQ-model has been used to represent Ormen Lange. This thesis, however, has implemented three two-terminal dc line models (converter models) to represent the facility.

The first part of the thesis starts with an overall introduction to the basic principles of configuration, operation and control of HVDC systems. The objective of this part is to provide an overview of the HVDC technology which is treated in detail later in the thesis.

The software tool "Power System Simulator for Engineering" (PSS/E) was used for both power flow and dynamic simulations performed in this thesis.

The second part of the thesis describes the power flow establishment, and constitutes the basis for both power flow and dynamic simulations. The main focus in this part is the modeling of the two-terminal dc line model which is implemented at Nyhamna. Data for the two-terminal dc line model is presented on three consecutive data records. Since these data enables not only power flow analysis but also establishes the initial steady-state for the dynamic analysis, a detailed description is presented in this section. The latter data is based on technical information provided by ABB and default values in PSS/E.

The third part of the thesis presents the power flow simulations. The objective of this part is to gain knowledge about the performance of the two-terminal dc line model implemented at Ormen Lange. This knowledge facilitates the understanding of the following dynamic simulations. Two cases were studied to simulate the action of the converter control system when exposed to a depression in rectifier bus voltage. In the first case the rectifier transformer tap settings were adjustable. In the second case the rectifier tap settings were locked to its initial value. The purpose of locking the tap setting was to represent a transient situation where the tap changer action is too slow and hence not considered.

The result showed that with adjustable rectifier tap settings, the depression in rectifier bus voltage is handled by reducing the rectifier transformer tap position and firing delay angle. This increased the voltage on the valve side of the rectifier transformer and enabled the rectifier to maintain dc current control. Consequently, the scheduled dc values were unaffected by the depression in rectifier bus voltage. However, with the rectifier tap setting locked, the transformer did not boost the voltage on the valve side of the rectifier transformer. This caused the control logic to reduce the rectifier firing delay angle to its minimum, and the inverter assumed control of the dc current. With the inverter in control of the current, the scheduled dc current was reduced by a fraction equal to the current margin along with the remainder dc values. Hence, the presence of an adequate rectifier transformer setting is essential for the two-terminal dc line model to maintain scheduled dc values during voltage depression.

All simulations showed that a voltage depression at the rectifier bus leads to a reduction in rectifier reactive power consumption. This is due to the action from the control logic which reduced the rectifier firing delay angle to counteract the voltage depression. The greatest reduction in rectifier reactive consumption was experienced when the rectifier firing delay angle was reduced to its minimum value. Hence, in situations with depressed bus voltage, the latter operation of the converter control logic causes the two-terminal dc line model to exhibit less stress to the ac system than the PQ-model.

The fourth part of this thesis contains a detailed description of the dynamic modeling of the two-terminal dc line model (CDC4T). Many of the chosen parameters are based on an example in [15], and do not necessary represent realistic values.

The final part of this thesis presents the dynamic simulations. The objective of this part is to analyze the control actions of the CDC4T model under normal regulation and during temporary overriding the normal regulation. This was performed by introducing ac system faults which depressed the rectifier bus voltage to a varying degree.

Further, this part analyzed the consequence of using the dynamic model CDC4T to represent Ormen Lange instead of a PQ-model. The purpose was to determine whether the response from the ac system differs when using the CDC4T model instead of a PQ-model. It is important to emphasize that this part does not evaluate stability issues associated with the implementation of CDC4T.

The results from the dynamic simulations showed that CDC4T exhibited an instantaneous response to changes in rectifier ac voltage. This is because CDC4T is a pseudo steady-state dynamic model which omits the L/R dynamic of the dc system and high frequency firing angle controller dynamics.

Further, the results revealed an important characteristic of the CDC4T model. After fault clearance, the rectifier bus exhibited small voltage fluctuations. The rectifiers compensated these fluctuations by adjusting their firing delay angles correspondingly. Consequently, the latter resulted in fluctuations in reactive power consumption. This means that the ac system perceives the CDC4T model as a varying reactive load following fault clearance.

Comparing the ac system response when using the CDC4T model and when using the PQ-model, the results showed that the main difference was CDC4T's generation of reactive power fluctuations. These fluctuations were experienced in the transmission line going into Nyhamna and Viklandet, and were substantial compared to the initial loading of the transmission lines. Two arguments were used to substantiate why the response from the CDC4T model only differs from the PQ-model in terms of reactive power fluctuations:

I. The calculated value of the short circuit ratio at Nyhamna indicated a strong interconnected ac/dc system.
II. The dynamic behavior of the pseudo-steady state model, CDC4T, is limited. Both the L/R dynamic of the dc line, smoothing reactors and high frequency controller dynamics are omitted.

In further studies where converter modeling at Ormen Lange is considered, a more complex dynamic dc model should be utilized to represent the converters. This model should include L/R dynamic of the dc system and high-speed controller dynamics, and will thus influence the ac system to a greater extent than CDC4T. Further, the model establishment should focus on achieving a sufficiently realistic load representation of Ormen Lange. In this manner, the converters' influence on system stability can be evaluated.

Table of content

1 Introduction

This chapter gives a brief description of the background and the scope of this master thesis. Finally, an outline of the thesis is presented.

1.1 Background

Mid-Norway have several large industrial loads and modeling of these loads can be crucial for the system performance. One of these loads is Ormen Lange, where large motors are supplied by converter stations based on power electronics. Traditionally, these loads are represented as PQ-models in system analysis. The latter representation can be made conservative in terms of power consumption, however, it omits the possibility to uncover the impact such systems may have on dynamic performance.

1.2 Scope of the thesis

This master thesis is focused on steady-state and dynamic converter modeling in system analysis. With the facility at Ormen Lange as basis, this thesis implements three *two-terminal dc line models* to represent the converter stations at Ormen Lange. The simulation tool "Power System Simulator for Engineering" (PSS/E) is used for both power flow and dynamic simulations. The system model utilized is the Nordic power model provided by Statnett.

The objective of this thesis is to describe converter modeling in PSS/E and illustrate the performance of the implemented converter model through power flow and dynamic simulations. Also, the simulations will illuminate the consequence of using a dynamic converter model to represent Ormen Lange instead of the traditional PQ-model. The purpose is to determine whether the response from the ac system differs when using the latter two models.

It is important to acknowledge that the actual converter system at Ormen Lange is a complex and complicated configuration. This impedes establishment of a realistic converter representation in simulation program like PSS/E. However, the latter is nor the purpose of this thesis. The evaluations made in this thesis are of a principal character and thus only valid for the assumptions made in the thesis. Since the simulations are of a principal character, the thesis does not evaluate stability problems associated with the implementation of the converter model.

General information
This thesis is a continuance of the preliminary study [9]. Hence, topics described in [9] will thus not be repeated in this thesis.

The converter modeling in PSS/E is an essential part of this thesis. Consequently, this is described in detail. Hopefully, this will facilitate further work associated with converter modeling in PSS/E.

In the initial phase of this thesis, a great deal of time was used to obtain relevant data to establish a realistic converter model of Ormen Lange. This turned out to be difficult. Hence, this thesis uses both default values in PSS/E and values obtained from the literature when

establishing the converter model. Consequently, the principal simulation results are of greatest interest in this thesis.

The discussion of the results is given consecutive as the results are presented to increase the readability.

1.3 Outline of the thesis

The thesis is organized as follows:

Chapter 2 This chapter gives an overall introduction to the basic principles of configuration, operation and control of HVDC systems. The chapter provides an overview of the HVDC technology which is treated in detail in the subsequent chapters.

Chapter 3 This chapter describes the establishment of the power flow model used in PSS/E and constitutes the basis for both power flow and dynamic analysis in the following chapters. The main focus of this chapter is the modeling of the *two-terminal dc line model*. This model does not represent Ormen Lange in realistic manner. The latter is nor the objective of this chapter.

Chapter 4 This chapter contains the power flow simulations performed in this thesis. The objective of this chapter is to evaluate the performance of the steady-state two-terminal dc line model. The simulations will illuminate the action of the control logic system, reactive power consumption and characteristics of the implemented model. The evaluations made in this chapter will facilitate the understanding of the dynamic simulations performed in the subsequent chapters.

Chapter 5 This chapter gives a detailed description of the modeling and operation of the dynamic *two-terminal dc line model (CDC4T)* implemented in PSS/E. Several of the parameter values used in the modeling are based on an example in [15], and do not necessary represent realistic values.

Chapter 6 This chapter contains dynamic analysis of the control action for the CDC4T model under normal regulation and during temporary overriding of the normal regulation. The simulations are performed by introducing ac system faults which depresses the rectifier bus to a varying degree.

Chapter 7 This chapter analyzes the consequence of using the dynamic model, CDC4T, to represent Ormen Lange instead of a PQ-model. The objective is to determine whether the response from the ac system differs when using the latter models. This chapter does not address stability issues associated with the implementation of CDC4T.

Chapter 8 This chapter contains the main conclusions which can be drawn from the results obtained in this thesis.

Appendix A This appendix contains results obtained from the power flow simulations in Chapter 4.

Appendix B This appendix contains some of the results obtained from the dynamic simulations in Chapter 6.

Appendix C This appendix contains a simplified calculation of the short circuit capacity (SCC) and short circuit ratio (SCR) at Nyhamna.

Appendix D This appendix contains PSS/E files and verification data. The appendix is attached electronically because it contains confidential information.

2 Theory about HVDC transmission

This chapter provides an overall introduction to the basic principles of configuration, operation and control of HVDC systems. The objective is to provide an overview of the HVDC technology which is treated in detail in the subsequent chapters.

For a more in-depth description of the topics addressed in this chapter, the reader may refer to references [1] and [2].

2.1 Introduction to HVDC

Remote generation and system interconnections lead to a search for efficient power transmission at increasing power levels. The problems of alternating current (ac) transmission particularly in long distance transmission, has lead to the development of high-voltage direct-current (HVDC) transmission. HVDC transmission has advantages over ac transmission in special situations and has become an important contributor to successful power system operation [1].

The first commercial application of HVDC transmission was between the Swedish mainland and the island of Gotland in 1954. The system used mercury arc valves and provided 20 MW at 100 kV. The mercury arc valves were utilized in HVDC systems until thyristor valves became commercially available in 1970. The introduction of thyristor valves made HVDC transmission even more attractive [1, 3].

In Norway the first HVDC link was build in 1976/77 between Kristiansund and Tjele in Denmark. The HVDC system consists of overhead lines and a submarine transmission cable. In 1977, this submarine cable was the longest cable ever set in operation and the facility was based on thyristor valve technology [4].

Today, the application of HVDC systems is well established. There are 16 dc linkes operating or under construction in the United States and 21 in North America. There are additionally numerous links throughout Scandinavia as well as Japan, Australia, South Africa and others; well over 100 world wide [5].

The main objective of a HVDC transmission is to transmit electrical power from one electrical point to another. The following are the types of application for which HVDC transmission has been used [3, 4]:

I. Bulk power transmission. Transmission of large amount of power over long distances by overhead lines. HVDC transmission is a competitive alternative to ac transmission for distances in excess of about 600 km.
II. Asynchronous networks. Asynchronous link between two ac systems where ac ties would not be feasible because of system stability problems or a difference in nominal frequency of the two systems.

III. Underground/submarine power feeders. ac transmission is impractical for underwater cables longer than 30 km. This is due to the high capacitance of the cable and the need for intermediate compensation stations.

HVDC systems also have the ability to rapidly control the transmitted power. Hence, they have a significant impact on the stability of the associated ac power systems.

An understanding of the characteristics of the HVDC system is essential for the study of system stability, and, especially for the understanding of the performance of the overall ac/dc system.

2.2 HVDC system configuration

HVDC links may broadly be classified into the following five groups:

I. Monopolar links
II. Bipolar links
III. Homopolar links
IV. Back-to-back links
V. Multi terminal links

This section gives a brief description of the latter groups and is mainly based on [3, 4].

2.2.1 Monopolar links

The monopolar HVDC link has one conductor, usually of negative polarity, and the return path is provided by ground or water. Sometimes metallic return is also used. Cost consideration often lead to the use of such systems, especially for cable transmission. This type of configuration may also be the first stage in the development of a bipolar system. A monopolar HVDC transmission scheme is illustrated in Figure 1.

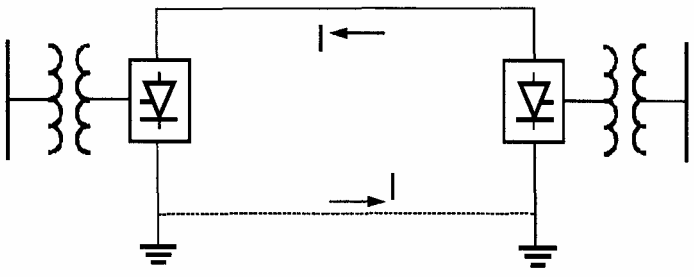

Figure 1 Monopolar HVDC transmission [4].

The metallic return path mentioned above, can be used in situations where the earth resistivity is too high or possible interference with underground/underwater metallic structures is objectionable. The conductor forming the return path is at low voltage.

2.2.2 Bipolar links

The bipolar HVDC link has two conductors, one positive and one negative. Each terminal has two converters of equal rated voltage, connected in series on the dc side. The junctions (the neutral point) between the converters are grounded. Normally, the currents in the two poles are equal, and there is no ground current. The two poles can operate independently. If one pole is isolated due to a fault on its conductor, the other pole can operate with ground and thus carry half the rated load or more by using the overload capabilities of the converters and line. A bipolar HVDC transmission scheme is illustrated in Figure 2.

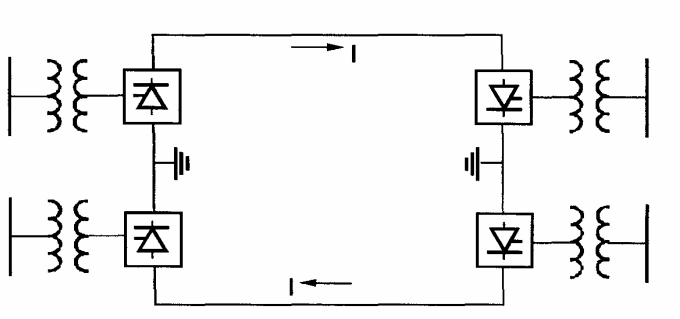

Figure 2 Bipolar HVDC transmission [4].

2.2.3 Homopolar links

The homopolar link has two or more conductors which all have the same polarity. However, negative polarity is often preferred because it causes less radio interference due to corona. The return path for this system is through ground. If there is a fault on one of the dc conductors, the entire converter is available for feeding remaining conductor(s) which, having some overload capability, can carry more than the rated power. A homopolar HVDC scheme is illustrated in Figure 3.

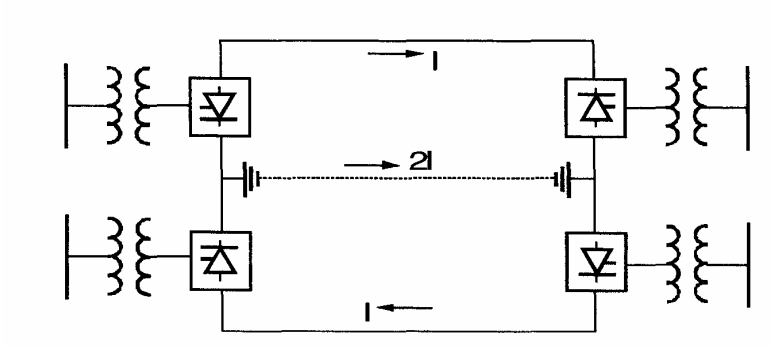

Figure 3 Homopolar HVDC transmission [4].

A homopolar HVDC link has the same advantages as a bipolar HVDC link. However, the difference between these two links is that homopolar link (with two poles in operation) has twice the ground current that it has with only one pole in operation.

2.2.4 Back-to-back links

Back-to-back HVDC links are used to connect two asynchronous operated ac power systems together. This configuration allows bidirectional power transfer between two ac systems. A back-to-back HVDC transmission scheme is illustrated in Figure 4.

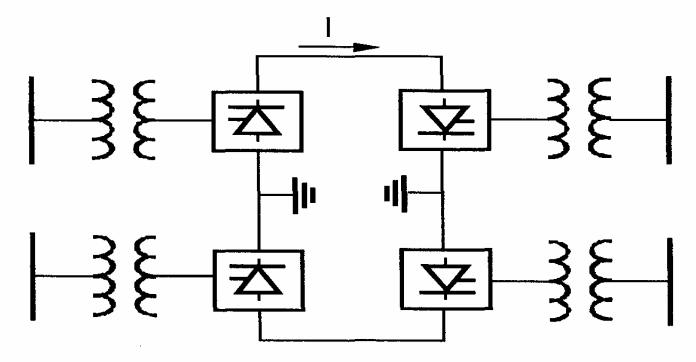

Figure 4 Back-to-back HVDC scheme [4].

A back-to-back HVDC system may be designed for monopolar or bipolar operation with different number of valve groups per pole. The number of valve groups depends on the purpose of the interconnection and the desired reliability. Note; back-to-back HVDC systems are operated without dc lines or dc power cables. Figure 4 illustrates a bipolar back-to-back HVDC scheme.

2.2.5 Multi terminal links

A multi terminal HVDC system is formed when the dc system is to be connected to more than two nodes on the ac network. The system consists of more than two converter stations, where some of the converters are operated as rectifiers and some are operated as inverters. A multi terminal HVDC transmission scheme is illustrated in Figure 5.

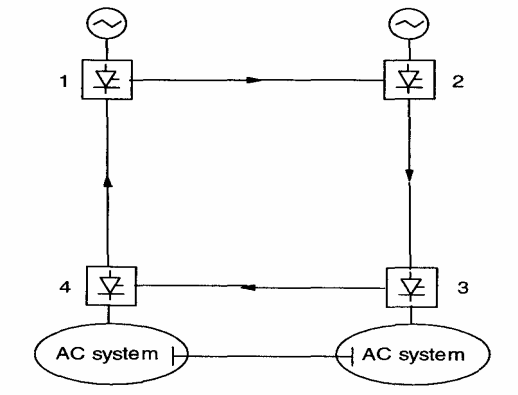

Figure 5 Multi terminal HVDC transmission system [4].

Figure 5 illustrates a series connected scheme. The latter scheme represents one among several possible configurations, e.g. meshed connection and parallel connection.

2.3 Components in a HVDC transmission system

This section describes the main components associated with a HVDC system. A schematic figure of the components addressed in this section is illustrated in Figure 6. This section is mainly based on [1, 4].

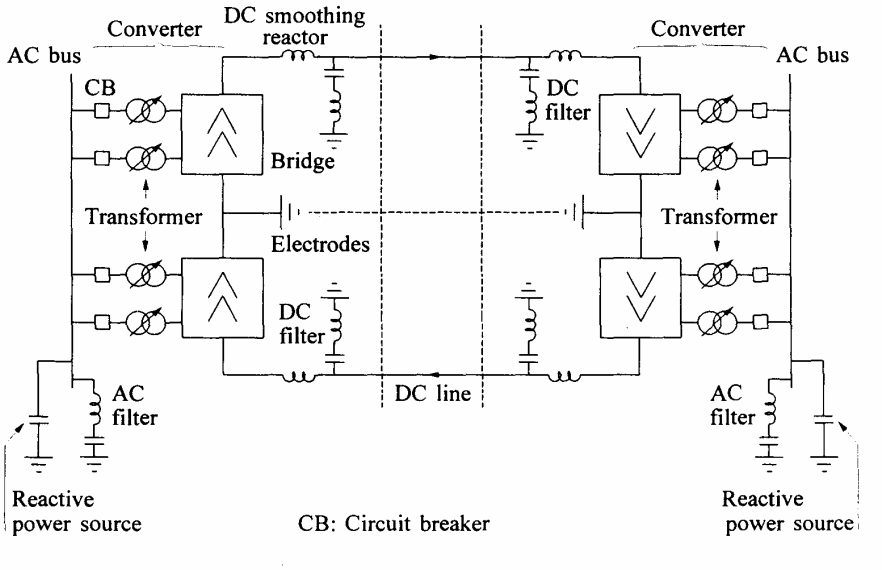

Figure 6 Schematic figure illustrating components in a HVDC system [3].

2.3.1 Converter unit

The converter units perform the ac/dc and dc/ac conversion, and consist of valve bridges and transformers with tap changers. Each valve is used to switch in a segment of an ac voltage waveform. The valve bridges consist of high-voltage valves connected in a 6-pulse or a 12-pulse arrangement. The valve firing signals are generated in the converter control at ground potential and are transmitted to each thyristor in the valve. Figure 7 shows a schematic illustration of a 12-pulse converter unit.

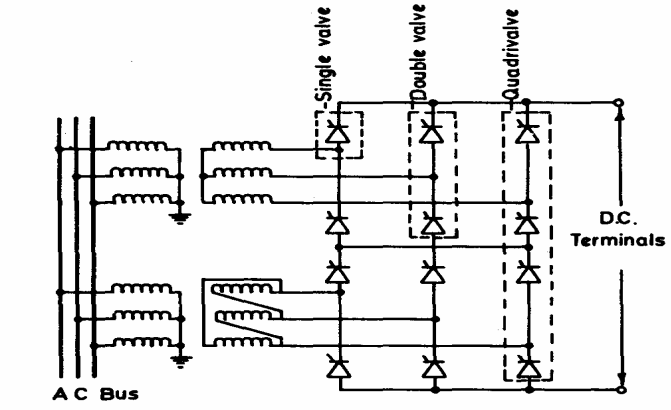

Figure 7 A twelve pulse converter unit [1].

The converter is fed by converter transformers connected in star/star and star/delta arrangements.

2.3.2 Converter transformer

The converter transformer can have different configurations – (i) three phase, two winding, (ii) single phase, three winding, (iii) single phase, two winding. If no transformer reserve is considered, the most economical alternative will be with three phase units.

Today, it is common to build a 12-pulse converter station per pole, i.e. each six-pulse bridge unit is supplied from separate transformers. To reduce harmonic interactions, one of the transformers is connected in star/star and the other in star/delta. The transformers in both the receiving and sending end are equipped with tap-changer control. The objective of this is to create an optimal voltage so that the converter can operate with an optimal firing angle. The control system of the converter transformers are slowly acting devices (T > 2-3 seconds) and do not need to be represented for transient studies, but for power flow studies only.

Note, the leakage reactance of the transformers is chosen to limit the short circuit currents through any converter valve.

2.3.3 Filter

Converters generate harmonic voltages and currents on both ac and dc sides. These harmonics may cause overheating of capacitors and nearby generators. Also, problems with interference with telecommunication systems are caused by harmonics. Filters are therefore used on both ac and dc side.

Filters also represent a reactive source that covers the reactive consumption of the HVDC link to a varying degree. Hence, the filters serve two purposes in the HVDC system:

I. Reduces harmonic currents and voltages in the ac power system.
II. Provides reactive power for the HVDC system.

There exist several types of filter used in HVDC systems. However, the latter will not be elaborated in this thesis. For more information on filters, see [1].

2.3.4 Smoothing reactor

The smoothing reactor serves an important part in the HVDC system. These are large reactors having inductances as high as 1.0 H, and are connected in series with each pole of each converter station [3].

The smoothing reactors serve the following purposes [3]:

I. Decrease harmonic voltages and currents in the dc line.
II. Prevent current from being discontinuous at light load.
III. Prevent commutation failure in inverters.
IV. Limit the crest current in the rectifier during short circuit on the dc line.

Even though increased reactance improves dc harmonic content, it also slows down the control response and reduces the resonance frequency. Hence, stabilization of current becomes more difficult.

2.3.5 Reactive power sources

Converter stations require reactive power supply. Under steady-state conditions, the reactive power consumed is about 50% of active power transfer. Under transient conditions, the reactive consumption may be much higher. Hence, reactive power sources are provided near the converters. For strong ac systems, these are usually in the form of shunt capacitors. In addition, synchronous condensers and static var systems (SVC) are used depending on requirements on the speed of the control system.

2.4 Principles of HVDC transmission

The static conversion of power from ac to dc and from dc to ac constitutes a central part of the HVDC transmission. To facilitate the understanding of the latter, it is essential to begin with a description of the converter principles and of the steady-state relationship of static power conversion.

The objective of this section is to give a basic understanding of the converter operation, the commutation phenomena and the rectification and inversion operation. Also, the reactive power demand and harmonic problems associated with converter operation are addressed in this section. This section is mainly based on [2].

2.4.1 General

The conversion from ac to dc and vice versa is done in HVDC converter stations by using three phase bridge converters. The configuration of the bridge is illustrated in Figure 8. This circuit is also known as the Graetz bridge. Although there are several alternative configurations possible, the Graetz bridge has been universally used for HVDC converters as it provides better utilization of the converter transformer and a lower voltage across the valve when conducting [3].

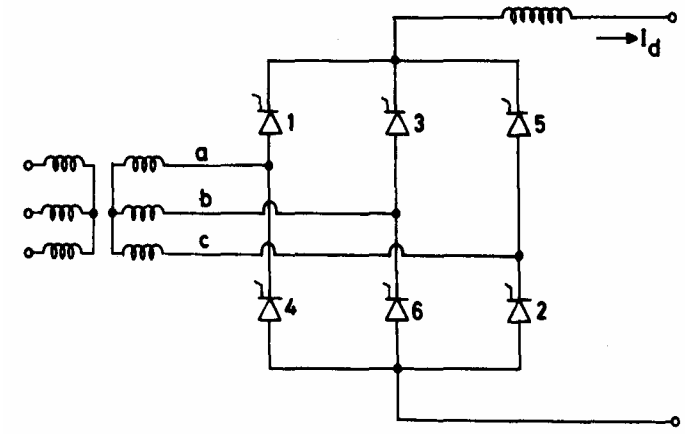

Figure 8 Graetz bridge [1].

The pulse number of a converter is defined as the number of pulsations, i.e. cycles of ripple, of direct voltage per cycle of alternating voltage. The valve can be treated as a controllable switch which can be turned on at any instant, provided the voltage across is positive. A diode is an uncontrolled switch which will turn on immediately after the voltage has become positive whereas the thyristor switching can be delayed by an angle α (alpha). The converters voltage sources are actually obtained from the transformer secondary windings [1].
The output voltage V_d of the converter consists of a dc component and a ripple whose frequency is determined by the pulse number [1].

2.4.2 Converter operation

To facilitate the understanding of converter bridge operation, this section will first consider the situation with negligible source impedance and no ignition delay. Thereafter the section will extend the analysis to include the effect of delaying the valve ignition and evaluate the effect of source impedance.

With no ignition delay

To understand the operation of the three-phase bridge rectifier, it is appropriate to first consider the idealized case where the converter bridge is connected to an infinitely strong power system. The latter corresponds to a situation with zero source impedance. Also, the bridge reactance is assumed so large that it is justified that the dc current is constant. Under this condition, the transfer of current (also noted commutation) between valves on the same side of the bridge takes place instantaneously. The switching sequence and the rectified voltage waveform are illustrated in Figure 9. This case corresponds to an uncontrolled bridge rectifier, i.e. on diode operation.

From Figure 9 it is clear that after instant A, valves 1 and 6 will conduct and the current flows in phase R and phase Y. This operating state continues up to point B, after which valve 2 becomes forward-biased and the dc current commutates naturally from valve 6 to valve 2. Similar argument applies at point C. A new valve becomes forward-biased every 60°, and the dc current will commutate to this valve.

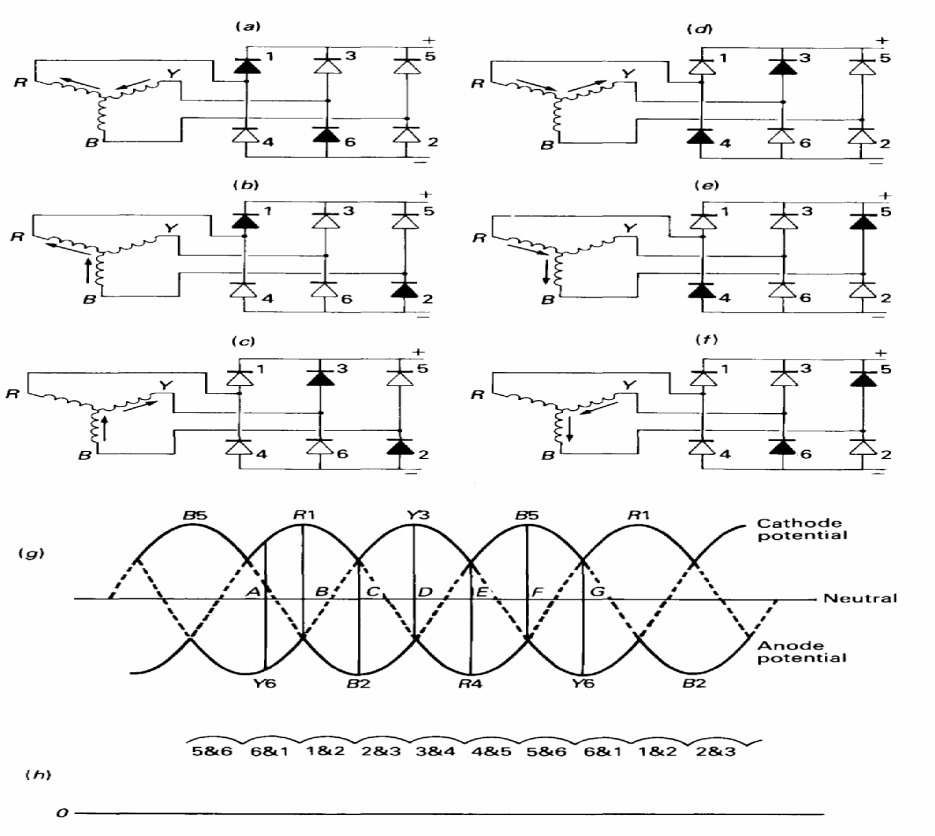

Figure 9 Bridge conducting sequence and dc voltage waveforms [2].

Figure 9 (h) shows the output voltage, i.e. the voltage of the positive pole with respect to the negative pole. It can be seen that the output voltage has ripple, or harmonic frequency, of six times the main frequency. Each valve carries the full value of direct current for one third of the cycle, and there are always two valves conducting in series.

With ignition delay

The ignition of the valves can be delayed by the grid or gate control. The "delay angle" is denoted α and corresponds to time delay of α/ω seconds. This thesis also uses the term firing delay angle in notation of α. Figure 10 illustrates the effect of ignition delay on voltage waveforms.

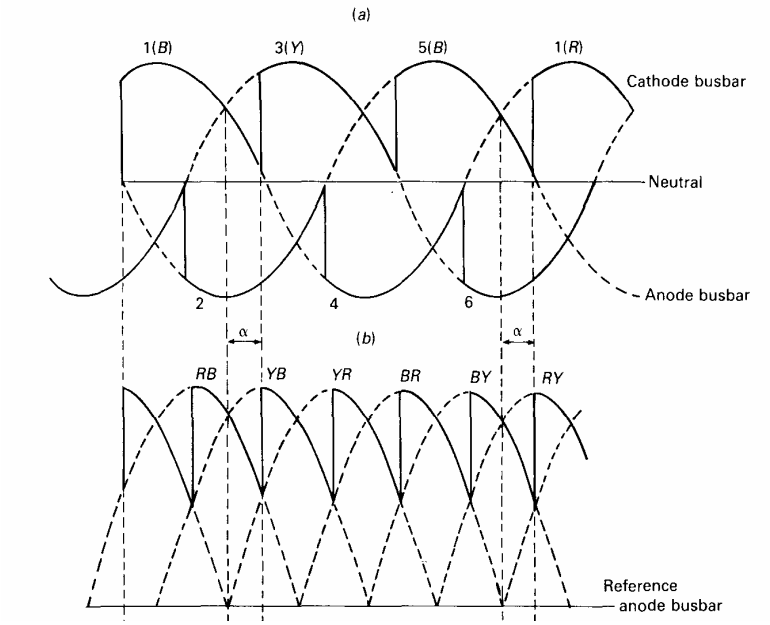

Figure 10 Effect of ignition delay on voltage waveforms [2].
(a) Common anode and common cathode voltages
(b) dc voltage

It is noticeable from Figure 10 that the voltage area, and therefore the mean direct voltage, is reduced in proportion with the magnitude of the delay. Hence, the effect of delayed ignition is a reduction in the direct voltage. For delay angles above 60° some negative periods begin to appear. If a pure resistance were connected to the bridge output, the bridge unidirectional current conduction property would prevent reverse current flow during these negative periods, and the operation would then be intermittent. However, the large smoothing reactor maintains positive current flow during the negative periods, and the energy is transferred from the reactor magnetic field to the ac system.

Figure 11 illustrates the voltage waveforms with 90° ignition delay. The figure shows that the negative cycle of the voltage waveform equals the positive cycle. Hence, the mean direct voltage becomes zero with 90° delay.

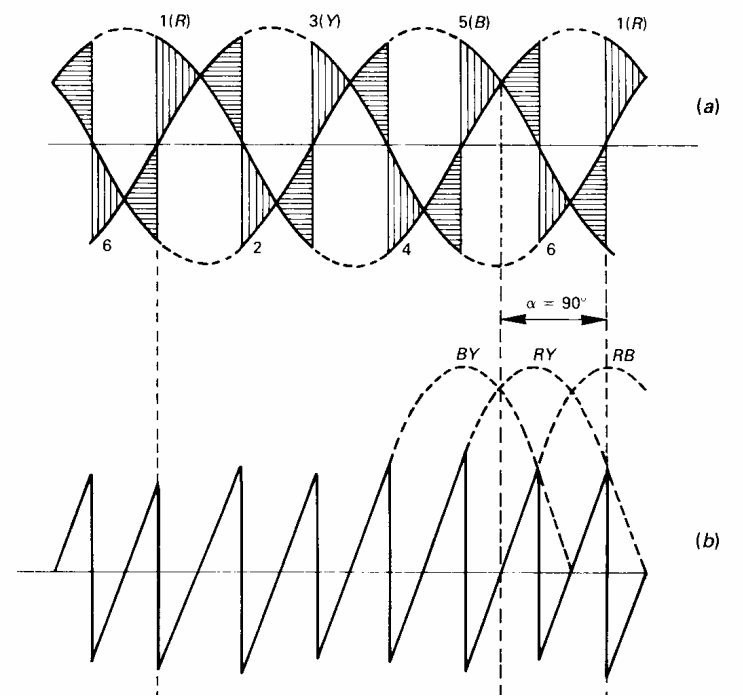

Figure 11 Voltage waveforms with 90 degrees ignition delay [2].
(a) Common anode and common cathode voltages
(b) dc voltage

If the delay angle is greater than 90°, the converter acts as an inverter instead of a rectifier. This means that the mean value of the direct current becomes negative and thus the active power is transferred from the dc side to the ac side [6].

The real commutation process

In a real situation the zero impedance supply required to produce the voltage waveforms in the previous sections does not exist. Even though the ac system impedance might be negligible, there will be a considerable transformer leakage reactance between the converter and the ac system.

Before analyzing the real commutation process it is important clearly define what is meant by commutation voltage and commutation reactance. [2] gives the following two definitions:

I. The commutation voltage is the voltage appearing on the dc line during the periods when no commutation is taking place.
II. The commutation reactance is the reactance between the commutation voltage and the converter valves.

To facilitate the study of the commutation process, see Figure 12. This figure considers the commutation process between valve 1 and 3 of a converter bridge, connected to a system with a source voltage v_c, a commutation reactance per phase X_c and negligible resistance.

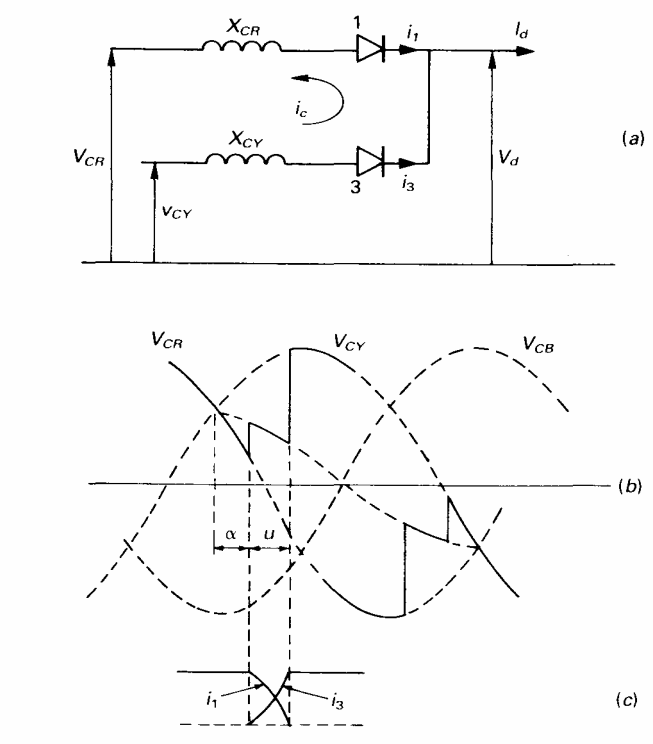

Figure 12 The commutation process [2].
(a) Equivalent circuit of the commutation from valve 1 to valve 3
(b) Voltage waveforms showing early rectification and late inversion commutations
(c) The commutation currents

With reference to Figure 12, the commutation from valve 1 to valve 3 can start any time after the upper voltage crossing between v_{CR} and v_{CY}. Due to $v_{CY} > v_{CR}$, a commutating current i_c (=i_3) builds up at the expense of i_1. Hence, $i_1 + i_3 = I_d$.

From the circuit in Figure 12 and assuming $X_{CR} = X_{CY} = X_C$, the following expression can be derived:

$$v_{CY} - v_{CR} = 2\frac{X_c}{\omega}\frac{di_c}{dt} = \sqrt{2}V_c \sin \omega t \tag{2.1}$$

where:

X_{CR}, X_{CY} and X_C are the commutation reactances.
v_{CY} and v_{CR} are phase voltages in phase Y and phase R respectively.
V_c is the phase-to-phase rms voltage.

The instantaneous expression for the commutation current, given below, can be derived from the above relation. However, the complete derivation is omitted in this thesis but can be found in [2].

$$i_c = \frac{V_c}{\sqrt{2}X_c}\left[\cos\alpha - \cos(\omega t)\right] \tag{2.2}$$

Substituting the final condition, i.e. $i_c=I_d$ at $\omega t = \alpha + u$ yields

$$I_d = \frac{V_c}{\sqrt{2}X_c}[\cos\alpha - \cos(\alpha + u)] \tag{2.3}$$

Rectifier operation

To illustrate the operation of a rectifier, see Figure 13. This figure illustrates a typical voltage and current waveform of a bridge operating as a rectifier with the commutation effect included. P indicates a firing instant (e.g. P_1 is the firing instant of valve 1), S indicates the end of a firing instant (e.g. at S5 valve 5 stops conducting) and C is a voltage crossing.

The average output voltage can be derived with reference to the waveforms of Figure 13, and is given as:

$$V_d = \frac{1}{2}V_{c0}\left[\cos\alpha + \cos(\alpha + u)\right] \tag{2.4}$$

where V_{c0} is the maximum average dc voltage and u is the commutation angle. For the three-phase bridge configuration $V_{c0} = \left(3\sqrt{2}/\pi\right)V_c$, and V_c is the phase to phase rms commutating voltage referred to the secondary (or valve side) of the converter transformer.

Since the value of the commutation angle is not normally available, a more useful expression for the dc voltage, as a function of the dc current, can be derived from Equations (2.3) and (2.4):

$$V_d = V_{c0}\cos\alpha - \frac{3X_c}{\pi}I_d \tag{2.5}$$

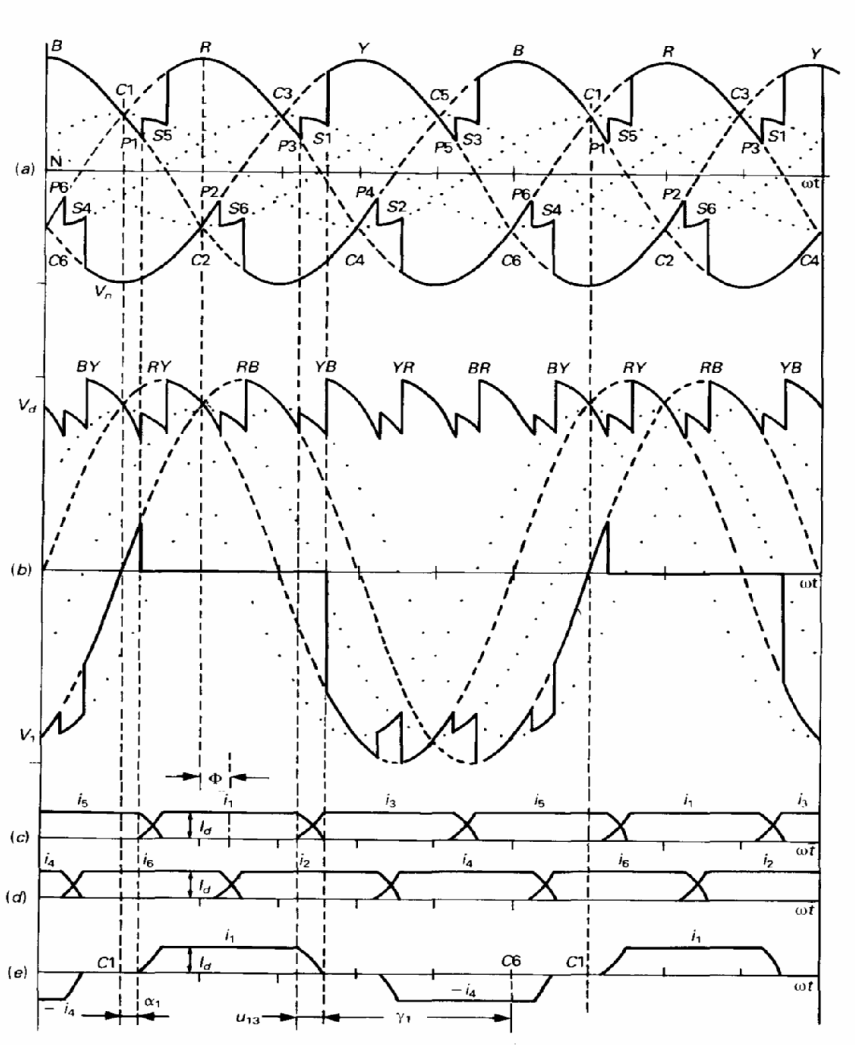

Figure 13 Typical 6-pulse rectifier operation [2].
(a) Positive and negative dc voltages with respect to the transformer neutral
(b) dc bridge voltage V_d, and voltages across valve 1
(c), (d) Valve currents i_1 to i_6
(e) ac line current of phase R

The rms magnitude of the rectangular current waveform (neglecting the commutation overlap) is often used to define the converter transformer MVA, i.e.

$$I_{rms} = \sqrt{\left\{ (1/\pi) \int_{\pi/3}^{\pi/3} I_d{}^2 d(\omega t) \right\}} = \sqrt{2} I_d \sqrt{3} \qquad (2.6)$$

However, since harmonic filters are normally provided at the converter terminals, the current flowing in the ac system contains only fundamental component frequency and its rms magnitude is:

$$I_1 = I_d \sqrt{6} / \pi \qquad (2.7)$$

Note; Equation (2.7) is obtained from Fourier analysis. This derivation is omitted in this thesis, but can be found in [2].

Inverter operation

The analysis of the inverter operation is not different from that of rectification and will thus not be repeated in this section. However, the inverter equations are often expressed in terms of the extinction angel γ (=π-α-u). Omitting the negative sign of the inverter dc voltage, the following expression applies:

$$V_d = V_{c0}\cos\gamma - \frac{3X_c}{\pi} I_d \tag{2.8}$$

The expression for the direct current is:

$$I_d = \frac{V_c}{\sqrt{2}X_c}\left[\cos\gamma - \cos(\pi - \alpha)\right] \tag{2.9}$$

Power factor and reactive power

Figure 14 illustrates a vector diagram of current and power for both the rectification and inversion operation. Due to the firing delay (earlier referred as ignition delay) and commutation angles, the converter current in each phase lags its voltage. This means that both the rectifier mode and the inverter mode consume reactive power. The latter can be seen from Figure 14.

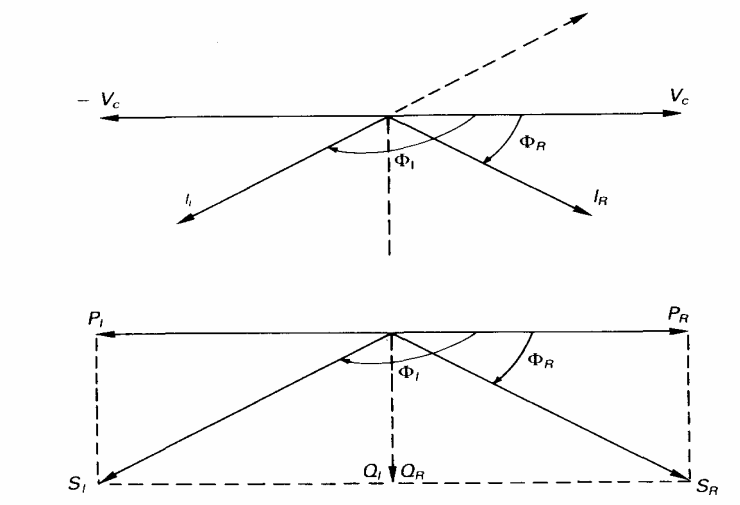

Figure 14 Current and power vector diagram [2].
R for rectification, I for inversion.

From a power system perspective, a minimization of reactive power consumption is desirable. This is due to the fact that reactive power influences the losses and the need for compensation. It can be shown that the extinction angle (γ) for the inverter mode, and the firing angle (α) for the rectifier mode should be as small as possible to obtain a optimal power factor. This is done below with the assumptions of no harmonic currents injected in the ac network. Also, its assumed no losses in the converter [6].

The active power P is the same as the dc power, i.e:

$$P = \sqrt{3} V_c I \cos\phi = V_d I_d \tag{2.10}$$

The power factor is:

$$\cos\phi = \frac{V_d I_d}{\sqrt{3} V_c I} \tag{2.11}$$

The fundamental component in the ac current, I, correspond to Equation (2.7). Substituting V_d and I_d from Equation (2.4) and (2.7) in Equation (2.11) the following approximate expression is obtained:

$$\cos\phi = \frac{1}{2}\left[\cos\alpha + \cos(\alpha + u)\right] \tag{2.12}$$

The reactive power is often expressed in terms of active power, i.e.:

$$Q = P \cdot \tan\phi \tag{2.13}$$

where $\tan\phi$ are defined by the following expression:

$$\tan\phi = \frac{\sin(2\alpha + 2u) - \sin 2\alpha - 2u}{\cos 2\alpha - \cos(2\alpha + 2u)} \tag{2.14}$$

Equation (2.10), (2.12) and (2.13) show that the active and reactive powers of a controlled rectifier vary with the sine and cosine of the control angle. Thus, when operating on constant current, the reactive power demand at low powers ($\phi = 90°$) can be very high. However, the latter situation is prevented in HVDC converters by the addition transformer tap changer, which tries to reduce the steady-state firing angle (or the commutation margin angle) to the minimum specified.

Note, in a normal power load condition the reactive power needed is about 50-60% of the transmitted active dc power at full load [4].

Converter harmonics

This section will only give a brief introduction to the concepts related to converter harmonics. A detailed description of converter harmonics can be found in [1, 2]. This section is mainly based on [1, 2].

The term harmonics is used to define the sinusoidal components of a repetitive waveform. These waveforms consist exclusively of frequencies which are exact multiples of the fundamental frequency. The full set of harmonics forms a Fourier series which completely represents the original waveform.

A HVDC converter introduces both ac and dc harmonics. These harmonics are injected into the ac system and dc line, respectively. There are several problems associated with the injection of harmonics and these are listed below:

I. Overvoltages due to resonance.
II. Telephone interference.
III. Extra power losses and consequent heating in machines and capacitors connected in the system.
IV. Instability of converter controls.

It is important to acknowledge that the orders of the "characteristic" harmonics are related to the pulse number of the converter configuration. A converter of pulse number p ideally generates only characteristic voltage harmonics of order pk on the dc side, and current harmonics of order pk ± 1 on the ac side (k is any integer). Hence, the greater the pulse number is, the greater is the lowest order of harmonics that is produced by the converter.

2.5 Principles of HVDC control

The system control in a HVDC link tends to be quite complex with a hierarchy of controllers. This section will thus present basic principles and functions of the HVDC control which constitutes a basis for the analysis performed in the following chapters. The control system is described in detail in the subsequent chapters, hence, an overall description will be presented in this section. This section is mainly based on [2, 4].

2.5.1 General

The transmitted dc current in a HVDC transmission is proportional to the difference in dc voltage in the sending and receiving end, respectively. The latter situation is illustrated in Figure 15. The figure shows a schematic one-line diagram which illustrates the power flow in a dc transmission. In this situation the dc current flows from the rectifier to the inverter. Thus, also the active power flows from the rectifier to the inverter. However, it is possible to reverse the active power flow by reversing the dc voltage.

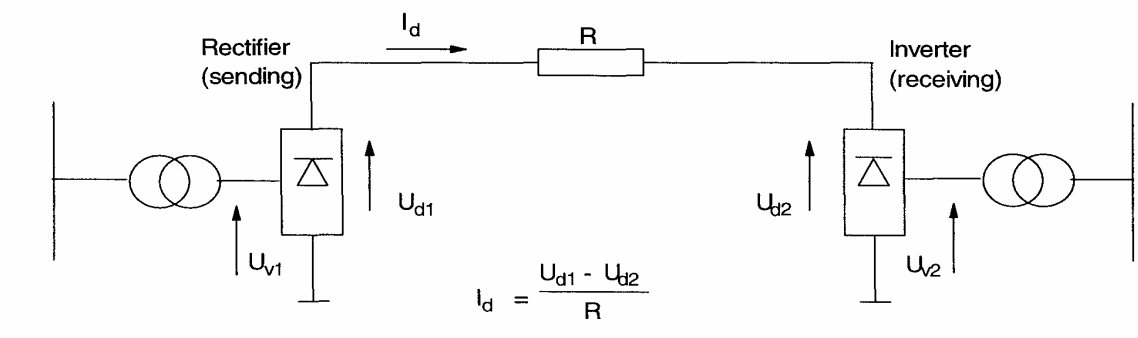

Figure 15 Schematic figure illustrating power flow in a dc transmission [4].

In a HVDC system, one of the converter stations is controlling the dc voltage. Normally, this is done by the inverter station. The other terminal station, usually the rectifier, adjusts the direct voltage on its terminals so that the dc current is controlled to the desired transmitted power. The objective of the transformer tap changers is to handle slow variations on the ac side, and therefore, maintain scheduled dc voltage on both sides.

Each converter has a closed loop current control system. The input controlling parameter to this system is the desired dc current. The latter is also called the current order. Each converter tries to adjust the dc voltage until there is no difference between the current order and the measured dc line current, or the maximum voltage is reached when the firing is at minimum delay angle. If the measured dc current is greater than the current order, the dc voltage is decreased.

The HVDC link provides the sending station with a slightly larger current order than the power receiving station. The difference between the two current orders is called the current margin.

Further, the converter which can generate the highest voltage will also control the current. The rectifier control angle ($\alpha = \alpha_{min}$) is normally smaller than the inverter control angle ($\gamma = \gamma_{min}$). Hence, the rectifier will control the current. The inverter will thus control the voltage with constant control angle ($\gamma = \gamma_{min}$).

2.5.2 Normal operation

To illustrate the control condition in normal operation, see Figure 16. This figure illustrates the V_d/I_d characteristic in normal operation. The operating current is set by the constant current control at the rectifier end. The inverter end current controller then detects an operation which is greater than its setting and tries to reduce it by raising its own voltage, until it hits the ceiling determined by the minimum extinction angle controlled at point A.

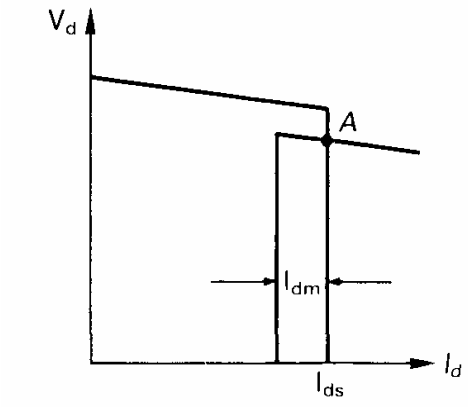

Figure 16 Steady-state characteristic and operation point under rectifier current control [2].

This constitutes the normal steady-state operation point, which presumes a higher natural voltage characteristic at the rectifier end. For the rectifier, the firing angle is measured and maintained approximately constant by making adjustments to rectifier transformer tap changers.

2.5.3 Operating during disturbances

Consider a situation where the ac voltage at the rectifier end has been reduced to an extent that the dc voltage ceiling (the natural voltage) of the rectifier becomes lower than that of the inverter. In absence of a current controller at the inverter, the voltage across the line is reversed and the current reduces to zero (current through the valve cannot reserve). However, an inverter current controller will prevent a current reduction below its current order by reducing its firing angel (inverter margin angle), thus changing from extinction angle to constant current control. A visualization of the situation is given in Figure 17.

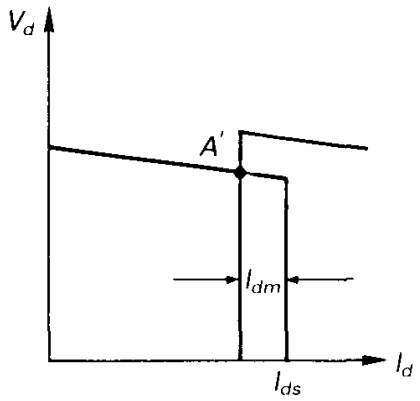

Figure 17 Steady-state characteristic and operation point under inverter current control [2].

The HVDC link is now under inverter current control. From Figure 17 it can be seen that the new operation point is A'. This operation point occurs at a current reduced by the current margin. The firing angle of the rectifier will now be at its extreme minimum since this terminal is trying to increase the dc voltage and thereby increase the dc current. However, at the inverter the firing angle has been decreased in order to control the dc current.

2.5.4 Voltage dependent current limit (VDCL)

In situations where the ac voltage is low, it may not be desirable or possible to maintain rated direct current or power. Two reasons for this are [3]:

I. When the voltage at a converter drops, the reactive power demand of the converter increases, and this may have an adverse effect on the ac system. The reduced ac system voltage also significantly decreases the reactive power supplied by the filters and capacitors, which often supply much of the reactive power consumed by the converters.
II. With reduced voltages, there is a risk of commutation failure and voltage instability.

The latter two problems associated with converter operation under low voltage conditions may be prevented by using a voltage dependent current limit (VDCL). The VDCL reduces the maximum allowable dc current when the voltage drops below a predefined value. The VDCL characteristic is illustrated in Figure 18 [3].

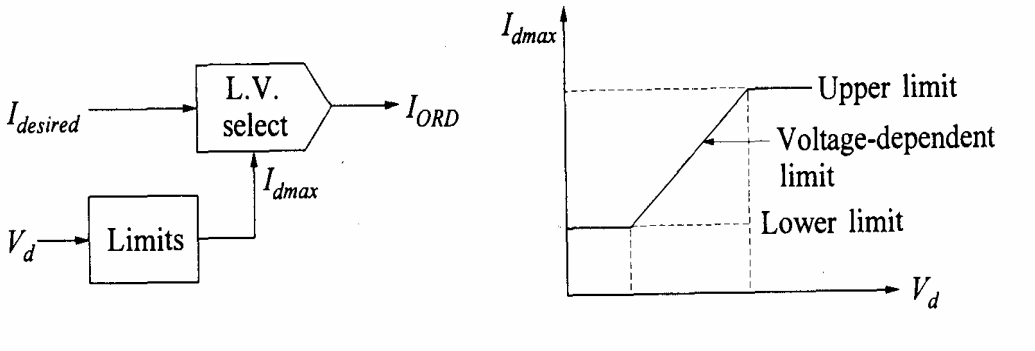

Figure 18 VDCL with current limit as a function of dc voltage [3].

In Figure 18 the VDCL characteristic is a function of the dc voltage. The VDCL characteristic can also be given as a function of the ac commutation voltage. However, the latter situation is omitted in this thesis because the VDCL characteristic used in the following chapters has a dc voltage characteristic.

For VDCL operation, the measured dc voltage is passed through a first-order time lag element. Normally, the time lag is different for increasing and decreasing voltage conditions. If the voltage is going down, fast VDCL action is required, and consequently, the time lag is small. However, if the same short time lag is used during voltage recovery, it may lead to oscillations and possibly instability. Therefore, a larger time lag is used when the dc voltage is recovering [3].

2.6 Influence of ac system strength on ac/dc system interaction

The performance of a HVDC system is significantly impacted by the relative strength of the ac system to which it is connected. The “weaker the ac system”, the greater will the ac/dc interactions be. This section addresses factors that require consideration when implementing a HVDC link terminated in a “weak” ac system. However, before the latter considerations are made, it is necessary to formally define what defines the strength of a system [7]. This section is mainly based on [4, 7].

2.6.1 ac/dc system strength

The ac system can be considered as “weak” from the following two aspects:

I. The ac system impedance is high relative to the dc power at the point of connection.
II. The ac system mechanical inertia is inadequate relative to the dc power infeed.

The term ”weak ac power system” means that the short circuit capacity in the ac system is low with respect to the nominal capacity of the HVDC transmission system. This situation can arise when either of (I) or (II), listed above, is valid. Both the short circuit ratio (SCR) and the effective short circuit ratio (ESCR) usually give a fundamental indication of the strength, and thereby, the performance of the HVDC system.

Short circuit ratio (SCR)

The SCR is obtained from the following equation:

$$SCR = \frac{S}{P_{d1}} \tag{2.15}$$

where S is the ac system three-phase symmetrical short circuit in megavolt-amperes (MVA) at the converter terminal ac bus with 1.0 pu ac terminal voltage. P_{d1} is the rated dc terminal power in megawatts (MW). In this thesis, P_{d1} is considered to be equal to the nominal dc power.

Effective short circuit ratio (ESCR)

The effective ac system impedance can be significantly increased if shunt capacitors including ac filters are connected at the ac terminal of a dc link. To allow for this, the effective short circuit ratio (ESCR) is defined as follows:

$$ESCR = \frac{S - Q_c}{P_{d1}} \tag{2.16}$$

where Q_c is the value of the three-phase fundamental MVAr in per unit of P_{d1} at per unit ac voltage of shunt capacitors connected to the converter ac bars.

Hence, the main different between SCR and ESCR is that ESCR includes the effect of ac system side equipment associated with the HVDC link.

In general, an interconnected ac and dc power system can be classified as:

$\lvert SCR \rvert < 2$	weak connection
$2 < \lvert SCR \rvert < 4$	medium connection
$4 < \lvert SCR \rvert$	strong connection

In evaluations based on the SCR and the ESCR, it is important to be aware of:

- Synchronous machines connected at, or near a converter station terminal and included in the system short circuit strength, should be represented by the subtransient reactance in the calculations of the short circuit ratios.
- HVDC schemes may have compensation equipment or filters connected to the converter transformer tertiary windings, which may complicate the relative meaning of the ESCR.
- The SCR and ESCR should be calculated carefully for each application.
- Evaluations and classification based on these values are only means for preliminary assessment of potential ac/dc interactions problems. Detailed studies are necessary.

2.6.2 Problems associated with weak ac/dc connections

This section will briefly discuss the main problems associated with the operation of a dc system connected to a weak ac system. A more detailed description of these problems can be found in [7]. This section is mainly based on [4].

Frequency instability

Frequency instability is often mentioned in relation to weak ac/dc power system considerations. However, this is not a phenomenon caused by low SCR of the ac system. Frequency instability is a result of low mechanical inertia of the connected ac system. The latter can be the situation if the HVDC transmission is connected to a small isolated network, when only a synchronous condenser is connected to the HVDC terminal.

Harmonic resonance

Problems with harmonic resonance are often due to parallel resonance between ac capacitors, and the ac power system at low harmonics. Capacitors tend to lower the natural resonance frequencies of the ac power system, while inductive elements tend to increase the frequencies. If a large numbers of capacitors are added, the natural frequency seen by the commutation bus may drop to 4^{th}, 3^{rd} or even 2^{nd} harmonic. If a resonance at one of these frequencies occurs, there can be a high impedance parallel resonance between the inductive and capacitive elements on the commutation bus. A low impedance resonance condition could arise in remote points in the system. Harmonic voltages from these remote points would tend to be amplified. The avoidance of low-order harmonic resonance is extremely important to reduce transient overvoltages.

High temporary overvoltages (TOV)

HVDC converters consumes large amount of reactive power, equal to about 50 to 60 percent of converter MW rating. When there is an interruption of the dc power transfer, the reactive power consumption of the HVDC converter drops to zero. With a low ESCR system, the resulting increase in ac voltage due to shunt capacitors and harmonic filters could be excessive. TOV may cause damage on customer equipment. Special schemes may be necessary to protect the thyristors in case of restart delays.

Countermeasures to TOV are:

- To use breakers to connect resistors for element switching or use metal-oxide arrestors. These schemes are called TOV control.
- To equip a converter station with control schemes using fast firing angle control to reduce TOV.

Voltage interaction

The active and reactive power characteristic of the converter influences the ac terminal voltage at the HVDC station. In order to minimize the voltage variations, it is important to control the reactive power demand. The variation in terminal voltage depends also on the total change in reactive power consumption in addition to components connected at the ac converter terminal. Examples of the latter components are filters, local loads, SVC and

synchronous compensators. Also, the SCR of the connected ac power system will influence the voltage variations.

During transient disturbances the reactive power consumption of the HVDC may vary widely, depending on the HVDC control system.

These variations in reactive power and voltage level can cause the following problems:

- Voltage flicker
- Voltage instability
- Cascading events

Voltage flicker
Shunt capacitors are normally installed as discrete banks equipped with breakers. Switching of these shunt banks at the converter station can cause large voltage changes with weak ac systems. This is called voltage flicker. To avoid customer complaints because of erratic and bothersome voltage fluctuations, consideration should be given to the maximum allowable shunt reactive bank size that can be switched [8].

Voltage instability
Another phenomenon which can occur when a weak ac power system is connected to a dc system is voltage instability. The latter is especially true for the inverter side of the converter. The ac as well as the dc voltages are sensitive to changes in loading and an increase in dc current is accompanied by a fall in ac voltage. The actual increase in power transfer may then be small. Control of voltage and recovery from disturbances will become difficult and the dc system response may even contribute to collapse of the ac power system.

The dc system controls may contribute to voltage instability by responding to a reduction in ac voltage as follows:

- Power control increases dc current to restore power.
- Inverter may increase γ to maintain commutation margin.
- Inverters draw more VAR with reduced voltage at the same time as the capacitors produce less.
- The ac voltage is further reduced.

Note; problems associated with interaction can be solved by increasing the SCR of the ac system or dynamic compensation of variations in reactive power.

Cascading events
The robustness and dynamic behavior of the terminal will be of great importance in case of disturbances with network splitting, low voltage periods etc. A short circuit situation in the terminal area could for instance lead to voltage problems which may affect the commutation condition for the converter. A consequence of commutation failure is tripping of the converter. In a particular network where all the converters operate under approximately the same conditions, the possibility of loosing all the terminals is high.

3 Power flow modeling in PSS/E

This chapter describes the establishment of the power flow model used in PSS/E and constitutes the basis for both power flow and dynamic analysis in the subsequent chapters. First, this chapter describes the changes made in the data set provided by Statnett. Second, a brief description of the facility at Ormen Lange is given. Finally, a detailed description of the power flow modeling of Ormen Lange is presented. The main focus in the latter is the modeling of the converters at Ormen Lange.

3.1 Modification of data set

This section describes the changes made in the power flow data set provided by Statnett. The changes made in this section are primarily based on knowledge gained from the preliminary study [9], and can be verified by studying Appendix D.

3.1.1 Changes made in the Statnett model

The changes made are mainly modifications on the existing data set, with the objective to obtain a more realistic model in terms of reactive power support in Mid-Norway. However, it is important to emphasize that the modifications made in this section are not essential for the power flow simulations in the following chapter. This is because the main focus of the next chapter is to analyze the principal behavior of the two-terminal dc line model. Hence, the degree of realism in the remaining power system is of less importance in such principal analyses.

These modifications are mainly implemented for the following dynamic simulations. Three changes are made in the "Statnett model". The following subsections describe the changes in detail.

3.1.1.1 Disconnection of SVC at Viklandet

The SVC connected to Viklandet will not be installed before 2008. From [9] it is clear that the SVC at Viklandet will provide a considerable amount of reactive power during system faults in Mid-Norway. The SVC is thus disconnected to give a more realistic reactive support in Mid-Norway (pro anno 2007).

3.1.1.2 Disconnection of capacitor bank at Klæbu

During the process of writing this thesis information of an error in the power flow data set was obtained. The initial data set included a large capacitor bank connected to a bus in Klæbu, which in reality, does not exist. Since this information was first obtained after the power flow simulations in Chapter 4 were completed, the simulations in this chapter are performed with the capacitor bank at Klæbu connected. However, since the objective of Chapter 4 is to analyze the principal behavior of the two-terminal dc model, the capacitor bank offers no undesirable effect on the simulation results.

Note, in all dynamic simulations the capacitor bank at Klæbu is removed from the data set.

3.1.1.3 Adjusting generator production and generator aggregation

In order to obtain a more stressed power situation in Mid-Norway the generator production in Mid-Norway is reduced with approximately 50 %. The load in the area remains unchanged, however, the generator production in West-Norway and Nort-Norway are increased by the same amount as the decrease in Mid-Norway. Hence, the net change in generator production is unchanged.

From the preliminary study [9], it became clear that the generator aggregation in Mid-Norway represents an unrealistic operational condition. Generators within the same power plant are operated at low ratings. This results in an unrealistic high reactive support in the area. Therefore, changes are made in the generator aggregation in Mid-Norway to obtain a more realistic reactive support in the area.

Status before changes are made

In the following, definition of the geographical areas Mid-Norway, North-Norway and West Norway are presented. Also, the total production within each area is given. The latter values can be verified by Appendix D.

- Generators in the following area constitute the production in Mid-Norway
    - 65 DRM.SVST
    - 66 DRM.MIDT
    - Total production 2310.90 MW
    - Max production 2962.6 MW

- Generators in the following area constitute the production in North-Norway
    - 67 DRM.NORD
    - 68 DRN.SOR
    - 69DRN.NORD
    - Total production 4043,7 MW
    - Max production 4644,5 MW

- Generators in the following area constitute the production in West-Norway
    - 61 DRSV.SKL
    - 62 DRSV.BKK
    - 64 DRSV.SFE
    - Total production 3011,7 MW
    - Max production 3929,9 MW

Power production in Mid-Norway after the production is reduced

In Appendix D, all generators with their respective production are given. In order to analyze a system which represents a situation with less reactive support, the production in Mid-Norway is reduced with approximately 1112.5 MW. This is approximately a 50% reduction.

The generators listed in the latter appendix are divided into groups. Each group represents generators in the same power plant or in the same geographical area. The purpose of these groups is to scale down the production within each group in a manner that gives a more realistic reactive power support. Instead of having e.g. three generators within a group operating at 30% power rating, two of the three generators are shut down and the remaining generator operates at 100%. Thus, the reactive power support in the area is reduced and represents a more realistic generator aggregation.

Power production in North-Norway after the production is increased

The power production in the northern part of Norway is increased with 500 MW. This equals a 12.3 % power increase. In this region generator aggregation is not considered, and the power increase is performed by using the scaling function in PSS/E.

The scaling process is not a dispatch activity; it merely scales the existing active power output of online machines such that the ratio of machine to total power is retained.

Aggregation of generators is not considered in this area because the analysis focuses on the situation in Mid-Norway.

Power production in West-Norway after the production is increased

The power production in the western part of Norway is increased with 610 MW. This equals a 20.3 % power increase.

In this region the generator aggregation is not considered, and the power increase is performed by using the scaling function in PSS/E.

3.2 Description of Ormen Lange

This section gives an overall description on how Ormen Lange is implemented in the PSS/E model. The main focus when establishing Ormen Lange is the converter modeling and this will be described in detail in the subsequent section. Modeling of the synchronous generator and the two-winding transformer will only be briefly described.

Figure 19 illustrates how Ormen Lange has been implemented in the PSS/E model. The configuration is based on technical information provided by ABB and Hydro. Due to confidentiality, only a brief description of the Ormen Lange facility is presented.

Three two-terminal dc line models are implemented to represent the respective converters at Ormen Lange. These converters feds three separate synchronous motors which are represented as three synchronous generators in PSS/E. The facility is connected to the 130 kV bus at Nyhamna through three separate four winding transformers. The tertiary transformer winding of each transformer is connected to a filter system. However, in PSS/E the four winding transformers are represented by two-winding transformers with the filter system connected directly to the 130 kV bus.

The remaining auxiliary components are represented as static PQ-loads.

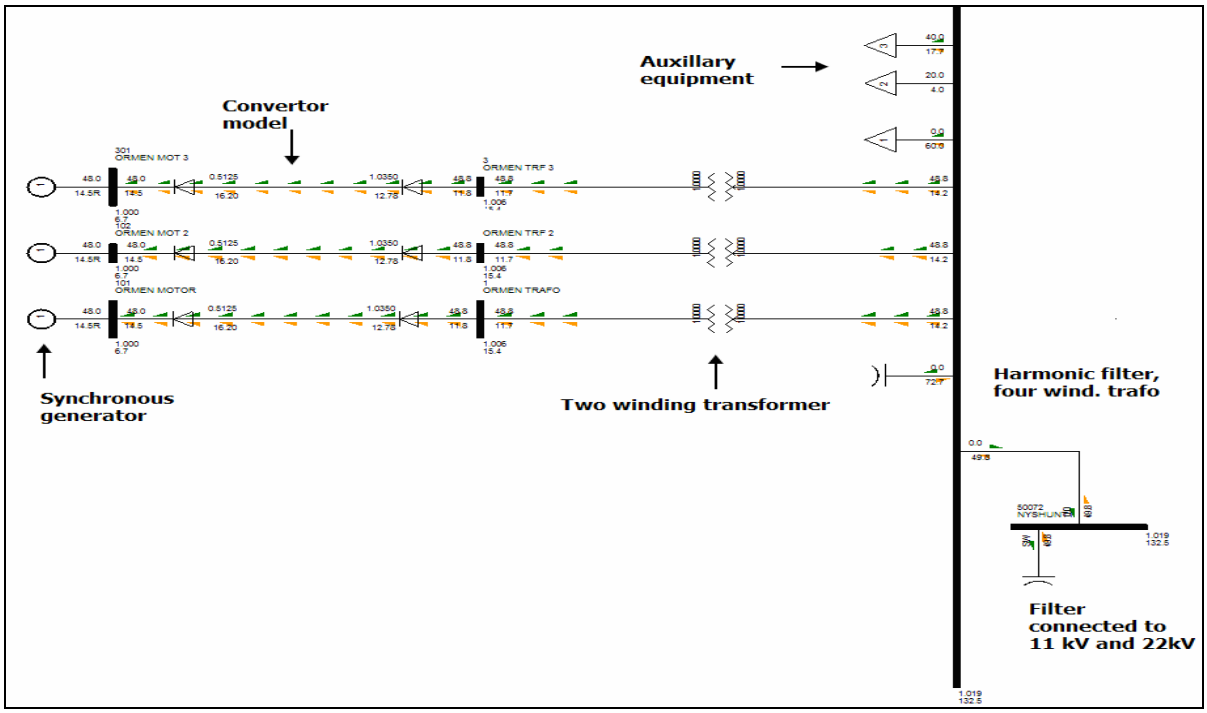

Figure 19 Illustration of Ormen Lange.

3.3 Converter modeling

This section gives a detailed description of the two-terminal dc line modeling in PSS/E. First, a detailed parameter description is given. Second, a thorough description of the converter configuration is presented.

It is important to emphasize that the modeling presented in this section does not represent Ormen Lange in a realistic manner. The latter is nor the objective of this section. The objective is merely to establish an alternative converter model which differs from the traditional PQ representation, and will constitute the basis for the dynamic model presented in Chapter 5.

The data used in the steady-state model enables not only power flow analysis but also establishes the initial steady-state for dynamic analysis. Thus, a detailed description is presented in this section.

3.3.1 Parameter evaluation

This section presents the data used for the two-terminal dc line model implemented in PSS/E. This section is mainly based on [10, 11].

The data requirements can be divided into the following three groups:

I. Control parameters and set-points.
II. Converter transformers.
III. The dc line characteristic.

Data for the two-terminal dc line model are specified on three consecutive data records. These data records, with their chosen parameter values, are presented in the following three records.

Some of the parameters specified are based on technical information provided by ABB. However, since the power flow simulations evaluate the principal response of the two-terminal dc line model, default values is also used.

The values are only presented for one of the three two-terminal dc line models. This is because all models are implemented in the same manner.

Data Record 1
Parameters defining line quantities and control parameters are given below.

Control mode (MDC)
Chosen value: MDC=2

The line can either be instructed to hold a desired dc current or a desired dc power. By choosing MDC=2 the line is instructed to hold a desired dc current.

Current or power demand (SETVL)
Chosen value: SETVL= 2840.2

When MDC is two, a positive value for SETVL specifies desired current in amps.

DC line resistance (RDC)
Chosen value: 0.1

This value equals the dc line resistance entered in ohms.

Compounding resistance (RCOMP)
Chosen value: 0

This is the compounding resistance entered in ohms. By using the value 0, the inverter end dc voltage VDCI is controlled. To control the rectifier end dc voltage VDCR, RCOMP is set to the dc line resistance, RDC. RCOMP = 0 by default.

Margin entered in per unit of desired dc power or current (DELTI)
Chosen value: 0.1

This is the percentage for which the order is reduced when alpha (rectifier firing delay angle) is at its minimum and the inverter is controlling the line current.

The difference between the rectifier current order and the inverter current order, also called current margin, is usually set at 10-15% of rated current. This is to ensure that the two constant current characteristics do not cross each other to errors in measurements or other causes [3].

Scheduled compounded dc voltage (VSHD)
Chosen value: 16.9

VSHD is the scheduled compounded dc voltage entered in kV. The value entered is based on information from ABB.

Minimum compounded dc voltage (DCVMIN)
Chosen value: 0

DCVMIN, entered in kV, is set to 0 because it's only used in constant gamma operations when the inverter tap setting is held constant and the ac transformer tap is adjusted to control the dc voltage. DCVMIN = 0 by default.

Mode switch voltage (VCMOD)
Chosen value: 0

If the line is in power control (MDC=1) and the inverter voltage falls below VCMOD (entered in kV) the line switches to current control mode. VCMOD = 0 by default.

Metered (METER)
Chosen value: I

Metered end code of either rectifier (R) or inverter (I). METER = I by default.

CCCITMX
Chosen value: 20

CCCITMX is the iteration limit for capacitor commutated two-terminal dc line Newton solution procedure. CCCITMX = 20 by default.

CCCACC
Chosen value: 1

Acceleration factor for capacitor commutated two-terminal dc line Newton solution procedure. CCCACC = 1 by default.

Data Record 2 and 3
Parameters defining rectifier end data, inverter end data and control parameters are given below. Parameters describing the rectifier are ended with the letter "R" and parameters describing the inverter are ended with the letter "I". Note; the control angle alpha for the rectifier is replaced with the control angle gamma for the inverter.

Number of bridges in series (IPR/IPI)
Chosen values: IPR = 2, IPI = 2

Nominal maximum rectifier firing angle (ALFMX)
Chosen value: ALFMX = 25

ALFMX is the maximum rectifier firing angle, entered in degrees. The maximum firing angle is only objective (not a firm limit). The converter may be operated above this limit.

Nominal maximum inverter firing angle (GAMMX)
Chosen value: GAMMX = 90

GAMMX is the maximum inverter firing angle, entered in degrees. The maximum firing angle is only objective (not a firm limit). The converter may be operated above this limit.

Minimum steady-state rectifier firing angle (ALFMN)
Chosen value: ALFMN = 5

ALFMN is the minimum rectifier firing angle, entered in degrees. The minimum rectifier firing angle is entered to ensure adequate voltage across the valve before firing [3].

ALFMN is a firm limit and the bridges will therefore not be operated in power flow solutions with firing angles below these values.

Minimum steady-state inverter firing angle (GAMMN)
Chosen value: GAMMN = 15

GAMMN is the minimum inverter firing angle, entered in degrees.

The minimum inverter firing angle (also noted extinction angle) is entered to avoid commutation failure. Because of the possibility of changes in direct current and alternating voltage even after commutation has begun, sufficient commutation margin above GAMMN must be maintained. Typically, the value for GAMMN with acceptable margins is 15° for 50 Hz systems and 18° for 60 Hz systems [3].

GAMMN is a firm limit and the bridges will therefore not be operated in power flow solutions with firing angles below these values.

Commutation transformer resistance (RCR and RCI)
Chosen value: RCR = 0
RCI = 0

RCR and RCI are, respectively, the rectifier and inverter commutating resistance per bridge, entered in ohms.

Note, if a commutating resistance value, not equal to zero, is input, PACR or PACI (dc line equivalent ac load) will not be equal to the desired dc power because of the losses in RCR and RCI.

RCR and RCI accounts for the voltage drop due to commutation overlap. It does not, however, represent a real resistance and consumes no power [3].

Commutating transformer reactance per bridge (XCR and XCI)
Chosen value: XCR = 0.01
XCI = 0.01

XCR and XCI are, respectively, the rectifier and inverter commutating reactance per bridge, entered in ohms.

The reactive consumption of the converter can vary greatly depending on the operating α or γ and on the commutating reactance (usually the converter transformer leakage reactance). The commutation reactance should include the leakage reactance of the converter transformer and other reactances in the commutation circuit that may influence the commutation process [7].

Increasing the commutation reactance reduces the rate of change of the dc currents. The converter bridge design is very dependent of the commutation reactance [12].

Primary base voltage (EBASR and EBASI)
Chosen value: EBASR = 15.3
EBASI = 6.7

EBASR and EBASI are, respectively, the rectifier and inverter primary ac voltage, entered in kV. The values entered are based on information provided by ABB.

Transformer ratio (TRR and TRI)
Chosen value: TRR = 0.44
TRI = 0.50

TRR and TRI are, respectively, rectifier and inverter transformer ratio.

Maximum tap setting (TMXR abd TMXI)
Chosen value: TMXR = 1.5
TMXI = 1.5

TMXR and TMXI are, respectively, rectifier and inverter maximum tap setting. TMXR and TMXI are 1.5 by default.

Minimum tap setting (TMNR and TMNI)
Chosen value: TMNR = 0.51
TMNI = 0.51

TMXR and TMXI are, respectively, minimum rectifier and inverter tap setting. TMNR and TMNI are 0.51 by default.

Tap step (STPR and STPI)
Chosen value: STPR = 0.00625
STPR = 0.00625

STPR and STPI are, respectively, rectifier and inverter tap step. STPR and STPI are 0.00625 by default.

Remaining parameters
The remaining parameters are used with their respective default values.

3.3.2 Converter configuration

This section describes both general converter configuration and the converter control system in PSS/E. This section is mainly based on [13].

3.3.2.1 General considerations

The two-terminal dc line model (also referred to as converter model) used in this thesis consists of a coordinated rectifier-inverter pair. These pairs place a coordinated set of special boundary conditions on the ac buses where the line is connected. The two-terminal dc line model consists of line commutated converters and is illustrated in Figure 20.

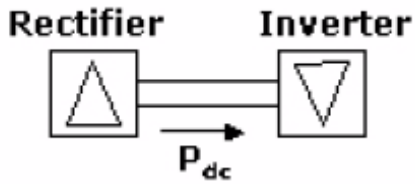

Figure 20 Simplified illustration of the two-terminal dc line model [10].

The constraints for the converter model consist of a series of linear and nonlinear equations. These equations are symmetrical between the rectifier and the inverter. The rectifier and inverter are only coupled by the transmission line equation. This means that the control equations for the converter (rectifier and inverter) are decoupled. The converter state can be obtained by solving the following converter equations.

Equations for the rectifier:

$$V_{dcr} = N_r \left(\frac{3\sqrt{2}}{\pi} E_{acr} \cos(\alpha) - \frac{3X_{cr} I_{dc}}{\pi} - 2R_{cr} I_{dc} \right) \tag{3.1}$$

$$\mu_R = ARCCOS\left(\cos(\alpha) - \frac{\sqrt{2} I_{dc} X_{cr}}{E_{acr}} \right) - \alpha \tag{3.2}$$

$$TAN\left(\phi_R\right)=\frac{2\mu_R+\sin(2\alpha)-\left[\sin 2(\mu_R+\alpha)\right]}{\cos(2\alpha)-\left[\cos 2(\mu_R+\alpha)\right]} \tag{3.3}$$

$$I_{acr}=\frac{\sqrt{6}N}{\pi}I_{dc} \tag{3.4}$$

Equations for the inverter:

$$V_{dci}=N_i\left(\frac{3\sqrt{2}}{\pi}E_{aci}\cos\left(\gamma\right)-\frac{3X_{cr}I_{dc}}{\pi}+2R_{cr}I_{dc}\right) \tag{3.5}$$

$$\mu_I=ARCCOS\left(\cos\left(\gamma\right)-\frac{\sqrt{2}I_{dc}X_{cr}}{E_{acr}}\right)-\gamma \tag{3.6}$$

$$TAN\left(\phi_I\right)=\frac{2\mu_I+\sin(2\gamma)-\left[\sin 2(\mu_I+\gamma)\right]}{\cos(2\gamma)-\left[\cos 2(\mu_I+\gamma)\right]} \tag{3.7}$$

$$I_{aci}=\frac{\sqrt{6}N}{\pi}I_{dc} \tag{3.8}$$

Equation for the transmission line:

$$V_{dci}=V_{dcr}-R_{dc}I_{dc} \tag{3.9}$$

The definitions for the above parameters are given in Table 1. Parameters describing the rectifier are ended with the letter "r" and parameters describing the inverter are ended with the letter "i".

Table 1 Two-terminal dc line parameter definitions.

Parameter	Explanation
V_{dcr}, V_{dci}	dc line voltage, [V]
E_{acr}, E_{aci}	Open circuit line-to-line voltage on the dc side of converter transformer, [V]
N_r, N_i	Number of bridges in series
X_{cr}, X_{ci}	Converter transformer dc side winding commutating reactance, [Ω/phase]
R_{cr}, R_{ci}	Converter transformer dc side winding commutating resistance, [Ω/phase]
I_{dc}	dc line current, [A]
I_{acr}, I_{aci}	Total ac line current flowing into the ac side of converter transformer.
$\cos_r$, $\cos_i$	ac power factor.
α	Rectifier firing delay angle.
γ	Inverter margin angle.
μ_R	Rectifier overlap angle.
μ_I	Inverter extinction angle.

3.3.3 Converter control

This section describes the control system and operation of the converter in PSS/E.

The rectifier and inverter are represented as shown in Figure 21 (see Section 3.3.1 for parameter explanation). The power flow solution logic adjusts the bridge control angle, α and γ, and the transformer tap position to control the dc voltage and current.

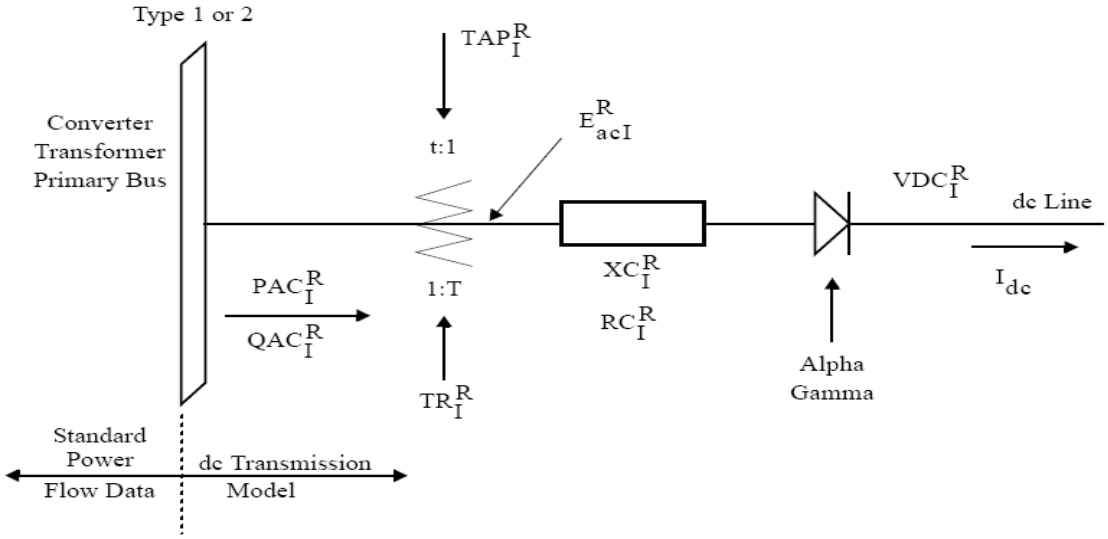

Figure 21 Rectifier/inverter representation in PSS/E [13].

To understand the principals which are applied to control the dc voltage and current, it is necessary to understand the relationship between the rectifier and inverter characteristic in PSS/E. The converter characteristic can be divided in to states. The first state is called normal operation, and applies for situations where the ac voltage at both rectifier and inverter are close to normal. This situation is illustrated in Figure 22. In this situation γ is adjusted to maintain the specified voltage on the dc line. The voltage control is current compounded to allow the voltage to be specified at a designated point along the line. The inverter will adjust γ to maintain line voltage at the set value, as long as the rectifier is able to control the line current.

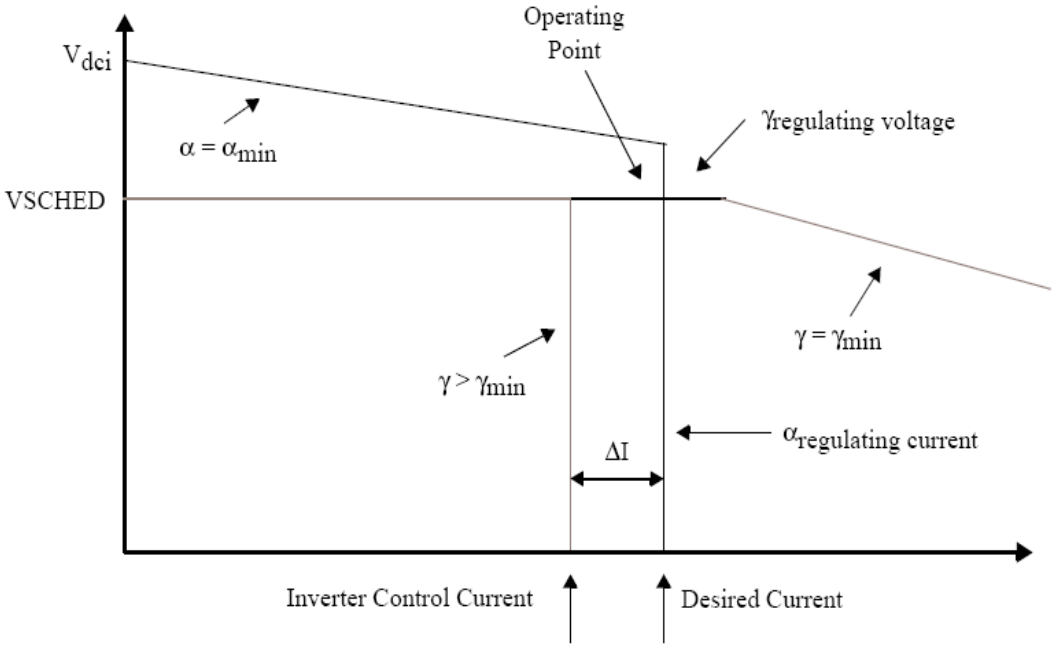

Figure 22 Converter characteristics in normal operation [13].

The second state represents the situation when the ac voltage at the rectifier is depressed. Figure 23 illustrates the converter characteristics for the latter state. In this state the control of the dc voltage is abandoned and γ is adjusted to maintain the dc current. The dc current, which the inverter is to control, is defined by the current margin, ΔI. The current margin is specified in "Data record 1" by the parameter "DELTI". The inverter will now control the dc current to a value reduced by a fraction DELTI compared to the desired current.

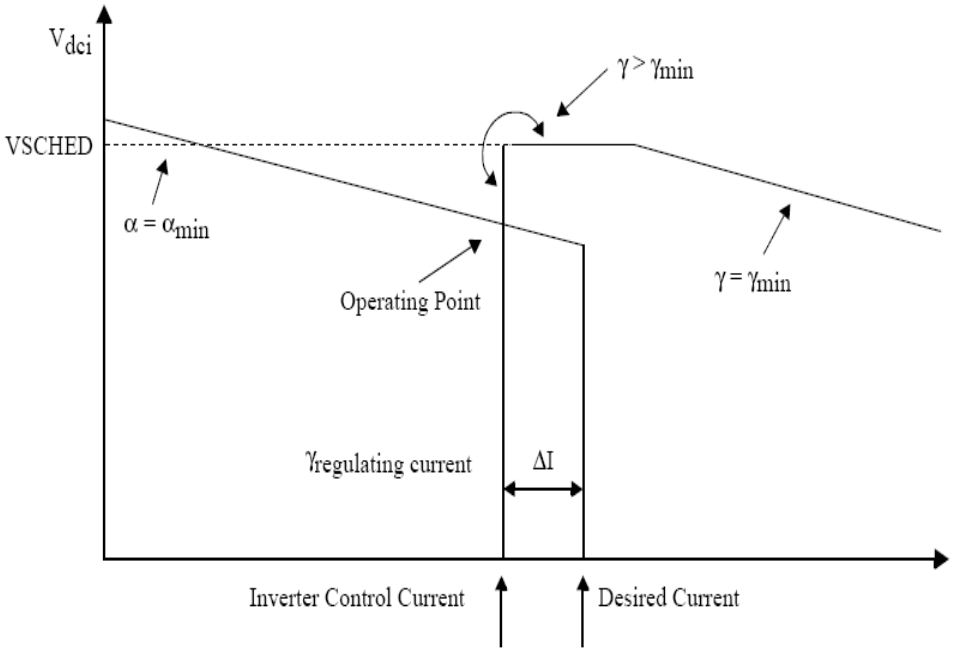

Figure 23 Converter characteristics when the rectifier ac voltage is depressed [13].

Converter transformer

The converter transformer tap position is adjusted by the control logic to attempt to hold the bridge firing angle above the predefined minimum and maximum values. The minimum values for α and γ are firm limits. This means that the converter will not be operated below these limits.

The converter taps are only adjusted until α and γ are between their specified maximum and minimum values. This means that the control logic does not adjust the taps to minimize α and γ when they fall between their maxima and minima.

The converter transformer is characterized by its leakage impedance and both its nominal absolute turn ratio and its per unit ratio in relationship to nominal value. These parameters are specified in "Data record 2" for the rectifier transformer and "Data record 3" for the inverter transformer.

Note; during every power flow solution the following variables are calculated:

Table 2 Power flow calculated variables.

Calculated variable	Description
$P_{ac}(R,I)$, $Q_{ac}(R,I)$	dc line equivalent ac load, [MVA]
α	Rectifier firing delay angel, [degrees]
γ	Inverter margin angle, [degrees]
$V_{dc}(R,I)$	dc line voltage, [V]
I_{dc}	dc line current, [A]
TAP (R,I)	Off-nominal tap setting, [pu]

3.4 Synchronous generator and two winding transformer

The focus in this thesis is to establish and analyze the converter model in PSS/E. The other components are only implemented as a necessity for the converter model to operate properly. Hence, there will be given no detail description of the generator and transformer modeling in this section.

Synchronous generator

The following non default values are used for the generator parameters:

- Mbase(MVA) = 53.98 Based on information from ABB
- R Source (pu) = 0.007 Standard value for this generator rating
- X Source (pu) = 0.300 "Standard value"

The remaining parameters are used with their default values. The reader may refer to attached save-file in Appendix D for parameter information.

The generators are modeled as swing buses, i.e. with a type code 3, and are held at constant voltage and phase angle. After each power flow solution the active and reactive power are set such that the mismatch at the bus is zero [10].

Two winding transformer

There will be given no description of the parameters used for the two-winding transformers implemented at Ormen Lange. The reader may refer to attached save-file in Appendix D for parameter information.

4 Power flow simulations

This chapter contains the power flow analysis performed in this thesis. The objective of this chapter is to gain knowledge about the performance of the steady-state two-terminal dc line model implemented at Ormen Lange. This knowledge will serve as basis for the dynamic simulations in the subsequent chapters.

This chapter uses the term converter model to refer to the two-terminal dc line model.

4.1 Introduction

In this chapter the following points are investigated:

I. The control logic system of the converter model in PSS/E. The investigation clarifies the behavior of the converter when exposed to a voltage depression at Nyhamna. The rectifier constitutes the link to the remaining power system and is therefore the main focus in these simulations.
II. Parameters influencing the reactive consumption of the converter.
III. The consequence of implementing a swing bus at the inverter.
IV. Principal comparison of the converter model and the PQ-model.

The knowledge obtained from the power flow simulations will serve as a basis for the following dynamic simulations. Some of the figures illustrated in this chapter are identical to figures used in Chapter 3. However, the figures are included to increase the readability.

4.2 Initial conditions and assumptions

This section presents the initial conditions and assumptions made for the power flow simulations presented in this chapter.

4.2.1 Power flow assumptions

The power flow file used in this chapter is "*Converter_model_chapter4.sav*" and can be found in Appendix D.

The following assumptions, which differ from the default setting provided in PSS/E, were made when establishing the power flow file:

- Switched shunt adjustments locked.
- Constant MVA loads converted with the following real power distribution:
    - 40 % constant current
    - 40 % constant admittance
    - 20 % constant power

- Constant MVA loads converted with the following reactive power distribution:
    - 0 % constant current
    - 100 % constant admittance
    - 0 % constant power

The initial conditions for the converter model are given in the table below. These data are obtained by solving the power flow for the file "*Converter_model_chapter4.sav*". Explanations for the parameters presented below are given in Table 1 and Table 2 in Chapter 3.

Initial values:

Table 3 Initial values.

DC converter data					AC system data			
V_{dcr} [kV]	V_{dci} [kV]	I_{dc} [A]	α [deg]	γ [deg]	Tap(R)	E_{acr} [kV]	P_{ac}(R) [MW]	Q_{ac}(R) [MVAr]
17.2	16.9	2840.2	12.78°	16.20°	1.035	6.55 *	48.8	11.8

Initial values in per unit:

Table 4 Initial values in per unit.

DC converter data					AC system data			
V_{dcr} [pu]	V_{dci} [pu]	I_{dc} [pu]	α [deg]	γ [deg]	Tap(R)	E_{acr} [pu]	P_{ac}(R) [pu]	Q_{ac}(R) [pu]
1	1	1	12.78	16.20	-	1 *	1	1

(*) The value entered for E_{acr} is calculated from the following equation:

$$V_{dcr} = N_r \left(\frac{3\sqrt{2}}{\pi} E_{acr} \cos(\alpha) - \frac{3X_{cr} I_{dc}}{\pi} - 2R_{cr} I_{dc} \right) \quad (4.1)$$

The figure below shows the rectifier side of one of the three converters implemented in PSS/E. This figure is identical to Figure 21 on page 39. XCR is the rectifier commutating transformer reactance, TRR is the rectifier transformer ratio and TAPR is the rectifier tap setting. The terms used in relation to the rectifier side is based on the figure below.

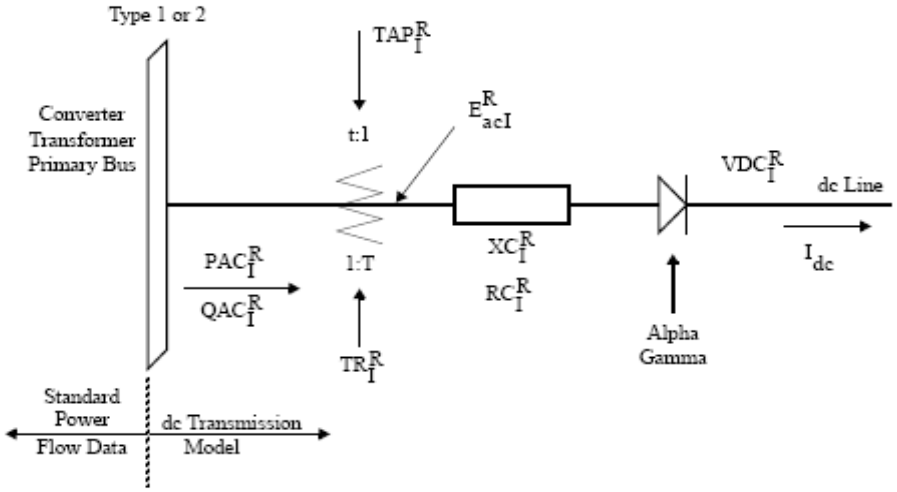

4.3 Application of the disturbance

Two disturbances are introduced in this section. The first disturbance is loss of 70 MVAr local shunt compensation at Nyhamna. The second disturbance is loss of 70 MVAr + 48 MVAr compensation at Nyhamna. The object of these disturbances is to clarify the performance of the converter model when exposed to a voltage depression at Nyhamna. The disturbances introduced do not represent a realistic scenario seeing that a loss of this amount of compensation will result in a shutdown of the plant. However, these disturbances act as an effective means to depress the bus voltage at Nyhamna to a varying degree.

The cases studied are given in the following tables.

Disturbance 1

Table 5 Case summary for Disturbance 1.

Case	Case explanation
A_1	Loss of 70 MVAr compensation at Nyhamna. Rectifier tap setting adjustable.
B_1	Loss of 70 MVAr compensation at Nyhamna. Rectifier tap setting locked.

Disturbance 2

Table 6 Case summary for Disturbance 2.

Case	Case explanation
A_2	Loss of 70 MVAr + 48 MVAr compensation at Nyhamna. Rectifier tap setting adjustable.
B_2	Loss of 70 + 48 MVAr compensation at Nyhamna. Rectifier tap setting locked.

4.4 Calculated solutions

This section presents the simulation results. The discussion is given consecutive as the results are presented to increase the readability.

Table 7 shows the results from Disturbance 1.

Table 7 Calculated solutions after loss of 70 MVAr compensation.

DC converter data						AC system data			
Case	V_{dcr} [pu]	V_{dci} [pu]	I_{dc} [pu]	α [deg]	γ [deg]	Tap(R)	E_{acr} [pu]	$P_{ac}(R)$ [pu]	$Q_{ac}(R)$ [pu]
A_1	1	1	1	8.35	16.20	1.01	0.986	1	0.695
B_1	0.99	1	0.9	5	16.48	1.035	0.973	0.913	0.424

Table 8 shows the results from Disturbance 2.

Table 8 Calculated solutions after loss of 70 MVAr+48 MVAr compensation.

DC converter data						AC system data			
Case	V_{dcr} [pu]	V_{dci} [pu]	I_{dc} [pu]	α [deg]	γ [deg]	Tap(R)	E_{acr} [pu]	$P_{ac}(R)$ [pu]	$Q_{ac}(R)$ [pu]
A_2	1	1	1	8.25	16.20	0.985	0.985	1	0.686
B_2	0.97	0.970	0.9	5	21.25	1.035	0.950	0.873	0.415

The results presented in Table 7 and Table 8 are also illustrated in single line diagrams in Appendix A.

4.5 Discussion of the results

This section contains discussion of the results presented in the previous section. It is important to emphasize that the evaluations made in this section is only valid for the assumptions made in this chapter and the parameter settings defined in Chapter 3.

4.5.1 Case A_1

The voltage depression at Nyhamna causes the control logic to reduce the rectifier transformer tap position to attempt to hold the rectifier firing angle α above its minimum and below its maximum value. The rectifier tap position is reduced from 1.035 to 1.01. The objective is to increase the voltage on the valve side of the rectifier transformer (E_{acr}). However, the change in tap position also changes the reactive consumption of the rectifier. In this case the reactive consumption of the rectifier is reduced to 0.695 per unit. Since the commutating reactance is held constant, the reduction in reactive consumption of the rectifier, $Q_{ac}(R)$, is due to the reduction of α from 12.78° to 8.35°.

Since the voltage on the valve side of the rectifier transformer is maintained close to its nominal value, I_{dc}, V_{dcr}, and V_{dci} are unaffected when exposed to the disturbance defined by

case A_1. It is also clear that since I_{dc} and V_{dcr} is unaffected by this disturbance, $P_{ac}(R)$ is also unaffected.

The operation of the converter when exposed to the disturbance defined by A_1, can be illustrated by the figure below. This figure is identical to Figure 22 on page 40. This figure illustrates the relationship between the rectifier and the inverter characteristics when the ac voltage at both the rectifier and inverter are close to normal. As the inverter is given a current order lower than the rectifier by the value of the current margin, it is forced into minimum commutation margin control, which gives the maximum dc voltage for a given ac voltage applied to the inverter.

The intersection of the two characteristics determines the mode of operation. The rectifier is operating with constant current control and the inverter is operating at constant (almost minimum) extinction angle.

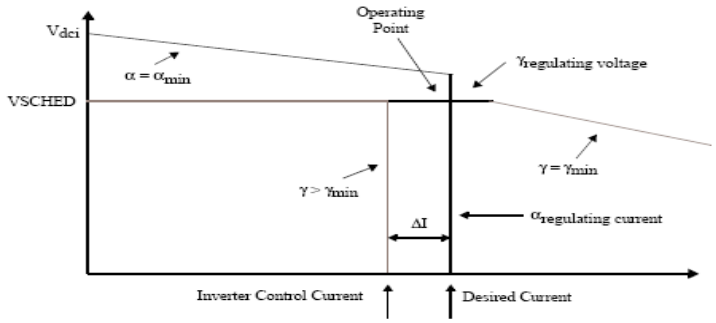

Due to the reduction in tap setting of the rectifier transformer, the ac voltage at the rectifier is still within its "normal" range when exposed to the voltage depression. Hence, the converter is in normal operation, with the rectifier in control of the dc current.

Figure 24 is included to give a visual picture on how the control system is operated. This figure is simplified and do not represent the correct model.

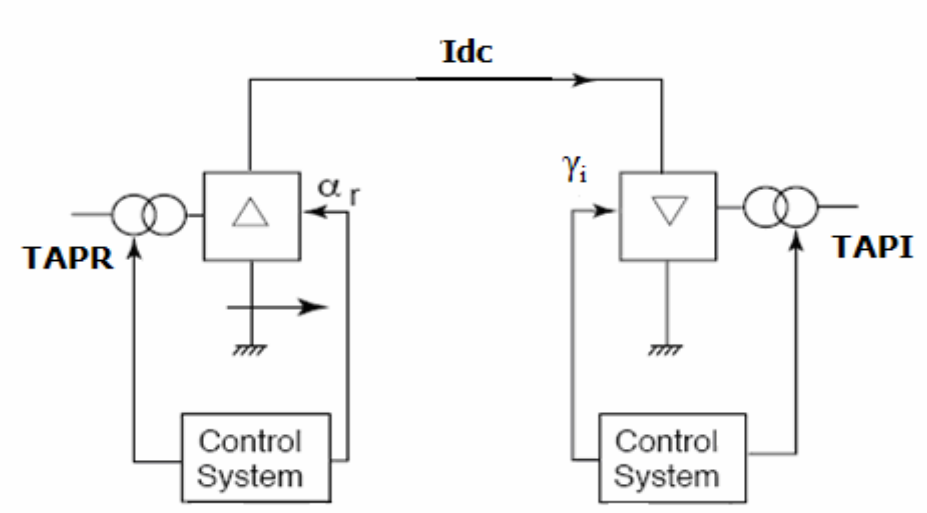

Figure 24 A illustrative model of the control system.

The converter taps are adjusted only until the corresponding bridge firing angles are between their specified minimum and maximum values. Hence, taps are not adjusted to minimize firing angle once they are between their maximum and minimum [13].

The latter explains why the inverter margin angle γ is slightly above its minimum value when the inverter is operating at constant extinction angle.

4.5.2 Case B_1

In this case the converter is exposed to the same disturbance as in case A_1, however, the rectifier transformer tap setting is locked to its initial value. The objective of this case is to evaluate the impact of a rectifier ac voltage depression without the influence of transformer tap changers. The latter may represent a transient situation were the tap changer action is too slow and hence not considered.

The converter response to Case B_1 can be illustrated in the figure below. This figure is identical to Figure 23 on page 40.

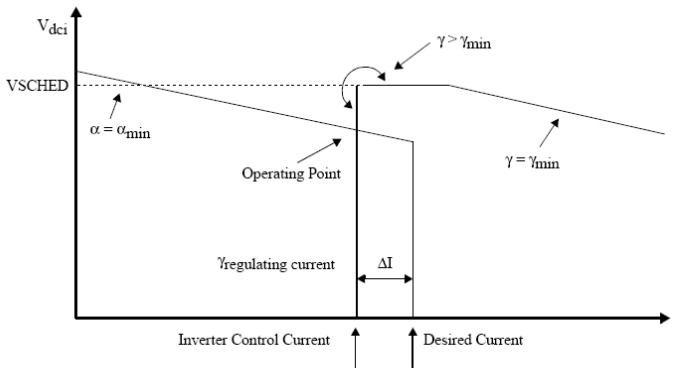

In normal operation the inverter margin angle, γ, is adjusted to maintain a specified voltage on the dc line. However, in case B_1 the control of the dc voltage is abandoned and γ is adjusted to maintain the dc current at a value which is the desired current reduced by the current margin, ΔI. In the data set used in these analyses, the parameter "DELTI" is used to specify the current margin. DELTI is set to be 0.1 per unit. This means that the current order is reduced by this fraction when α is at its minimum and the inverter is controlling the line current [13].

The results from Table 7 confirm the evaluation made above. Since the rectifier transformer tap setting is locked to its initial value, the rectifier transformer will not boost the valve side of the rectifier transformer. This means that E_{acr} is given by the ac voltage at the primary side of the rectifier transformer (called ORMEN TRAFO in PSS/E) multiplied with $\left(\frac{\text{Rectifier transformer ratio}}{\text{Rectifier tap setting}}\right)$. From Table 7 it can be seen that E_{acr} is reduced to 0.973 per unit. This reduction causes α to be reduced to its minimum value, $\alpha=\alpha_{min}=5°$. As described above, the inverter takes over the current control and the dc current is reduced to a fraction equal to the current margin, i.e. $I_{dc}=0.9$ per unit. Due to the locked tap setting of the rectifier transformer, the rectifier dc voltage, V_{dcr}, is reduced to 0.944 per unit.

Since both the dc current and the rectifier dc voltage are reduced, $P_{ac}(R)$ is reduced to 0.913 per unit.

The rectifier reactive consumption, $Q_{ac}(R)$, is reduced to 0.424 per unit. This drastic reduction is a result of a reduction in the rectifier firing angle from $\alpha=12.78°$ to $\alpha=\alpha_{min}=5°$. It is thus clear that the rectifier reactive power consumption is reduced when α is reduced. A reduction in α also improves the power factor for the rectifier, thus reducing the reactive power consumption.

4.5.3 Case A_2 and B_2

From Table 6 it can be seen that Case A_2 and B_2 are defined in the same manner as Case A_1 and B_1. However, the disturbance introduces a compensation loss of approximately 118 MVAr at Nyhamna. This disturbance is called Disturbance 2 and is introduced to depress the ac bus voltage at Nyhamna further.

By evaluating the results from Case A_2 in Table 8, it is clear that the results are almost the same as for case A_1. Even though a 118 MVAr compensation loss leads to a greater voltage depression at the primary side of the rectifier transformer, the transformer reduces its tap settings and thus boosts the valve side of the rectifier. This is done by reducing the rectifier transformer tap setting from 1.035 to 0.985. Seen from the rectifier, a 118 MVAr compensation loss is approximately the same as a 70 MVAr compensation loss. This can be confirmed by comparing E_{acr} from Case A_1 with E_{acr} from Case A_2.

In other words; the rectifier transformer tap changer compensates the additional voltage depression. However, the latter is only valid when the rectifier minimum tap setting is adequate.

In case B_2, see Table 6, the converter is exposed to the same disturbance as in Case A_2, however, in Case B_2 the rectifier transformer tap setting is locked at its initial value. As described for Case B_1, the control of the dc voltage is abandoned by the inverter and γ is adjusted to maintain the dc current at a value which is the desired current reduced by the current margin, ΔI. Since the rectifier tap setting is locked, this disturbance leads to a greater voltage depression at the valve side of the rectifier transformer. Consequently, the rectifier dc voltage is reduced to 0.971 per unit, see Table 8. Due to current control at the inverter, the inverter increases the inverter margin angle (γ) from 16.20° to 21.25°. This causes a reduction in the inverter dc voltage, V_{dci}, and is necessary in order to maintain scheduled dc current. The increased inverter margin angle also results in an increased consumption of reactive power at the inverter, see Appendix A.

The reduction in $P_{ac}(R)$ and $Q_{ac}(R)$ can be explained in the same manner as for the previous cases. When comparing the reactive consumption of the rectifier for Case B_1 and Case B_2, one can see that the reactive consumption is slightly reduced for Case B_2. The difference in reactive consumption is due to the fact that the amount of active power going into the rectifier, $P_{ac}(R)$, in Case B_2 is less than in Case B_1.

The latter can be seen from the following equation:

$$Q_a = P_a * \tan\varphi$$

which is identical to Equation (2.13) in Section 2.4.2.

4.6 Reactive power consumption of the converter

When analyzing the influence of implementing a converter model in power flow simulations, the converter reactive consumption is a key factor that needs to be considered. From the previous sections it is clear that the reactive consumption of the converter can vary greatly depending on the operating α and γ. However, the reactive consumption also depends on the commutating reactance, and the latter will be illuminated in this section.

The commutation reactance should include the leakage reactance of the converter transformer and other reactances in the commutation circuit that may influence the commutation process. Due to the uncertainty of the commutation reactance in the previous simulations, and its influence on the converter reactive consumption, this section evaluates the effect of varying the rectifier commutation reactance. Only the rectifier commutation reactance is evaluated because the rectifier constitutes the link to the remainder power system, and affects the power system with its reactive consumption [7].

It should be noted that varying the control angle (α and γ), and by this, the consumption of reactive power in one converter station, can result in a corresponding variation in the control angle and reactive consumption in the other station. However, since the control equations for the rectifier and inverter are decoupled in power flow simulations, no considerations are made on a possible influence on the inverter reactive consumption [7, 13].

The figures listed below illustrate how the reactive consumption of the rectifier is influenced by varying the rectifier commutating reactance, XCR.

Figure 25 illustrates how marginal changes in the commutating reactance influence the reactive consumption of the rectifier. Figure 26 illustrates how a substantial increase in the commutating reactance influences the reactive consumption of the rectifier. In both figures, the reactive consumption is given in per unit of the nominal rectifier reactive consumption, i.e. $Q_{ac}(R) = 11.8$ MVAr.

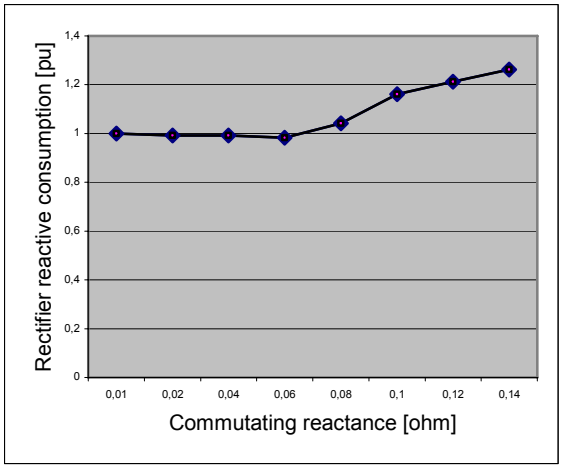

Figure 25 Rectifier reactive consumption for marginal changes in rectifier commutating reactance.

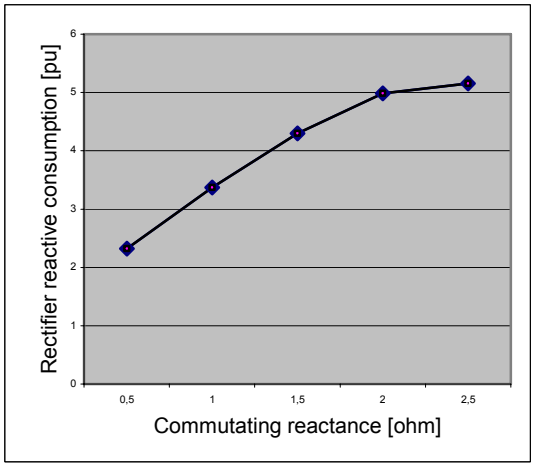

Figure 26 Rectifier reactive consumption for large changes in rectifier commutating reactance.

4.6.1 Discussion of the results

Figure 25 shows that an increase in the rectifier commutating reactance from XCR=0.01 Ω (which is the initial value) to XCR=0.08 Ω results in a small decrease in the rectifier reactive consumption. This contradicts with the statement above which implies that the reactive consumption increases with an increased commutating reactance. However, the small reduction in reactive consumption is caused by a corresponding reduction in rectifier firing angle, α. This means that when the commutating reactance increases to XCR =0.08 Ω, the reduction in α "compensates" for the actual increased reactive consumption from the commutating reactance.

Increasing the commutating reactance from XCR=0.08 Ω to XCR = 0.14 Ω leads to a gradual increase in the reactive consumption. Also in this situation there is a reduction in α as the commutating reactance increases. However, the contribution from the increased commutating reactance now dominates the reduction in α, thus resulting in a net increased consumption. Figure 25 shows that increasing the rectifier commutating reactance from XCR=0.01 Ω to XCR=0.14 Ω results in a 26 % increased reactive consumption at the rectifier.

In Figure 26 the same principals are illustrated, though with a greater increase in the commutating reactance. This figure illustrates how the rectifier reactive consumption changes when the commutating reactance varies from XCR=0.5 Ω to XCR=2.5 Ω. It is clear that the reactive consumption is drastically increased when the commutating reactance increases from the initial value to XCR=2.5 Ω. Increasing XCR to 0.5 Ω result in a reactive consumption of 2.32 per unit. If XCR is increased further, e.g. XCR = 2 Ω, the reactive consumption is increased to approximately 5 per unit.

Note; Figure 25 and Figure 26 do not give an unambiguous explanation on how the rectifier reactive consumption is influenced by the rectifier commutating reactance. Since there are several parameters in the rectifier model that changes as a consequence of changing the commutating reactance, it is not possible to conclude that the changes in reactive power

consumption is caused by the commutating reactance alone. The rectifier e.g. compensates the increased voltage drop by reducing the rectifier firing angle, α, and the rectifier transformer tap setting.

To avoid the influence of a reduction in α and rectifier transformer tap settings, it is possible to "force" PSS/E to maintain a constant α and transformer tap setting during the simulations. This is done by specifying the initial value for α as the minimum rectifier firing angle, ALFMN, and the initial value for the rectifier transformer tap setting as the minimum rectifier transformer tap setting, TMNR. However, this leads to a reduction of the active power going into the rectifier and will obviously influence the reactive consumption as well (see Equation (2.13)). Therefore, this is not considered in detail.

4.7 Influence from the swing bus on the inverter

From a system viewpoint, it is the rectifier side which is of most interest since this side is directly coupled to remaining power system and its behavior can have a significant impact on the ac system. Consequently, this chapter has mainly focused on the mechanisms taking place on the rectifier side of the converter.

When a two-terminal dc line model is implemented at Nyhamna, the inverter bus becomes decoupled from the remaining ac system. Consequently, the inverter bus must be defined as a swing bus in order to execute the simulations. Hence, this section gives a short introduction to the mechanisms taking place on the inverter side of the converter. The objective is primarily to give a description of how the behavior of the swing bus influences the results from the previous simulations.

Figure 27 shows the inverter side of one of the three converters implemented in PSS/E. XCI is the inverter commutating transformer reactance, TRI is the inverter transformer ratio and TAPI is the inverter tap setting. The machine connected to the swing bus illustrates the synchronous machine at Ormen Lange.

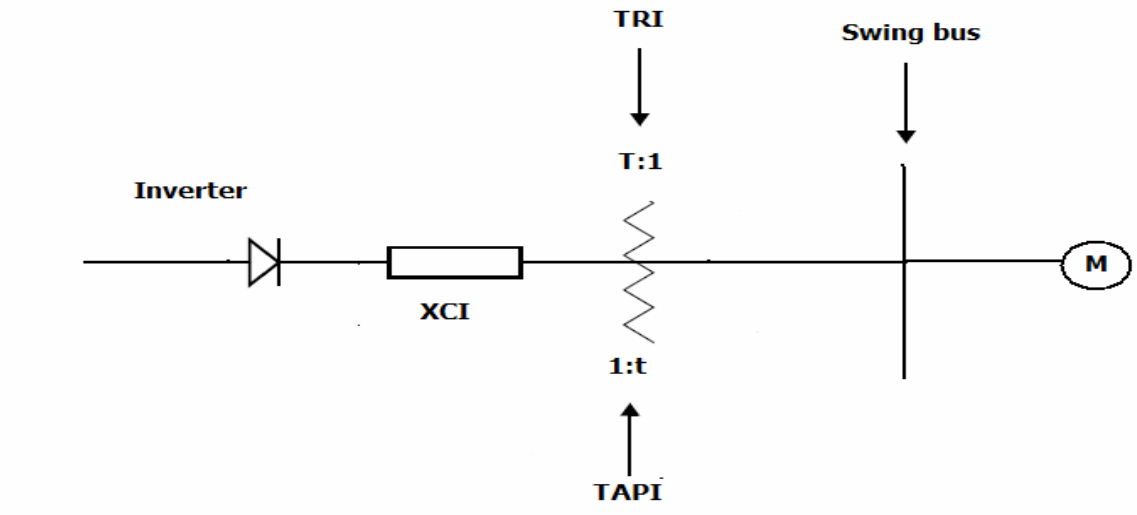

Figure 27 Inverter side of the converter at Ormen Lange.

From the previous analyses the effect of a voltage depression at the ac side of the rectifier were analyzed. The results showed that the rectifier transformer adjusts its tap setting to maintain the voltage on the valve side of the rectifier transformer close to its nominal value. From the results given in Appendix A, it is clear that this mechanism does not take place on the inverter side of the converter. This is due to the fact that during power flow solutions, the voltage magnitude and phase angle at each swing bus are held constant. The bus voltage at the swing bus, VS, is specified to be 6.7 kV and the phase angle, VA, is set to be 0°. The generator connected to the swing bus will adjust its power output to maintain the specified voltage and phase angle. Hence, a voltage depression at the valve side of the inverter transformer will never take place and there will be no tap adjustments on the inverter transformer [10].

When a disturbance introduced on the rectifier side causes the inverter margin angle (γ) to change, this leads to a new reactive consumption at the inverter. The generator handles the reactive change by adjusting its reactive output. The inverter is decoupled from the remaining system and all changes in the operation condition for the inverter is handled by the swing bus.

4.8 Converter versus PQ representation of Ormen Lange

This section gives a short principal evaluation of the consequence of representing Ormen Lange with a converter model instead of a PQ-model. The evaluation is focused on the reactive consumption of the latter models.

In power system simulation programs, one uses simplified models to represent complex facilities. Ormen Lange represents such a facility. In PSS/E there are several feasible ways of representing this facility. In previous studies, Statnett has used a PQ representation. This means that Ormen Lange is represented as a constant active and reactive load. When using a PQ representation, the active and reactive consumption is only dependent on the initial chosen set point (independent of system operational conditions). However, the latter is not applicable for a converter representation.

In order to numerically compare the response of two different models representing the same facility in a simulation program, the following criteria should be fulfilled:

I. The initial power flow in both models should be approximately the same.
II. Adequate input data and control parameters for the two-terminal dc line model should be used.

In the simulations performed in this chapter, neither of the above criteria's are fulfilled. The data for the converter model is uncertain, and it is therefore less meaningful to strive after an initial power flow which is identical to the PQ-model utilized by Statnett. Hence, the utilitarian value of performing a numerical comparison of the PQ-model and converter model is low, and will not be performed in this chapter.

4.8.1 Principal comparison

Even though numerical comparisons are less meaningful, principal comparisons can be made. As described above, the PQ-model will consume approximately the same amount of power independent of any faults introduced. It is thus of interest to analyze the principal response of the converter model when exposed to a system fault. In the previous sections, analyses on how a voltage depression at Nyhamna influences the rectifier were performed. In these steady-state simulations the change in rectifier reactive consumption, is of greatest interest to analyze. This is because the rectifier constitutes the junction to the remainder ac system, and its reactive consumption will directly influence the state of the ac system.

The results in Table 7 and Table 8 showed that a voltage depression at Nyhamna resulted in a reduction in the rectifier reactive power consumption. The latter can also be verified from Appendix A. The reduction in reactive consumption occurs because the power flow solution logic reduces the firing delay angle, α, to "counteract" the voltage depression.

Hence, in a situation with depressed voltage the latter operation of the converter solution logic causes the converter model to exhibit less stress to the ac system than the PQ-model. That is, the converter model reduces its reactive consumption in a situation where the ac system is already stressed.

Note, it is important to acknowledge that the power flow solution logic only adjust the converter taps until the corresponding bridge firing angles are between their specified maximum and minimum values. Hence, transformer taps are not adjusted to minimize reactive power consumption [13].

4.9 Summary

This section presents a brief abstract of the evaluations made in this chapter.

In *Section 4.3*, two disturbances were introduced. The objective of these disturbances was to analyze the performance of the converter model when the bus voltage at Nyhamna was depressed. For each of the latter disturbances, two sub-cases were defined. The first case represented a situation with adjustable rectifier tap setting and the second case represented a situation with locked tap setting. The purpose of locking the tap setting was to analyze a transient situation where the action of the tap changers was to slow to be considered.

The results from *Section 4.4* illustrated important characteristics of the implemented two-terminal dc line model. The rectifier tap setting was reduced when the voltage at Nyhamna was depressed. This reduced the rectifier firing angle, and the voltage on the valve side of the rectifier was maintained close to its nominal value. This means that the rectifier was still in control of the dc current, and all scheduled dc values were unaffected by the disturbance. However, with the rectifier tap setting locked, the transformer did not "boost" the voltage on the valve side of the rectifier transformer. The latter voltage reduction caused the rectifier firing angle to be reduced to its minimum, and the inverter assumed control of the dc current.

The dc current was reduced to a fraction equal to the current margin (defined as DELTI in Section 3.3.1) along with the remainder dc values.

Hence, the presence of an adequate rectifier transformer tap setting is essential for the two-terminal dc line model to maintain scheduled dc values during voltage depressions.

In *Section 4.6,* the influence of varying the rectifier commutation reactance was analyzed. The objective of these analyses was to investigate to what extent the commutation reactance influenced the rectifier reactive consumption. The results showed that a marginal increase in the commutation reactance caused a reduction in reactive consumption. The latter was a result of a corresponding reduction in rectifier firing delay angle (α). The reduction in α compensated the actual increase in reactive consumption. However, with a more substantial increase in the commutation reactance, the reduction in α did not compensate adequately, and the rectifier reactive consumption was greatly increased.

In *Section 4.7,* the mechanisms taking place on the inverter side were addressed. Since the inverter bus becomes decoupled from the remaining ac system, the inverter bus must be defined as a swing bus. This means that the generator connected to the swing bus will adjust its power output to maintain scheduled bus voltage and phase angle. Hence, a voltage depression on the inverter bus will never take place and there will be no tap adjustments on the inverter transformer. All change in operation condition for the inverter is handled by the swing bus, and will not influence the remaining ac system.

Section 4.8 discussed the principal difference between the PQ-model and the converter model. The main focus in this section was the reactive power consumption of the models. During a voltage depression at Nyhamna, the PQ-model will consume approximately constant reactive power. However, the latter is not true for the converter model. When the voltage on the valve side of the rectifier transformer is depressed, the converter solution logic reduces the rectifier firing angle. Consequently, the rectifier reactive consumption is reduced. Hence, the converter model exposes the ac system to less stress than the PQ-model during voltage depressions.

5 Dynamic modeling in PSS/E

This chapter gives a detailed description of the modeling and operation of the dynamic two-terminal dc line model, CDC4T. This chapter is a continuance of the corresponding power flow description given in Chapter 3, and constitutes the basis for the subsequent dynamic simulations.

The chapter consists of four sections. The three first sections give, respectively, a description of converter modeling, configuration and control. The last section briefly discusses the dynamic modeling and assumptions for the synchronous generator implemented on the inverter side.

This chapter uses the term converter model to refer to the dynamic two-terminal dc line model.

5.1 Converter modeling

It is important to acknowledge that the actual converter system at Ormen Lange is a complex and complicated configuration. Consequently, this impedes establishment of a realistic converter model in simulation programs like PSS/E. The latter is nor the objective of this section. The objective is merely to establish a dynamic converter representation of Ormen Lange, which differs from the traditional PQ representation. This section is mainly based on [14].

5.1.1 Parameter evaluation

This section presents the chosen values for the parameters constituting the dynamic two-terminal dc line model, CDC4T. It is important to emphasize that the values chosen in this section does not necessary represent realistic values. Many of the chosen values are inspired from an example given in [15].

Minimum alpha for dynamics (ALFDY)
Chosen value: ALFDY = 5

ALFDY is the dynamic firing delay angle entered in degrees. The dynamic angle limit constitutes the range on transient basis. The dynamic angle is often reduced compared to the steady state value (ALFMIN) because the firing angle limit of a dc transmission line generally has a wider range on a transient basis than in steady-state. See Figure 32 on page 65.

Minimum gamma for dynamics (GAMDY)
Chosen value: GAMDY = 15

GAMDY is the dynamic inverter margin angle entered in degrees. The dynamic angle limit constitutes the range on transient basis. The dynamic angle is often reduced compared to the steady state value (GAMMIN) because the firing angle limit of a dc transmission line generally has a wider range on a transient basis than in steady-state.

DC voltage transducer time constant (TVDC)
Chosen value: TVDC = 0.05

TVDC is the dc voltage transducer time constant entered in seconds. The chosen value is based on an example given in [15].

DC current transducer time constant (TIDC)
Chosen value: TIDC = 0.05

TIDC is the dc current transducer time constant entered in seconds. The value chosen is based on an example given in [15].

Note; by setting TVDC and TIDC to zero the measured dc voltage will be equal to the instantaneous dc voltage. This can be seen from Figure 33 on page 65.

Rectifier ac blocking voltage (VBLOCK)
Chosen value: VBLOCK = 0.6

VBLOCK is the rectifier ac blocking voltage entered in per unit. The rectifier and inverter will be shutdown, i.e. blocked, if the ac voltage at the rectifier falls below VBLOCK.

Rectifier ac unblocking voltage (VUNBL)
Chosen value: VUNBL = 0.65

VUNBL is the rectifier ac unblocking voltage entered in per unit. The value entered for VUNBL determines at which ac voltage the rectifier will restart.

Minimum blocking time (TBLOCK)
Chosen value: TBLOCK = 0.1

TBLOCK is the minimum blocking time entered in seconds. The value entered for TBLOCK will therefore be the minimum time the rectifier remains blocked (if already blocked). The chosen value is based on an example given in [15].

Inverter dc bypassing voltage (VBYPAS)
Chosen value: VBYPAS = 0.6

VBYPAS is the inverter dc bypassing voltage entered in kV.

Inverter ac unbypassing voltage (VUNBY)
Chosen value: VUNBY = 0.55

VUNBY is the inverter ac unbypassing voltage entered in per unit. If bypassed, the inverter may reestablish dc voltage when the voltage at its ac bus rises to the per unit value, VUNBY.

Minimum bypassing time (TBYPAS)
Chosen value: TBYPAS = 0.1

TBYPAS is the minimum bypassing time entered in seconds. If bypassed, the inverter remains bypassed for a minimum of TBYPAS seconds. The chosen value is based on an example given in [15].

Minimum dc voltage following block (RSVOLT)
Chosen value: RSVOLT = 6

RSVOLT is the minimum dc voltage entered in kV. Restarting from a blocking, the dc voltage is among other parameters specified by the parameter RSVOLT. See Figure 37 on page 68.

Minimum dc current following block (RSCUR)
Chosen value: RSCUR = 500

RSCUR is the minimum dc current following a block entered in amps. Restarting from a blocking, the dc current is among other parameters specified by the parameter RSCUR. See Figure 37 on page 68.

Voltage recovery rate (VRAMP)
Chosen value VRAMP = 5

VRAMP is the voltage recovery rate entered in pu/sec. See Figure 37 in Section 5.3 for more explanation. The chosen value is based on an example given in [15].

Current recovery rate (CRAMP)
Chosen value: CRAMP=5

CRAMP is the current recovery rate entered in pu/sec. See Figure 37 on page 68 for more explanation. The chosen value is based on an example given in [15].

Minimum current demand (C0)
Chosen value: C0 = 400

C0 is the minimum current demand entered in amps. See Figure 39 on page 69. However, the minimum current demand can be overridden during restart of the converter.

Voltage limit point 1 (V1)
Chosen value: V1 = 8

V1 is voltage limit point 1 entered in kV. V1 defines one of the points which constitute the voltage-dependent current limit (VDCL) profile, see Figure 39 on page 69.

Current limit point 1 (C1)
Chosen value: C1 = 1000

C1 is current limit point 1 entered in amps. C1 defines one of the points which constitute the VDCL profile, see Figure 39 on page 69

Voltage limit point 2 (V2)
Chosen value: V2 = 15.3

V2 is voltage limit point 2 entered in kV. V2 defines one of the points which constitute the VDCL profile, see Figure 39 on page 69.

Current limit point 2 (C2)
Chosen value: C2 = 3000

C2 is current limit point 2 entered in amps. C2 defines one of the points which constitute the VDCL profile, see Figure 39 on page 69.

Voltage limit point 3 (V3)
Chosen value: V3 = 15.3

V3 is voltage limit point 3 entered in kV. V3 defines one of the points which constitute the VDCL profile, see Figure 39 on page 69.

Current limit point 3 (C3)
Chosen value: C3 = 3000

C3 is current limit point 3 entered in amps. C3 defines one of the points which constitute the VDCL profile, see Figure 39 on page 69.

Minimum time stays in switched mode (TCMODE)
Chosen value: TCMODE = 0.1

TCMODE is the minimum time stay in switched mode entered in seconds. The chosen value is based on an example given in [15].

5.2 Converter configuration

This section describes the configuration and operation of the converter model used in PSS/E. This section is mainly based on [13, 15].

5.2.1 General considerations

The performance of the converter is dominated by its control. However, the bandwidth of the control is far greater than the bandwidth of the PSS/E simulation. Therefore it is not practical

to represent the detailed dynamic of these controls. Hence, this section gives a general introduction of the control of the converter model.

Figure 28 illustrates the arrangement of dc transmission control of a converter bridge. Each bridge is controlled by a local feedback loop of bandwidth consistent with the firing delay accuracy requirements of the rectification/inversion process. The local loops works independently to maintain bridge current or voltage at desired values. An outer control loop provides the desired values and acts in a supervisory role and coordinates the action of the several converter bridges and the ac power system.

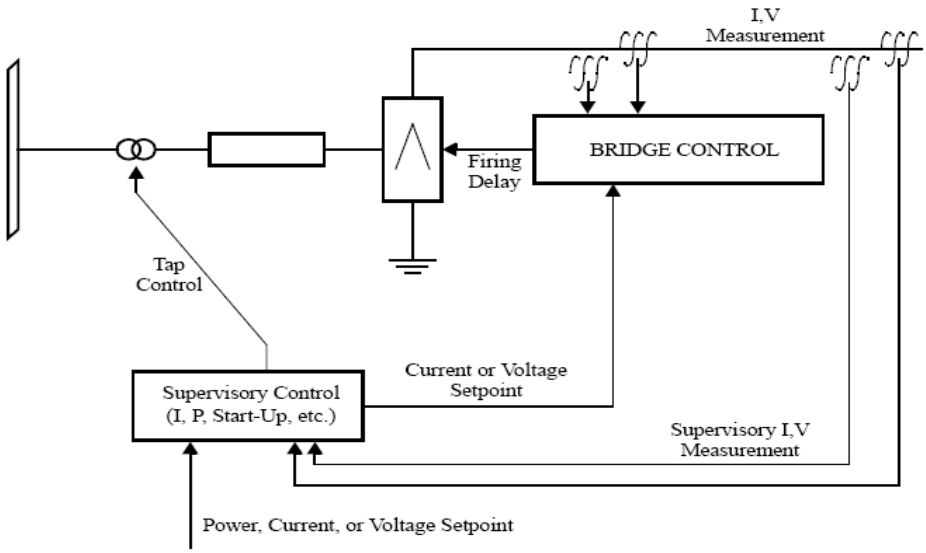

Figure 28 Illustration of dc transmission control [15].

To understand the behavior of the converter model, the behavior of the bridges and their inner control loops must be investigated. A rectifier bridge may be regarded as an adjustable voltage source forcing current though the transmission system resistance and inductance, against the constant back-emv of the inverter. An illustration of this is shown in Figure 29.

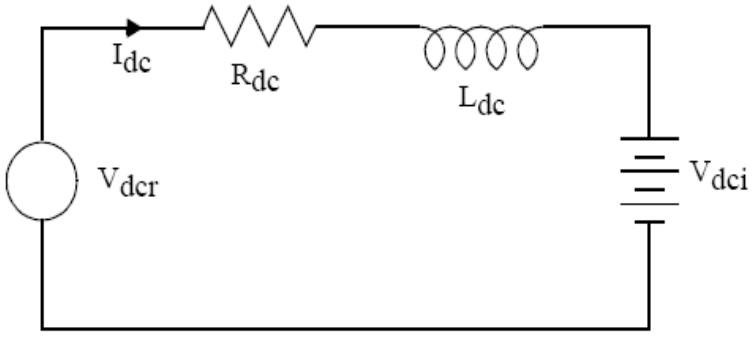

Figure 29 Illustration of a rectifier bridge [15].

By applying current setpoint changes to rectifier voltage on an open-loop basis, a simple current control could be set up with a gain equal to the dc resistance as shown in Figure 30.

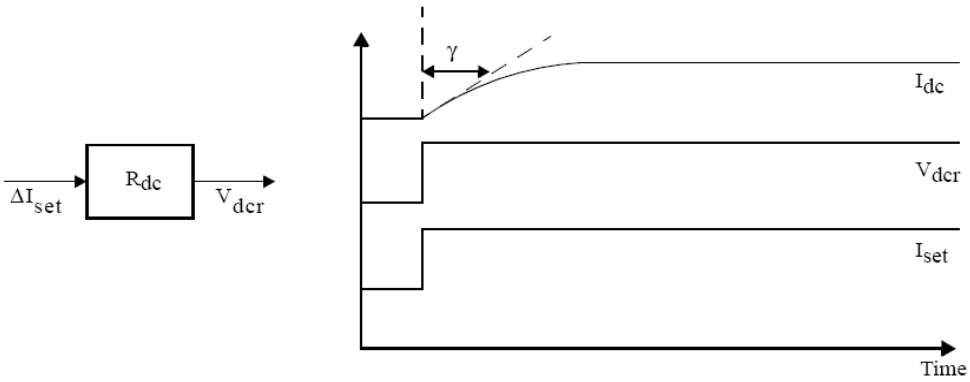

Figure 30 Open-loop rectifier current control [15].

The step change of current setpoint produces a time response as shown in Figure 30. The figure shows that the voltage changes in a step and the current follows with a delay time constant determined by inductance and resistance. The time response would be small compared to those of principal importance elsewhere in PSS/E, however, not negligible.

It is important to acknowledge that a real dc transmission rectifier is not operated by adjusting its output voltage in the open-loop manner as described above. In a real dc transmission rectifier, the local bridge is a feedback loop that adjusts firing angle delay to control the dc current to a set point. This is illustrated in Figure 31.

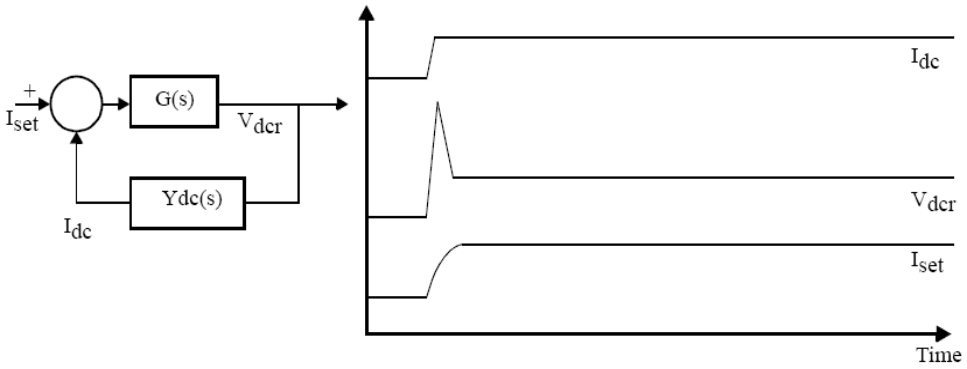

Figure 31 Rectifier current control in a real dc transmission rectifier [15].

The controller transfer function depends on details of the converter bridge design and is usually complex and nonlinear. The bandwidth is broad in relation to the 0 to 30 rad/sec bandwidth over which PSS/E simulations is applicable. Figure 31 shows a typical response of a bridge control loop to a step change of current setpoint. The feedback controller forces the dc current rapidly to its new value by transient overadjustment of the rectifier voltage. This rapid response is generally shorter than the shortest time interval that can be recognized within the bandwidth of PSS/E.

Since the local converter bridge control and its response are so rapid in relation to the time scale of most PSS/E simulations, several PSS/E models, e.g. CDC4T, CDC6, CEELRI and CMDWAS treat dc converter pairs as if they move instantaneously to their new operating point when any of their input signals or ac feed voltages are changed.

These *pseudo steady-state*, HVDC dynamic models calculate the active and reactive power loading of the HVDC converter using steady-state converter relationships similar to those described in Section 3.3. However, it is one important difference; in the dynamic models the transformer taps remain fixed. This means, as distinct from the power flow solutions, that the converter transformer tap position does not attempt to hold the bridge firing angle within its maximum and minimum values in dynamic simulations.

In the same manner as the ac network model is not concerned with the internal transient behavior of transformers and three-phase transmission lines, the PSS/E dc models are not concerned with the internal dynamic behavior of dc converters and lines.

The mode of operation where the rectifier firing angle is not at a limit and the inverter margin angle is also not at a limit or controlling voltage, is not possible to directly represent with the pseudo steady-state HVDC dynamic models. This is because this condition does not occur in steady-state. This dynamic condition may occur during startup and/or a cycle or two following a disturbance. If the recovery is slow (e.g. if the ac system is weak), then some pseudo steady-state models may depress direct current and dc voltage during a disturbance, and ramp up voltage and current at user specified rate following the disturbance.

Note; the model CDCVUP can represent the temporary dynamic condition when neither of the converters are at a firing angle or a margin angle limit, and both are fighting for control of current. However, this is not the case for the model used in this thesis.

Blocking and bypassing

If the inverter is bypassed, the dc side is shorted and the ac side is open. In this situation the rectifier will continue to circulate a low level of direct current through the shorted inverter at a low voltage. Hence, the rectifier will draw some vars but very little power from the ac system. The inverter will draw no power of vars.

Blocking, or turning off a converter can be simulated by changing the appropriate ICON or by raising the blocking parameter to force a block.

5.3 Converter control

This section describes the dynamic control system and operation of the converter model in PSS/E. This section in mainly based on [15].

In PSS/E the dc transmission models are concerned with the transient behavior of the outer, or supervisory, levels of the dc control. This is due to the fact that the handling of the dc power flow by its control has a strong influence on the ac system.

In PSS/E there are three distinct types of actions by the control:

I. Normal regulation of dc converter operation to maintain constant power or constant current with coordination of rectifier and inverter current setpoints.

II. Temporary overriding of dc converter normal operation setpoints as a result of ac system voltage disturbances.
III. Modulations of the dc power setpoint by supplementary control devices. The objective of this is e.g. to assist in the damping of rotor angle swings in the ac system.

The main focus in this thesis is the action by the control system during normal regulation and temporary disturbances. Hence, a detailed description is given on (I) and (II). It is important to acknowledge that the basic control system described in Section 3.3.3 underlies all dc transmission operation. Hence, modeling of the normal regulating of the dc converters includes the description given in the latter section. Various dc converter models represent different normal regime manipulations of the different setpoints given in Figure 22 and Figure 23 (see Section 3.3.3).

However, if the ac or dc voltages at the converters (rectifier/inverter) reach abnormal levels which may cause commutation difficulties, excessive currents, or unacceptable harmonics, the normal control action is overridden by special control actions. These overriding actions are activated when the positive sequence ac voltage or dc voltages at the converters reach specified levels.

It is important to recognize that the actions executed by the model used in this thesis, CDC4T, does not represent actions a real converter would take. However, it represents the user's decision to simulate the blocking, bypassing, unblocking or unbypassing of the converters when various disturbances encounters.

Also, the dynamic converter model has access to all the data and variables used in the load flow. If additional parameters and variables are needed, these are defined on individual model data sheets.

5.3.1 Characteristics of normal operation

From Section 5.1.1 it can be seen that a new parameter, ALFDY, is included in the dynamic data sheet. ALFDY is the dynamic firing angle. This parameter represents the fact that the firing angle limits of the dc model generally have a wider range on a transient basis compared to steady-state. This is illustrated in Figure 32.

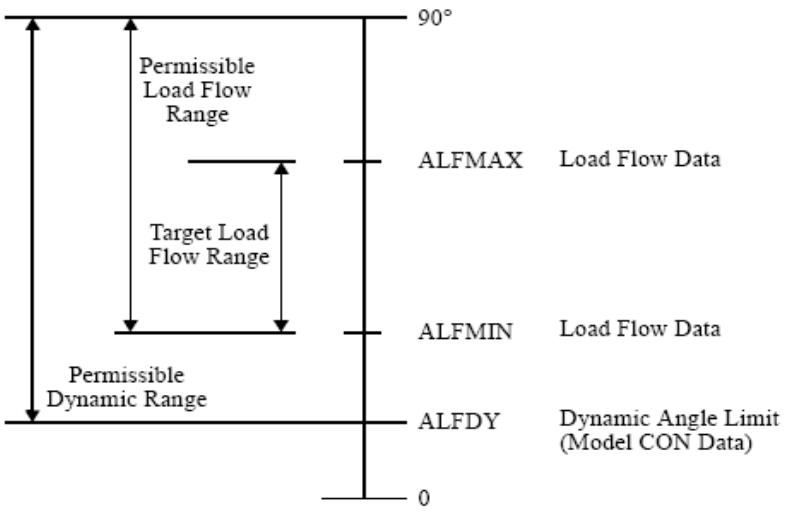

Figure 32 Alpha and gamma ranges in load flow and dynamic simulations [15].

CDC4T will adjust rectifier and inverter firing delay angles within the dynamic limits to operate the dc transmission in accordance with the characteristics given in Figure 22 and Figure 23 (see Section 3.3.3). As explained in the previous section, the scheduled dc voltage and dc current are specified in the load flow case (i.e. parameters VSHED, SETVAL and MDC in Section 3.3.1).

Figure 33 shows the dc transmission control arrangement for the model used in this thesis. From the figure it can be seen that the instantaneous current setpoint, I_{set}, is adjusted continuously if the line is in constant power mode, i.e. MDC=1 (see Section 3.3.1). The inverter current setpoint will follow the rectifier current setpoint to always provide the current margin, DELTI. DELTI is explained and defined in Section 3.3.1.

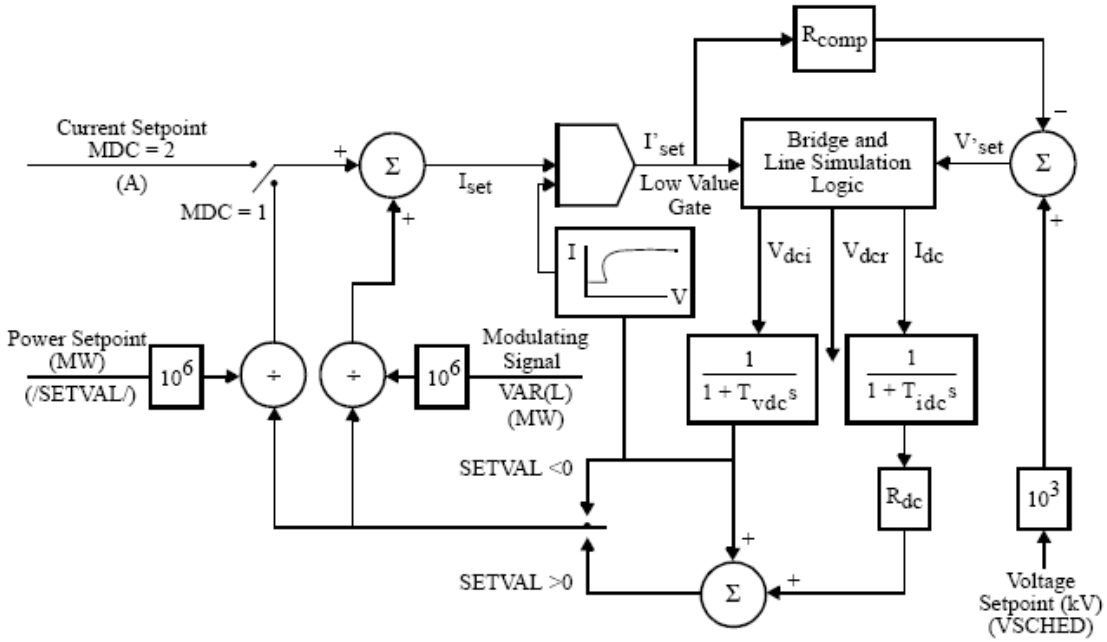

Figure 33 dc transmission control arrangements [15].

Note; when changing the dc operation setpoints VSCHED, SETVAL and MDC this has to be handled by the load flow working case.

If the rectifier firing delay angle reaches its dynamic lower limit during the simulations, the dc current will fall below the instantaneous rectifier current setpoint but not below the inverter current setpoint.

As mentioned earlier, the transformer taps will not be adjusted automatically during dynamic simulations. Transformer taps must be changed manually via the load flow case.

5.3.2 Characteristics of operation during transients

The converters must have actions that protect the converters from commutation failure during ac system disturbances. If an ac disturbance causes a commutation failure in the inverter it results in one pair of diodes conducting permanently in the inverter bridge. The latter situation is illustrated in Figure 34. The figure illustrates a situation where the commutation from valve 4 to valve 6 fails.

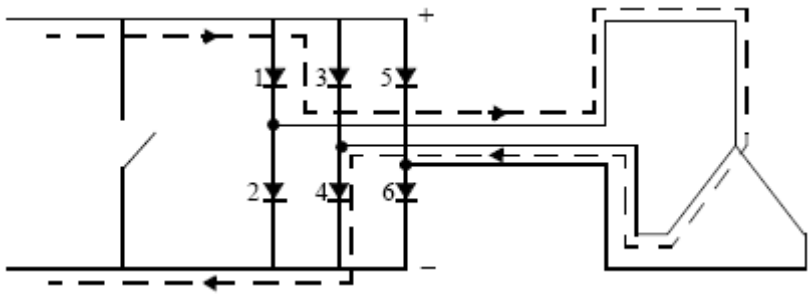

Figure 34 Commutation failure at inverter due to ac system disturbance [15].

The action made to extinguish the two conduction diodes is to bypass the inverter bridge as illustrated in Figure 35. The figure shows that the bypass switch is closed to allow valves 1 and 4 to be extinguished.

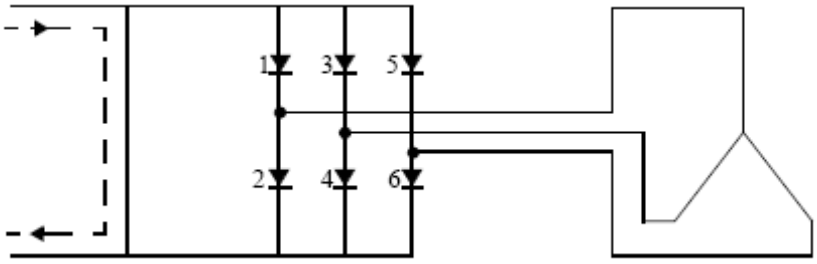

Figure 35 Bypassing of the inverter due to commutation failure [15].

For the inverter to regain its normal operation condition the bypass switch is opened, see Figure 36. Thus, the inverter operation is reestablished by starting valve 3 and 6 in proper sequence after a suitable delay.

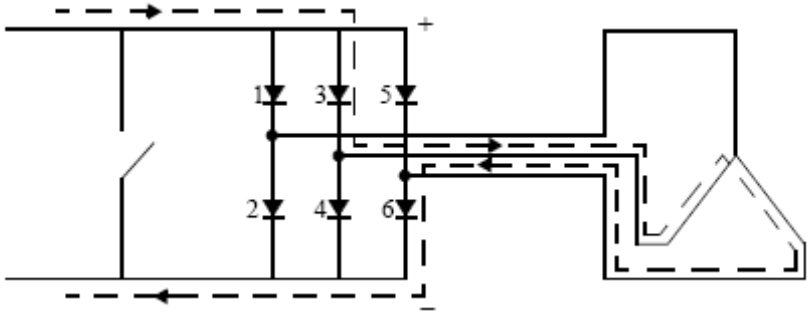

Figure 36 Unbypassing of the inverter [15].

The situation explained above constitute one of the two actions the converter model can take during an ac system disturbance. CDC4T has two actions that the converter can take during such ac system disturbances:

I. The rectifier and inverter are both shut down, i.e. blocked, if the ac voltage at the rectifier falls below the per unit value, VBLOCK.
II. The inverter bypass switch is closed if the inverter end dc voltage falls below VBYPAS. The rectifier will continue to maintain dc current at scheduled value.

When analyzing the control operation of the converter model in PSS/E it is essential to understand both what causes blocking and bypassing of respectively rectifier and inverter, and how the voltages and currents are reestablished following blocking and bypassing.

Note; low dc voltage does not cause blocking of the rectifier unless the rectifier ac voltage is low. Also, low ac voltage at the inverter does not cause bypassing unless the inverter dc voltage is low.

5.3.2.1 Reestablishment after blocking and bypassing

Figure 37 and Figure 38 are included to facilitate the understanding of how the voltage and current are reestablished following a blocking or bypassing. The parameters shown in Figure 37 and Figure 38 can be found in Section 3.3.1 and Section 5.1.1.

If the rectifier is blocked, it remains blocked for a minimum of TBLOCK seconds. If the per unit voltage at the ac bus rises to a value of VUNBL, the rectifier may restart. Figure 37 illustrates how the dc voltage and current instantaneous setpoints are reestablished following a blocking of the rectifier.

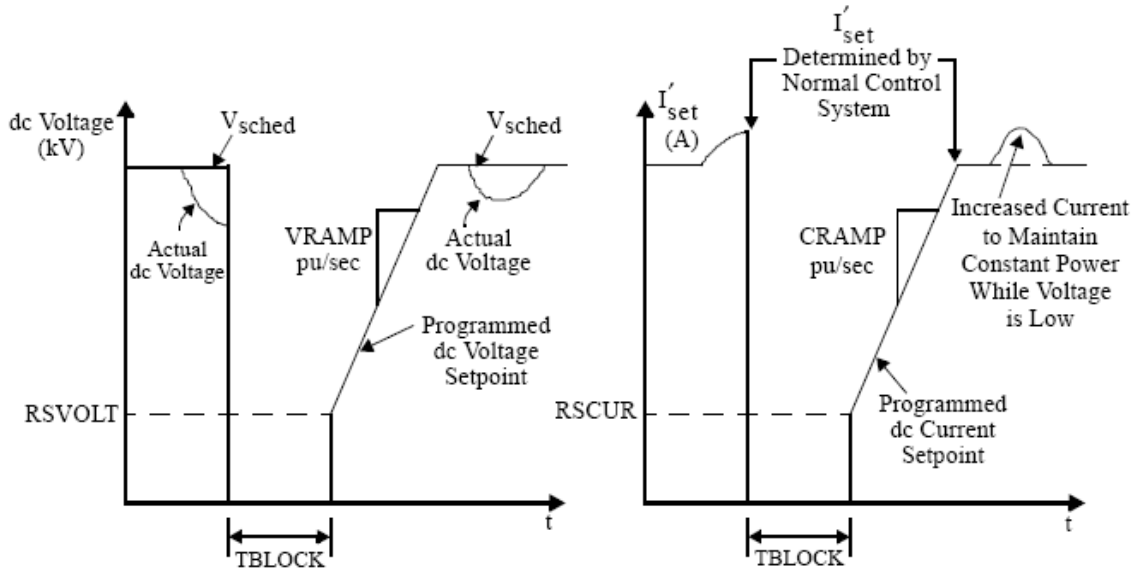

Figure 37 Voltage and current reestablishment following blocking [15].

Figure 38 illustrates how the voltage and current instantaneous setpoints are reestablished following a bypassing of the inverter. If the inverter is bypassed it remains bypassed for a minimum of TBYPAS seconds. If the voltage at the ac bus rises to the per unit value VUNBY, it may reestablish the dc voltage.

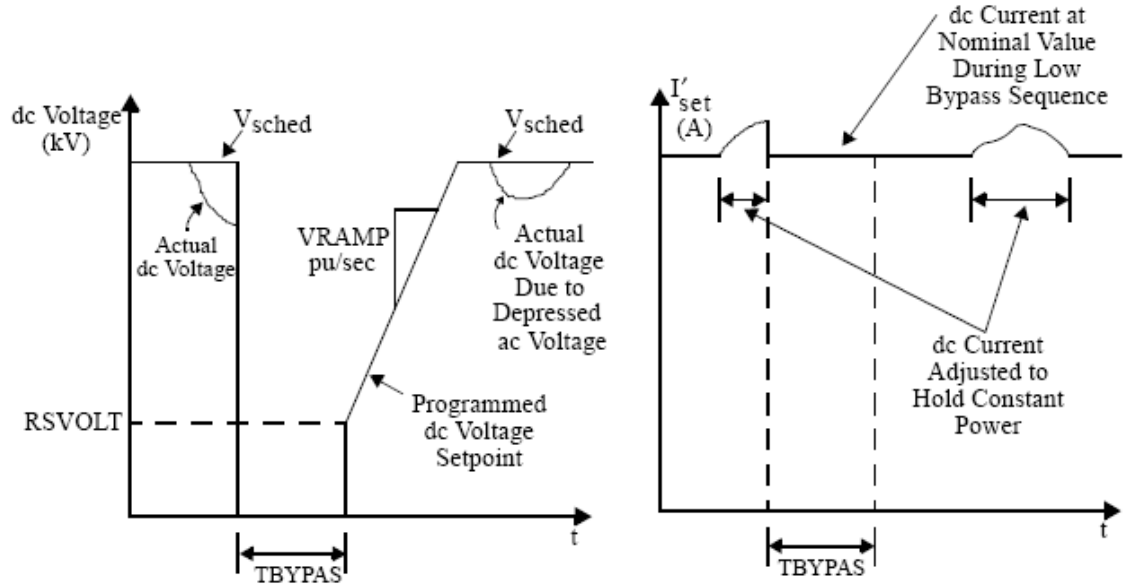

Figure 38 Voltage and current reestablishment following bypassing [15].

Figure 37 and Figure 38 illustrate that the voltage and current reestablishment are specified by the parameters RSVOLT, RSCUR, VRAMP and CRAMP. These values are specified by the user in the dynamic data sheet described in Section 5.1.1.

However, the current setpoints at both the rectifier and inverter are overridden at all times by a voltage-dependant current limit (VDCL). The VDCL for CDC4T is shown in Figure 39. The VDCL curve is defined by the three limit points (V_1, C_1), (V_2, C_2) and (V_3, C_3). These three limit points are specified by the user in the dynamic data sheet for CDC4T.

If the VDCL comes into play during dc voltage or current reestablishment, it will force the dc current to a value below the minimum current demand, C_0.

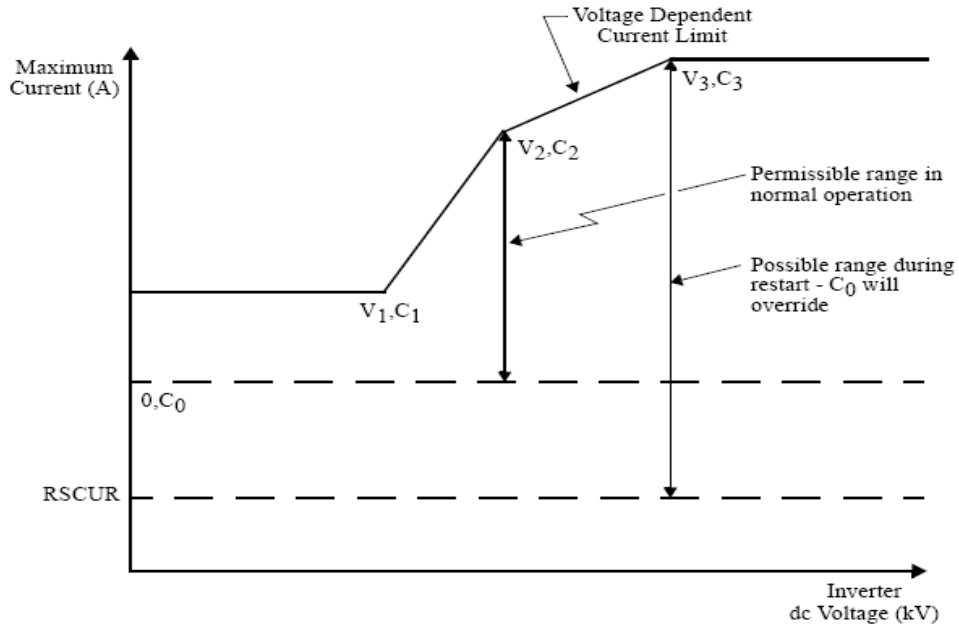

Figure 39 Voltage-dependant current limit for CDC4T [15].

5.3.3 Special considerations

It is important to recognize the distinction between the static and dynamic minima of the firing angle limits. CDC4T does not recognize the load flow firing angle limits ALFMIN and GAMMIN defined in Section 3.3.1. This has no consequence as long as the load flow solution is normal, i.e. neither alpha nor gamma is on its load flow limits, or when the dynamic limits ALFDY and/or GAMDY are the same as the respective load flow limits ALFMIN and/or GAMMIN.

However, the distinction between static and dynamic minima becomes a difficulty if the initial condition load flow has alpha or gamma at its static minimum. In this situation ALFDY and GAMDY will be different from the converted load flow solution which is the intended initial condition. The difference may result in a non-steady initial condition.

One approach the user can implement to avoid this difficulty is to change ALFMIN and GAMMIN to the dynamic limit values when a disturbance is applied. This is done by setting ALFDY equal to ALFMIN and GAMDY equal to GAMMIN in all initial setups and initial condition snapshots. When the disturbance is applied manually, change these values to the actual dynamic values.

Note; in the initial power flow condition used in this thesis the alpha and gamma is not at their static minimum. Consequently, the dynamic limits constitute no problem.

5.4 Generator modeling

The converters at Ormen Lange are operated to deliver active power to three synchronous motors. These motors are implemented as synchronous generators in PSS/E. The generators are connected to the inverter side of the converter, and are thus decoupled from the remaining ac system. Since the main focus in the following simulations are the rectifier and the ac system, this section only presents a brief description of the dynamic model used to represent the synchronous motors. This section is manly based on [14, 15].

5.4.1 Model and parameters implemented in PSS/E

The generator model used in this thesis is a round rotor generator model, also referred to as GENROU. This synchronous generator is operated as a motor in the simulations.

The parameters chosen for the generator model at Ormen Lange are based on standard parameters used for generators with approximately the same size elsewhere in the system. The parameters are based on the generator connected to bus (37256). This generator is almost of the same size as the one implemented at Ormen Lange.

Table 9 shows the parameter values used for the generator model implemented in PSS/E. The three synchronous machines at Ormen Lange are identical, thus only parameter values for one of the three machines are presented.

Table 9 Parameters used for the generator model

Parameter	IBUS	Name	I	T'_{do}	T''_{do}	T'_{qo}	T''_{qo}	H
Chosen value	101	GENROU	1	3.00	0.05	1.50	0.05	2.8
Parameter	**X_d**	**X_q**	**X'_d**	**X'_q**	**X''_d**	**X_l**	**S(1.0)**	**S(1.2)**
Chosen value	2.3	2.2	0.39	0.49	0.25	0.18	0.1089	0.37795

For a detailed parameter description, see the generator data sheet in [14].

5.4.2 Basis for chosen model

The synchronous machines at Ormen Lange are operated at a high speed. Hence, a synchronous generator with round rotor is chosen to represent the motor at Ormen Lange. Compared to salient pole machines, round rotor machines have the ability to withstand high centrifugal forces, and are generally used for high speed synchronous machines.

PSS/E contains several standard generator models. Among these standard models there are three models which represent synchronous generators with round rotor. These generator models are GENROE, GENROU and GENDCO. Both GENROU and GENDCO assume the saturation curve to be quadratic, while GENROE assumes the saturation curve to be exponential. However, GENDCO includes dc offset effects and is intended for use only in shaft torsional studies.

In this thesis the model GENROU is chosen in preference to GENROE only because GENROU is used by Statnett to represent similar round rotor machines. Thus, no

considerations are made on the effect of using a model with a quadratic saturation curve compared to a model with an exponential saturation curve. However, the latter procedure is not adequate if detailed dynamic simulations on the performance of the synchronous machine are to be performed. Since the dynamic effect of greatest importance in the machine is the development of synchronizing and damping torques, it's important to acknowledge which factors influence both synchronizing and damping torque. Synchronizing and damping torque are determined by the relative values of the synchronous, transient, and subtransient reactances which again are influenced by the magnetic saturation. Hence, in these simulations it is important to acknowledge and investigate the influence of magnetic saturation.

6 Dynamic simulations

This chapter contains dynamic analysis of the control actions for the converter model. The objective of these analyses is to illustrate the performance of the converter model. These analyses are a continuance of the corresponding simulations performed in Chapter 4.

This chapter uses the term converter model to refer to the dynamic two-terminal dc line model.

6.1 Introduction

In this chapter the following points are investigated:

I. Analysis of the control actions for the dynamic converter model under normal regulation.
II. Analysis of the control actions for the dynamic converter model during temporary overriding of the normal converter operation.

In this thesis three dynamic two-terminal dc line models (CDC4T) are implemented at Nyhamna. All three models are identical. Hence, the results from the simulations will only be given for one of the three implemented models. Figure 40 illustrates the system configuration for which the results are presented.

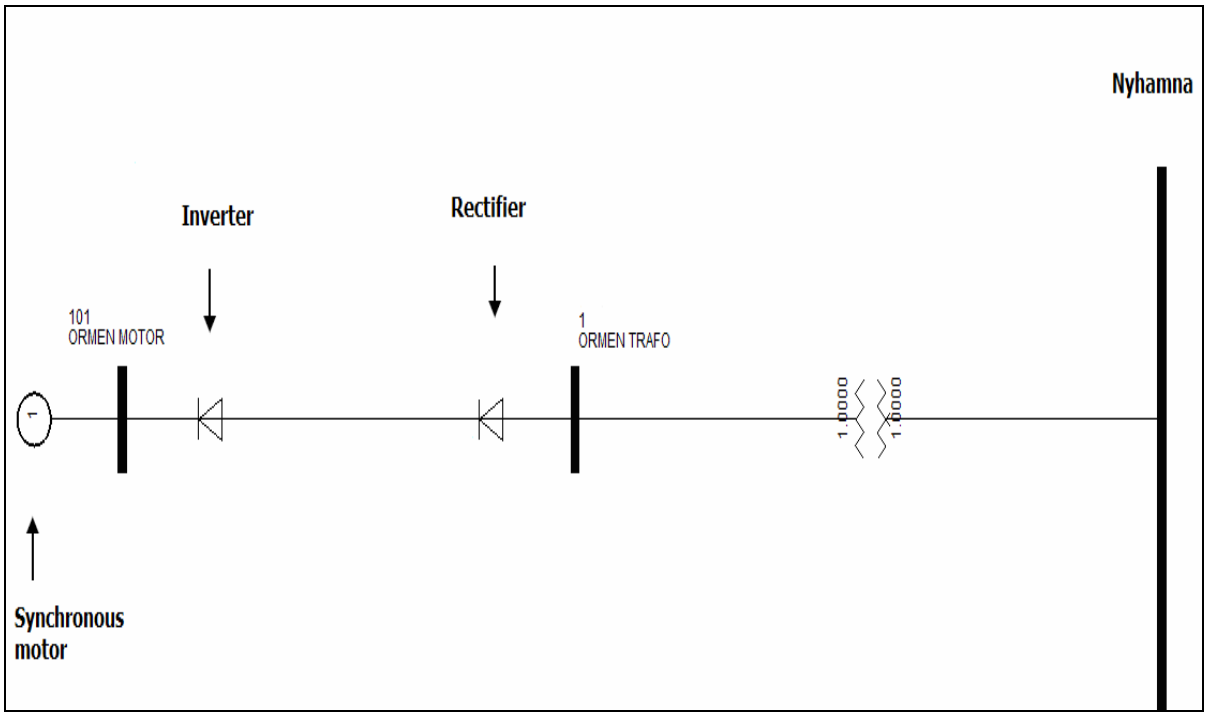

Figure 40 Illustration of one of the three converters connected to Nyhamna.

6.2 Initial conditions and assumptions

This section presents the initial conditions and assumptions made for the dynamic simulations presented in this chapter.

6.2.1 Power flow assumptions

The following power flow file is used in this chapter:

- Converter_model_cnv.sav

The following assumptions, which differ from the default setting provided in PSS/E, were made when establishing the power flow file:

- Switched shunt adjustments locked.
- Constant MVA loads converted with the following real power distribution:
    - 40 % constant current
    - 40 % constant admittance
    - 20 % constant power
- Constant MVA loads converted with the following reactive power distribution:
    - 0 % constant current
    - 100 % constant admittance
    - 0 % constant power

The power flow file can be found in Appendix D.

6.2.2 Dynamic assumptions

The following dynamic file is used in this chapter:

- NN.dyr

The dynamic file can be found in Appendix D.

Before running the dynamic simulations, the dynamic initialization activity, STRT, is invoked. This activity calculates the initial value of all variables as a function of the model's constant data and boundary condition at the bus in the working case at which it is referenced. Ideally, the following message should be printed after the activity is executed: "INITIAL CONDITIONS CHECK O.K.". This message indicates that no nonzero STATEs are found. The latter massage is not printed when executing the STRT activity in this chapter, however, the following message appears: "SUSPECT INITAIAL CONDITIONS". This message usually indicates some error in setup. Due to time limitations and the focus in this thesis, removing these suspect initial conditions has not been a priority [11].

However, it is important to acknowledge which situations may cause these suspect initial conditions. Hence, following are three situations which may cause such conditions [11]:

I. Model variables initialized out of limits.
II. STATE variables characterized by high gain and a short time constant.
III. Improperly specified data (e.g., zero time constants where they are not allowed, unrealistic limits etc.).

To minimize any possible influence from the suspect initial conditions, all simulations are run for a period of 2 seconds before any disturbances are applied. The objective is to insure that any non steady-state variables have reached a steady-state condition.

6.2.3 Initial values

The initial values for the dynamic simulations are given in Table 10. These data are obtained by running dynamic simulation with "Converter_model_cnv.sav" and "NN.dyr".

Table 10 Dynamic initial values.

DC converter data					AC system data					
V_{dcr} [kV]	α [deg]	V_{dci} [kV]	γ [deg]	I_{dc} [A]	$V_{ac,rec}$ [pu]	$P_{ac}(R)$ [pu]	$Q_{ac}(R)$ [pu]	$V_{ac,inv}$ [pu]	$P_{ac}(I)$ [pu]	$Q_{ac}(R)$ [pu]
17.2	11.4	16.9	16.2	2840.2	0.9767	0.0488	0.0106	1.0	-0.048	0.0145

The variables $P_{ac}(R)$, $Q_{ac}(R)$, $P_{ac}(I)$ and $Q_{ac}(I)$ are given in per unit of system base, i.e. 1000 MVA.

Table 11 contains a description of the variables used in Table 10. Some of the names used in Table 11 are also illustrated in Figure 40.

Table 11 Description of variables.

Variable	Description
V_{dcr}	Rectifier dc voltage
α	Rectifier firing delay angle
V_{dci}	Inverter dc voltage
γ	Inverter margin angle
I_{dc}	DC current
$V_{ac,rec}$	Bus voltage at ORMEN TRAFO
$P_{ac}(R)$	Rectifier ac real power
$Q_{ac}(R)$	Rectifier ac reactive power
$V_{ac,inv}$	Bus voltage at ORMEN MOTOR
$P_{ac}(I)$	Inverter ac real power
$Q_{ac}(R)$	Inverter ac reactive power

6.3 Application of the disturbance

This section presents the two cases which are analyzed in this chapter. Both cases represent a three phase line fault. However, the fault impedance varies for each case. The cases studied are given in the following table.

Table 12 Cases analyzed

Case	Case explanation
D	Branch fault on 130 kV line between Aura1(57013)-OSBU1(57403) with fault impedance R=30, X=30. The fault is applied for 400 ms.
E	Branch fault on 130 kV line between Aura1(57013)-OSBU1(57403) with fault impedance R=2, X=2. The fault is applied for 400 ms.

The purpose of Case D is to introduce a fault which depresses the voltage at Nyhamna to an extent that the control action of the converter remains in normal regulation. Hence, this case is a means for analyzing the converter operation under normal regulation. The objective of Case E is to introduce a fault which depresses the voltage at Nyhamna to an extent that temporary overrides the control action under normal regulation. Hence, this case is a means for analyzing the converter operation under abnormal regulation.

The fault impedance introduced does not necessarily represent a realistic impedance. However, the different impedances act as an effective means to depress the bus voltage at Nyhamna to a varying degree.

Note; the faults applied are three phase faults. The value of the fault admittance is calculated based on the settings of the “Unit” toggle switch, the impedance input field and “Base kV” input field in PSS/E. When the fault is executed the line shunt at the “from” bus end of the designated branch is replaced with the per unit admittance equivalent to the value entered for R and X [11].

The branch faults are applied for 400 ms after which the fault is removed. The duration of the fault is based on information from [16].

6.4 Results and discussion

This section presents the simulation results for Case D and Case E. The discussion is given consecutive as the results are presented to increase the readability.

The numerical values obtained from these simulations are of less importance and will not be commented in detail. This is because neither the converter model nor the initial condition used, do represent a realistic situation. Hence, this section will focus on the principal response obtained from the simulations.

It is important to emphasize that the following evaluations are only valid for the assumptions made in this chapter and parameter setting used in Chapter 5. Also, no verification with other simulation programs is performed to assure that the pseudo steady-state model, CDC4T,

exhibits realistic dynamic behavior. The dynamic behavior can only be evaluated from the expected behavior described in previous chapters.

Since this chapter analyzes the control actions for the dynamic converter model, the time period during fault and right after fault is of greatest interest.

6.4.1 Case D

This case introduces a remote three-phase line fault at time t = 2.0 between AURA1 and OSBU1 with a fault impedance equal to R=30 and X=30. This case will facilitate the understanding of actions performed by the converter control when normal regulation of the dc converter is performed to maintain specified setpoints. By introducing the latter fault impedance, the impact of the remote line fault is limited, and a desired voltage depression is obtained.

During fault, 2.0 < t < 2.4

The remote three-phase fault causes a voltage depression at the rectifier bus. Figure 41 shows the response of the ac variables at the rectifier side. This figure shows that the rectifier bus voltage is reduced from approximately 0.98 per unit to 0.94 per unit instantaneously when the fault is applied.

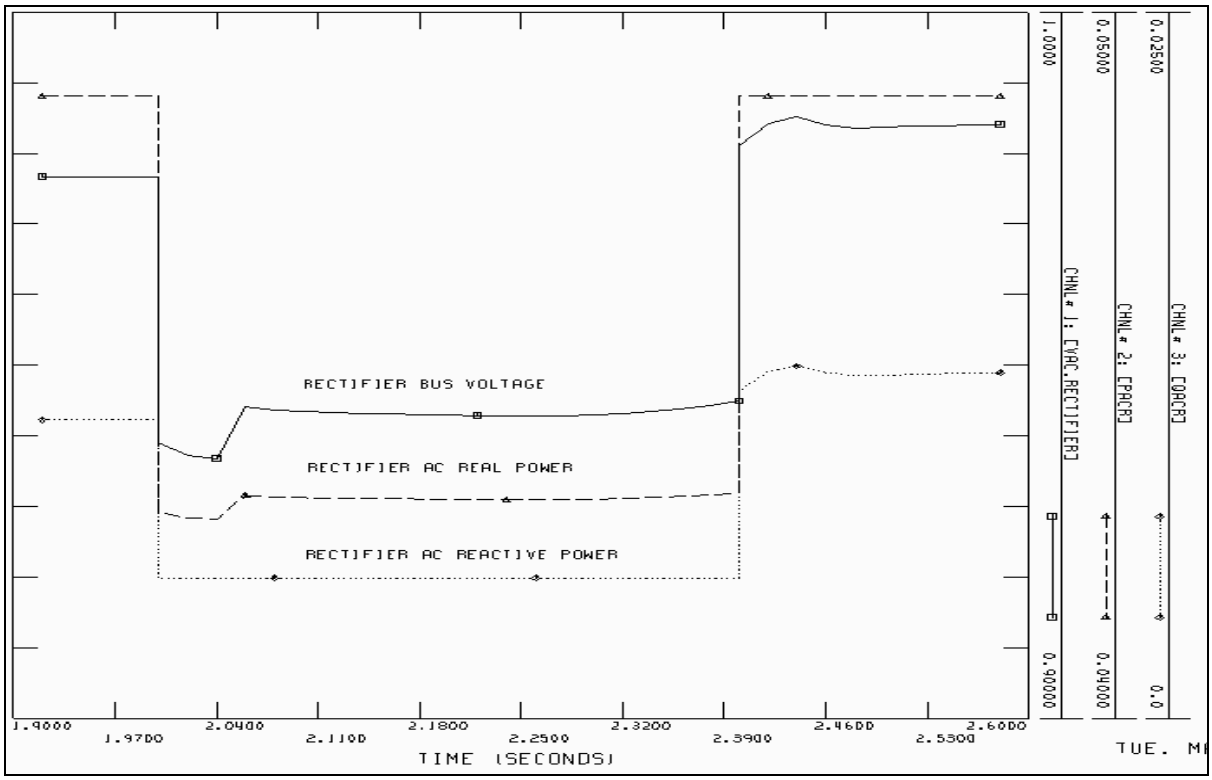

Figure 41 Rectifier bus voltage [pu], ac real power [pu] and ac reactive power [pu] during fault. The active and reactiv power are based on system base (1000 MVA).

In the pre fault situation, i.e. t < 2.0 seconds, the rectifier is controlling the dc current. When the fault is applied at t = 2.0 seconds, the rectifier loses control of the current order and the rectifier firing delay angle (alpha, α) is instantly reduced to its extreme minimum, alpha =

ALFDY = 5°. The latter is illustrated in Figure 42. ALFDY is a parameter specified by the user in the dynamic data sheet, see Section 5.1.1. The consequence of an instant reduction in alpha can be observed in Figure 41. The latter figure illustrates an analogues drop in the rectifier reactive consumption in the fault period. This reduction in reactive power consumption helps prevent further deterioration of the rectifier bus voltage.

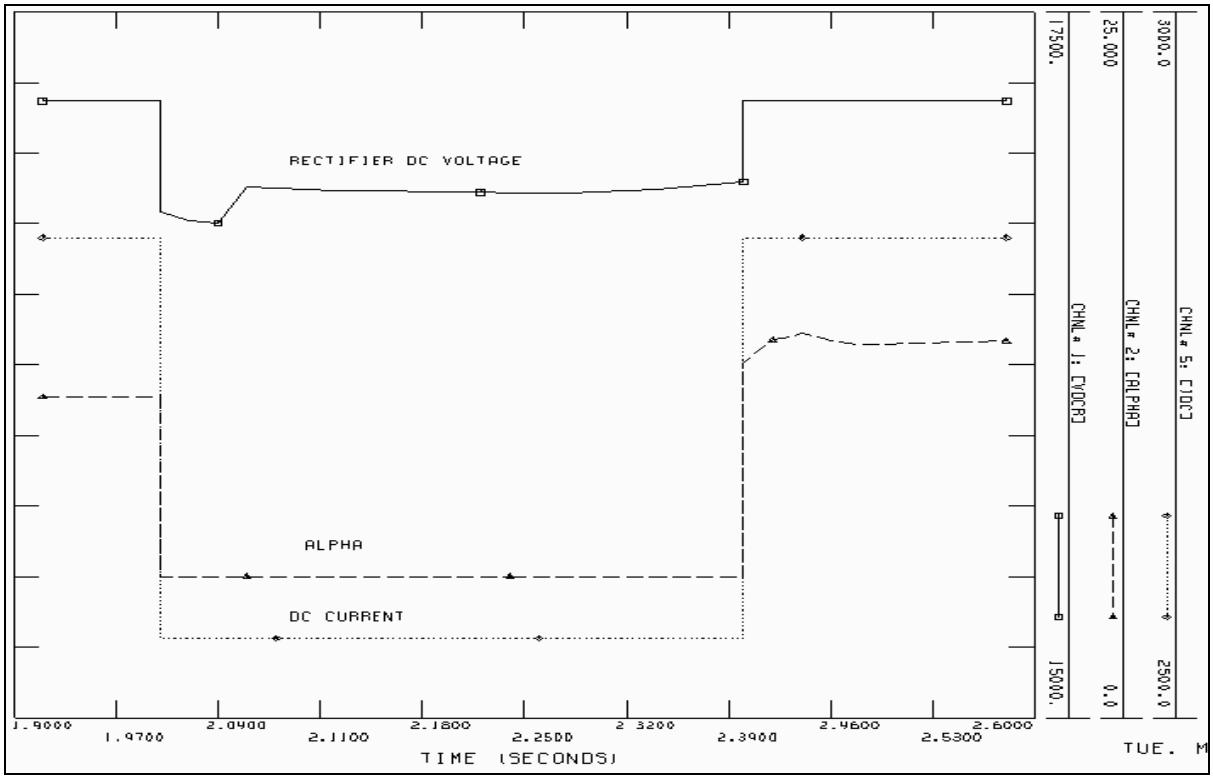

Figure 42 Rectifier dc voltage [V], rectifier firing delay angle [degrees] and dc current [A] during fault.

The inverter has abandoned the control of the dc voltage and is now regulating the inverter margin angle (gamma, γ) to control the dc current to a value which is the desired dc current reduced by the current margin, DELTI=0.1, see Section 3.3.1. Consequently, the reduction in dc current results in an analogous reduction in rectifier dc voltage shown in Figure 42. As a direct consequence of the reduced dc current and voltage, the active power transmitted through the rectifier is also reduced during fault. The latter is illustrated in Figure 41.

The inverter now continuously adjusts the inverter margin angle to maintain the specified dc current. This can be seen by comparing the rate of change for the gamma curve, see Figure 43, and the rectifier bus voltage curve, see Figure 41.

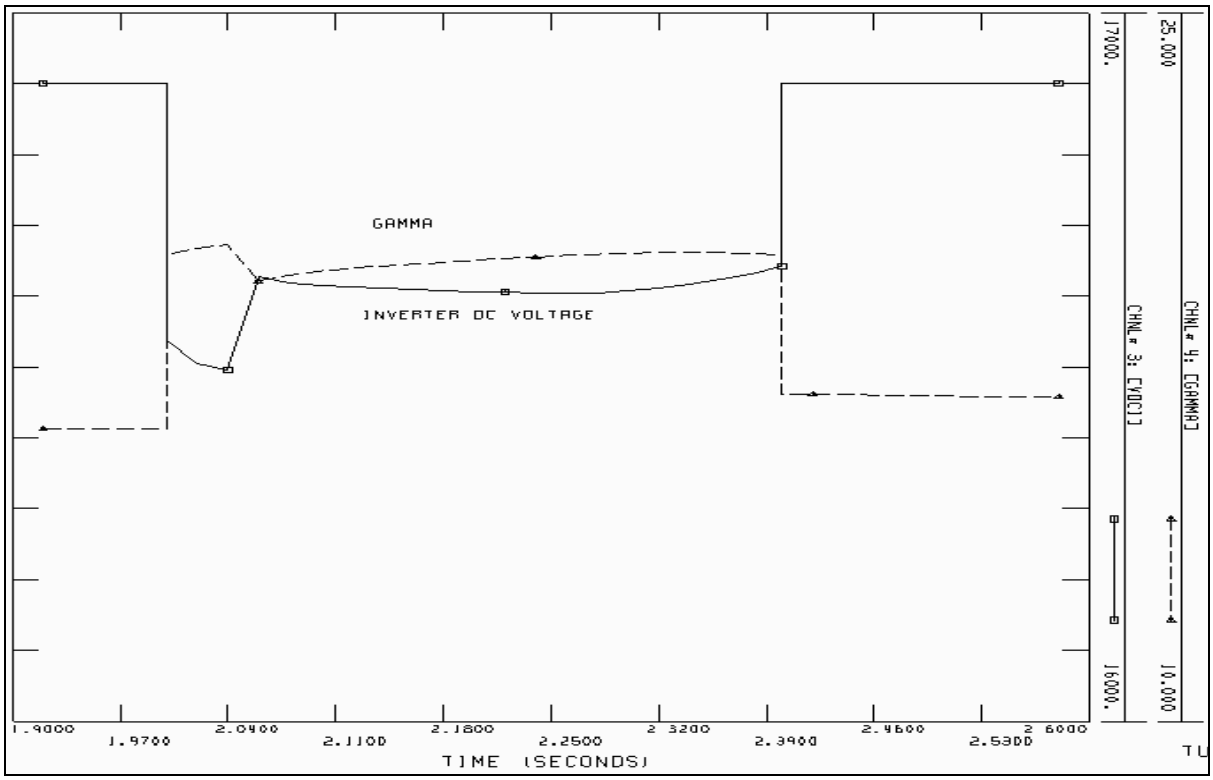

Figure 43 Inverter dc voltage [V] and gamma [degrees] during fault.

Figure 41 shows that the rectifier bus voltage curve consists of three time intervals within the period the fault is applied. The first time interval is between t = 2.0 and t = 2.04, the second is between t = 2.04 and t = 2.06 and the third interval is between t = 2.06 and t = 2.4. The same time intervals can be found in the gamma curve in Figure 43. Comparing these to curves within the same intervals it is clear that the rate of change is the same for both curves, however, the change is in opposite direction. As the rectifier bus voltage is reduced in the first time interval, gamma is increased. This result is evident since a reduction in the rectifier bus voltage causes a reduction in the rectifier dc voltage. Hence, to maintain the scheduled dc current, gamma is increased to reduce the inverter dc voltage. In the second time interval the rectifier bus voltage is increased, i.e. the rectifier dc voltage increases. This results in a reduction in gamma in order to maintain scheduled current. This situation continues till the fault is removed at t = 2.4 seconds.

Since the depressed rectifier bus voltage causes the inverter to abandon voltage control and assume current control, the increased inverter margin angle results in an increased reactive consumption at the inverter. An illustration of the latter is omitted in this section, but can be verified through simulations.

The fault is cleared, t > 2.4 second

As the fault is cleared, the rectifier regains control of the dc current. Both the rectifier dc voltage and dc current are instantly reestablished to their pre fault values, see Figure 44. Since the dc current and dc voltage is instantly reestablished to their pre-fault values, an identical response is expected from the rectifier real power. The latter can be verified by studying Figure 45.

Although the dc values and real power (see Figure 44 and Figure 45) are instantly reestablished, this is not true for the rectifier ac reactive power and alpha. Figure 44 and Figure 45 shows that alpha and the rectifier ac reactive power have the same development after the fault is cleared. This is expected since the rectifier ac real power is constant after the fault has been cleared.

The cause of the fluctuations in alpha and reactive power illustrated in Figure 44 and Figure 45, can be found by evaluating the rectifier bus voltage in the latter figure. Due to the small deviance between pre fault and post fault bus voltage, the rectifier adjust α accordingly to maintain scheduled dc current. Hence, rectifier bus voltage, reactive power and alpha exhibit similar responses after the fault is removed.

As long as there are voltage fluctuations on the rectifier bus, even small fluctuations, both alpha and reactive power will exhibit fluctuations. Due to these fluctuations in rectifier reactive power consumption, the ac system will perceive the rectifier as a varying reactive load.

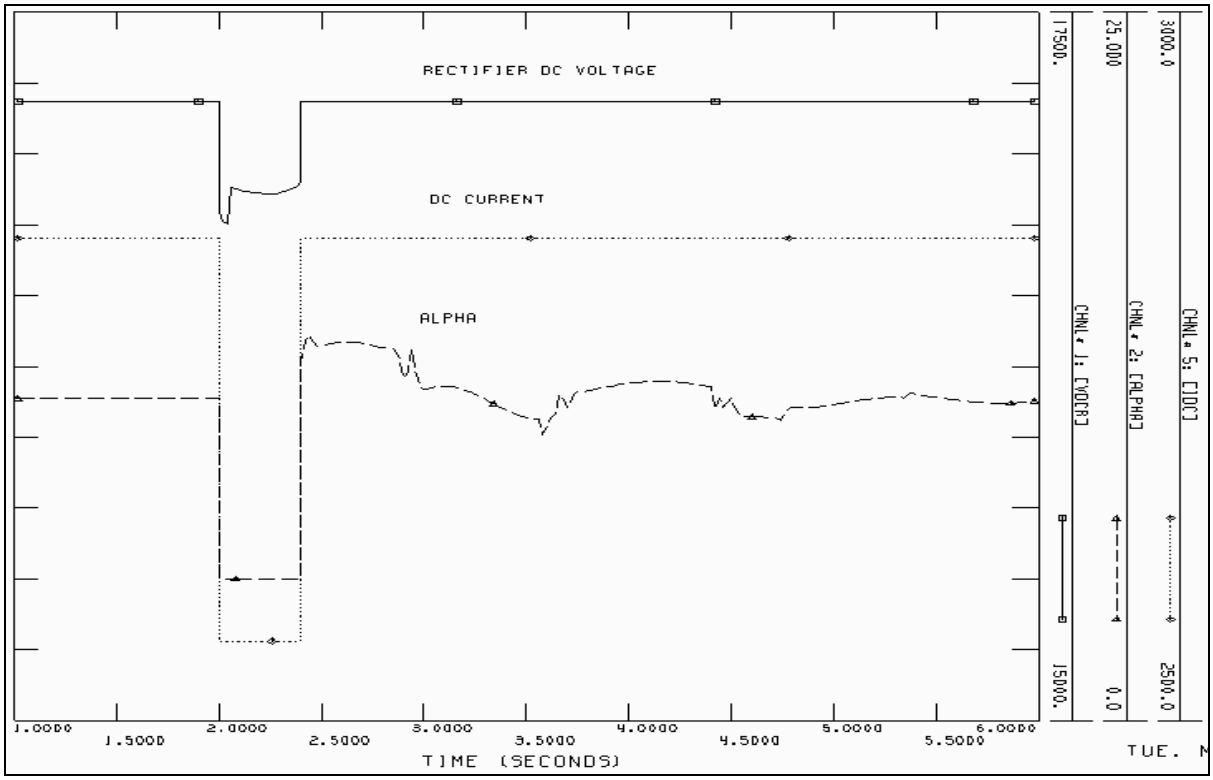

Figure 44 Rectifier dc voltage [V], dc current [A] and rectifier firing delay angle [degrees] after the fault is removed.

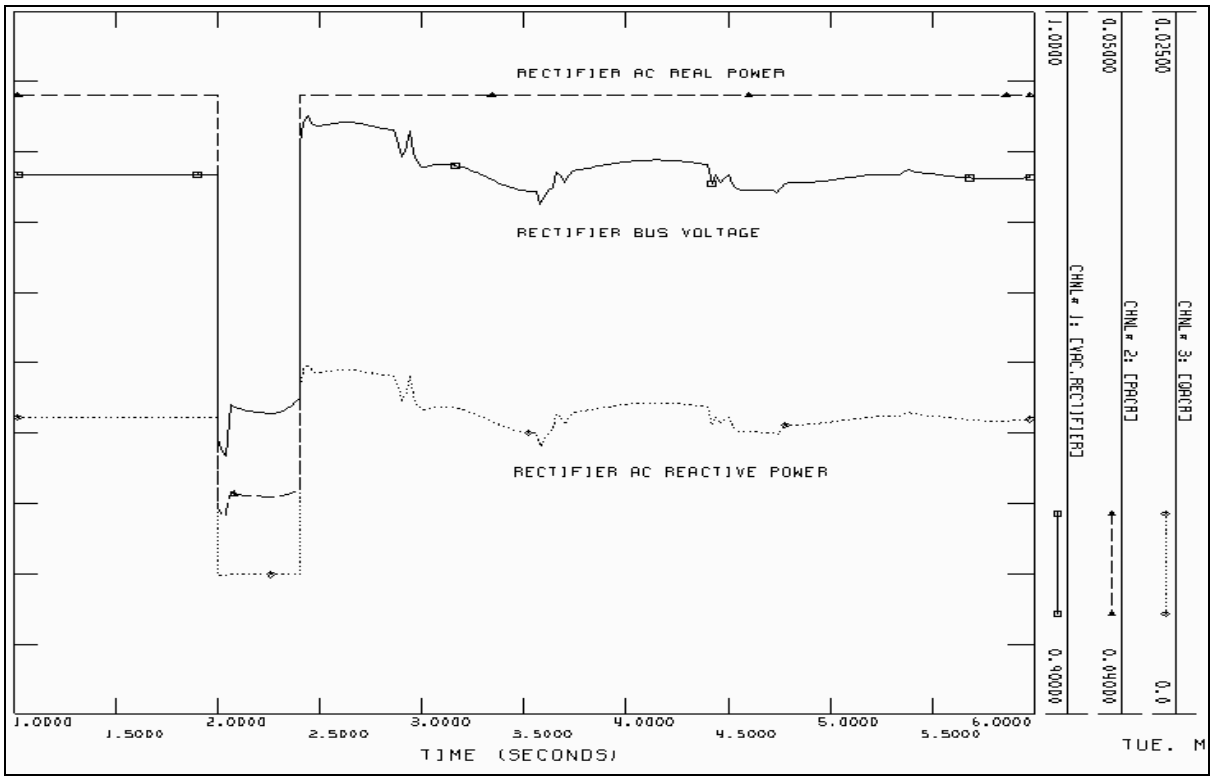

Figure 45 Rectifier bus voltage [pu], ac real power [pu] and ac reactive power [pu] after the fault is removed. The active and reactive power are based on system base (1000 MVA).

6.4.2 Case E

This case introduces a remote three-phase line fault at time t = 2.0 between AURA1 and OSBU1 with a fault impedance equal to R=2 and X=2. The purpose is to introduce a fault which depresses the bus voltage at Ormen Lange to an extent that results in a shutdown (also called blocking) of the converter bridges. This will facilitate the understanding of actions performed by the converter control when the normal operation setpoints are temporary overridden. Also, this case will illustrate the reestablishment of dc voltage and current following a converter blocking.

During fault, 2.0 < t < 2.4

The fault introduced results in a substantial voltage depression at the rectifier bus. As a consequence of this voltage depression, the real and reactive ac power at both rectifier and inverter falls instantaneously to zero at t = 2.0. Thus, no power is transferred over the dc link. This situation is illustrated for the rectifier in Figure 46. The corresponding response for the inverter is illustrated in Figure B1 in Appendix B. Hence, the remote line fault results in a converter blocking at t = 2.0 seconds.

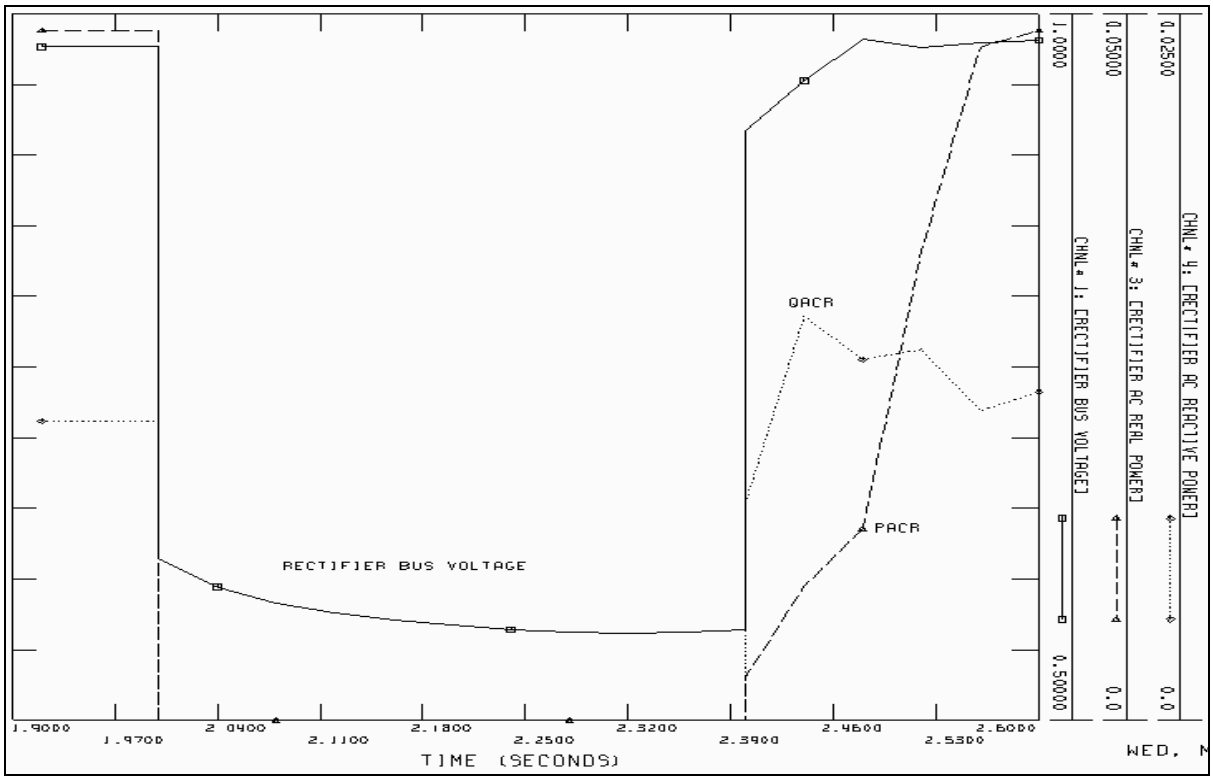

Figure 46 Rectifier bus voltage [pu], rectifier ac real power [pu] and rectifier ac reactive power [pu] during fault. The active and reactive power are based on system base (1000 MVA).

As the converter shutdown, the control system instantly increases alpha and gamma to 90°. The latter is illustrated in Figure 47. This value for alpha is greater than the nominal maximum rectifier firing angle (ALFMX) specified in the power flow data sheet (see Section 3.3.1) and is possible because ALFMX is no firm limit.

During the converter shutdown all dc variables are instantly reduced to zero, i.e. both rectifier and inverter dc voltage and dc current are reduced to zero, see Figure 47 and Figure 48. This is a consequence of alpha being increased to 90°. In a real converter, alpha = 90° causes the negative cycle of the output voltage on the dc side of the rectifier to be equal to the positive cycle. Consequently, the mean value of the output voltage on the dc side becomes zero, and no energy is transferred from one side of the converter to the other [6].

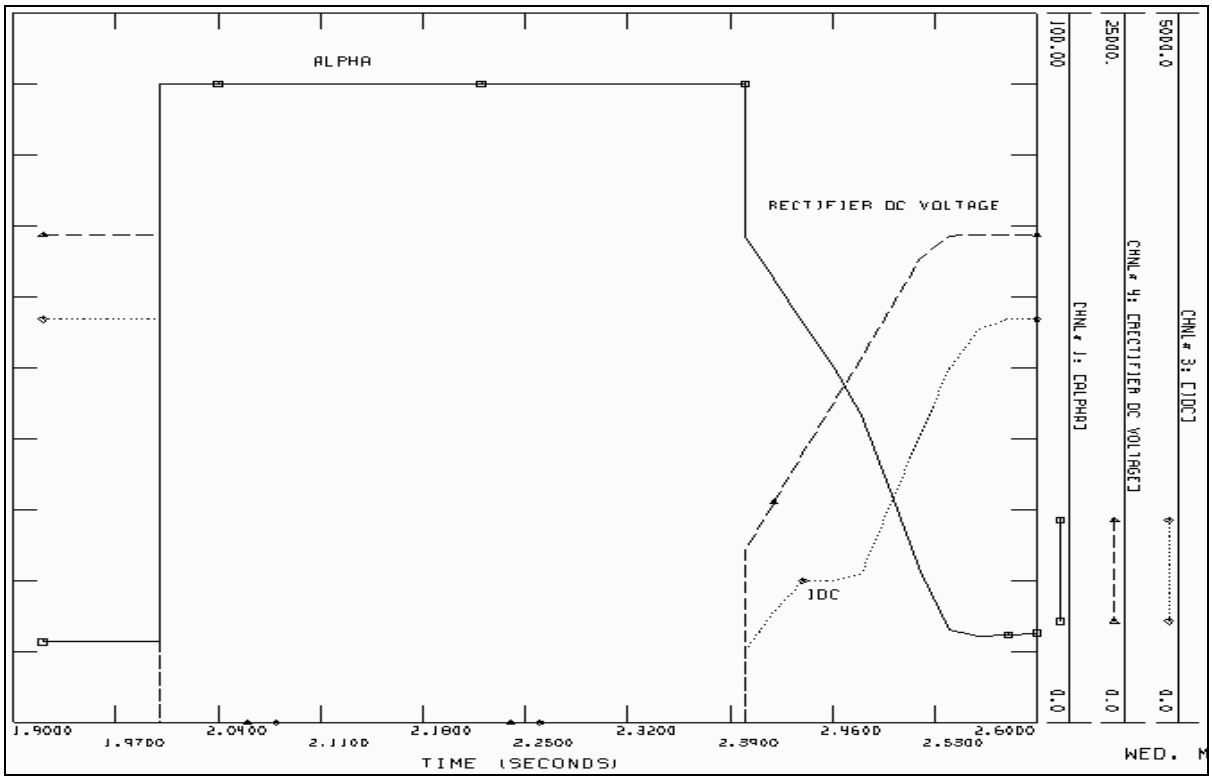

Figure 47 Alpha [degrees], rectifier dc voltage [V] and dc current [A] during fault.

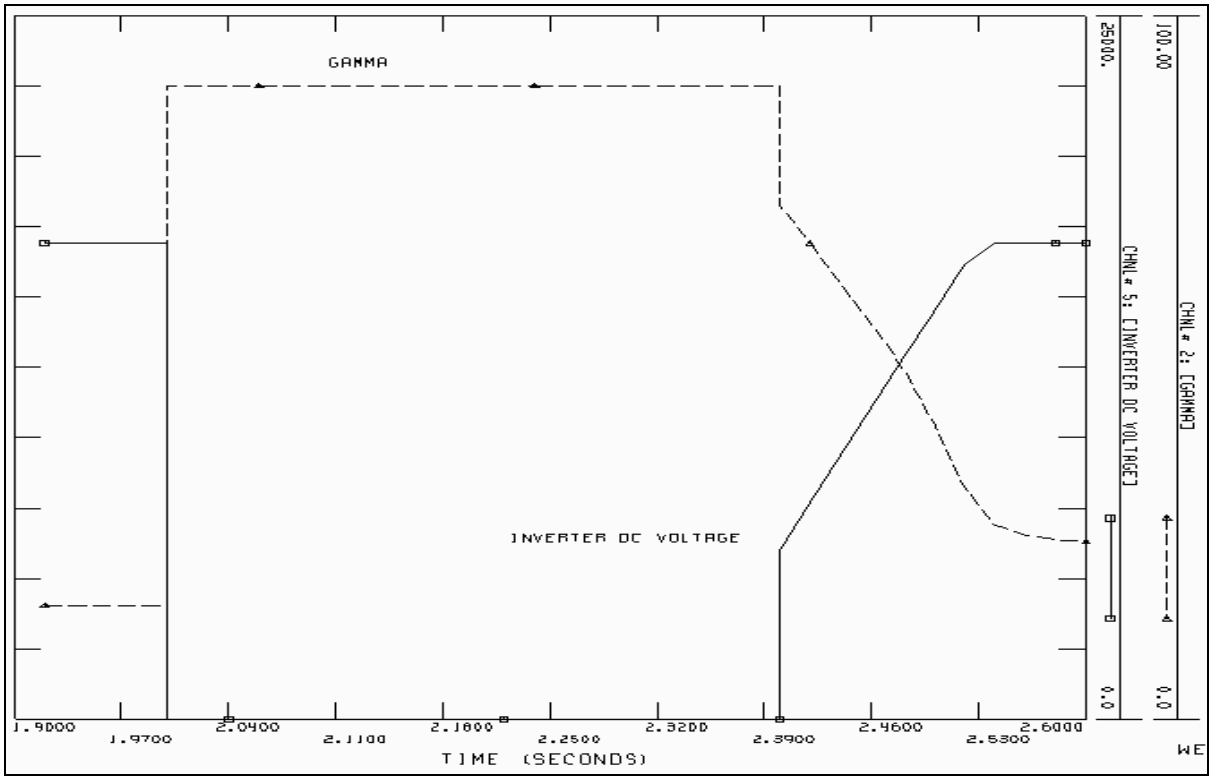

Figure 48 Gamma [degrees] and inverter dc voltage [V] during fault.

As stated in Section 5.3.2, the rectifier and inverter are both shutdown if the ac voltage at the rectifier falls below the per unit value, VBLOCK. In Section 5.1.1 the parameter VBLOCK is set to 0.6 per unit. The latter means that the converter will be shutdown if the ac rectifier voltage falls below this value. However, by investigating Figure 46, one can see that the

rectifier bus voltage falls to 0.6 per unit at time t = 2.029. This means that at time t = 2.0, when the converter is shutdown, the rectifier bus voltage is greater than 0.6 per unit. The explanation for the latter situation can be found by investigating Figure 21 on page 39. The rectifier bus voltage in Figure 46 is analogues to the "Primary bus" voltage in Figure 21. However, the rectifier ac blocking voltage is measured at the secondary side of the converter transformer and is denoted E_{ac}^{R}. Thus, the rectifier bus voltage in Figure 46 is somewhat greater that E_{ac}^{R} and the blocking occur seemingly at a greater value than VBLOCK.

The fault is cleared, t > 2.4 second

As the fault is cleared, Figure 46 shows that the rectifier bus voltage rises instantaneously to a value greater than VUNBL (the rectifier unblocking value), and thus, the converter is restarted. To facilitate the understanding of the reestablishment of dc voltage and current following this converter blocking, see Figure 49.

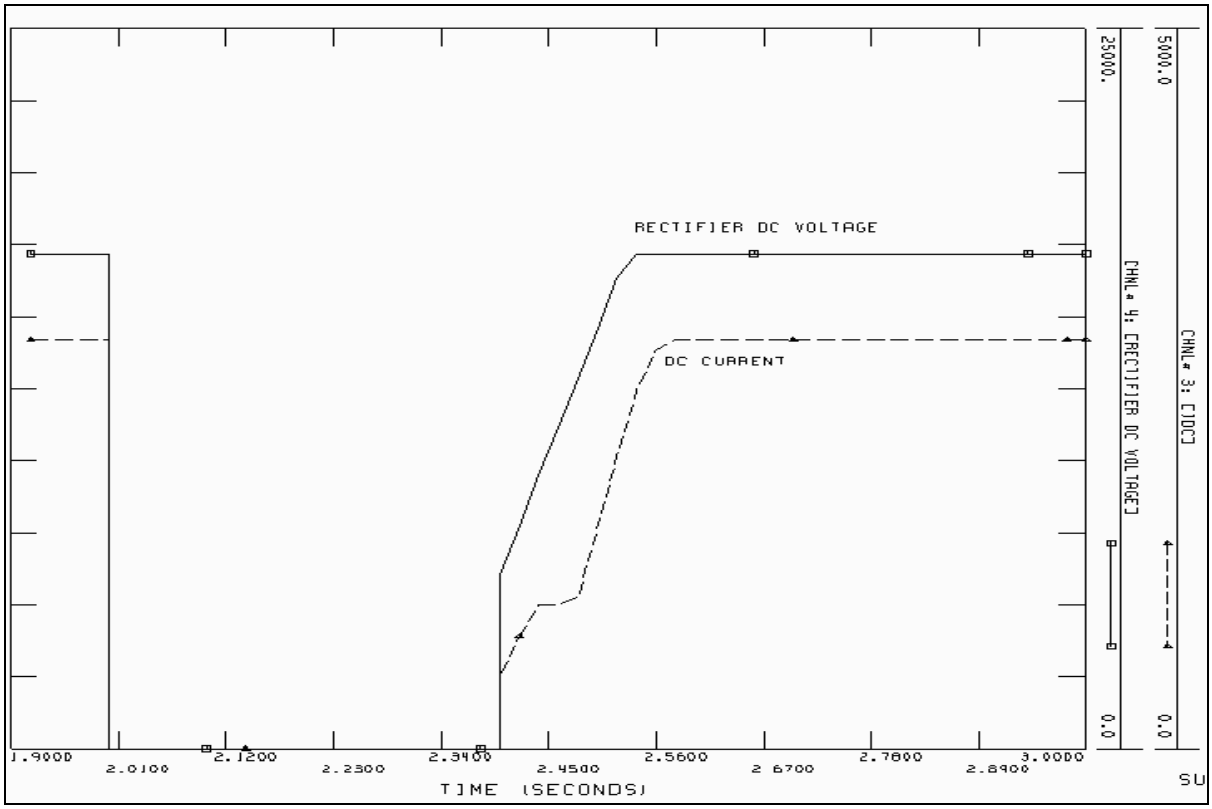

Figure 49 Reestablishment of rectifier dc voltage [V] and dc current [A] after the fault is cleared.

Figure 49 shows that the rectifier dc voltage and current at time t = 2.4 are 6 kV and 500 A, respectively. These values are the minimum dc voltage and current following a converter blocking, and correspond to the parameters RSVOLT and RSCUR defined in the dynamic data sheet in Section 5.1.1. The latter also applies for the inverter reestablishment.

Figure 37 on page 68 illustrates the principal reestablishment of dc voltage and current following a blocking. In this figure TBLOCK is the minimum time in seconds, the rectifier remains blocked. However, since the duration of the line fault is greater than the value specified for TBLOCK, the actual rectifier blocking time is determined by the duration of the fault.

The reestablishment of dc voltage and current are generally determined by the parameters RSVOLT, RSCUR, VRAMP and CRAMP defined in Section 5.1.1. From Figure 49 it can be seen that the rectifier dc voltage follows the predetermined parameters RSVOLT and VRAMP. However, the current setpoints at both the rectifier and the inverter are overridden by the voltage-dependant current limit (VDCL). VDCL for the dc converter is illustrated in Figure 39 on page 69. If the VDCL comes into play during the current reestablishment, it forces the dc current to a value below the instantaneous setpoint.

The latter situation can be observed in Figure 49. This figure shows that the dc current follows the parameters RSCUR and CRAMP till t = 2.44 seconds. However, in the period $2.44 < t < 2.49$, the VDCL comes into play and holds the dc current at a constant value of 1000 A. This value corresponds to the predefined current limit point 1, i.e. C1, in Figure 39 on 69. The time period in which the VDCL is active, see Figure 49, is determined by the dc voltage and current transducer time constant. The transducer constant is specified in the dynamic data sheet in Section 5.1.1. A figurative illustration of the transducer time constant is shown in Figure 33 on page 65. In this figure the time constants are denoted T_{vdc}^{s} and T_{idc}^{s}.

In order to obtain the current reestablishing profile illustrated in Figure 37 (on page 68), the VDCL profile and reestablishing rate for both the voltage and current has to be coordinated. It's also feasible to increase C1, i.e. current limit point 1 on the VDCL profile, to e.g. 3000 A. In the latter approach, the VDCL will not come into play, and the current reestablishing profile is determined by the parameters RSCUR and CRAMP. This situation is illustrated in Figure 50.

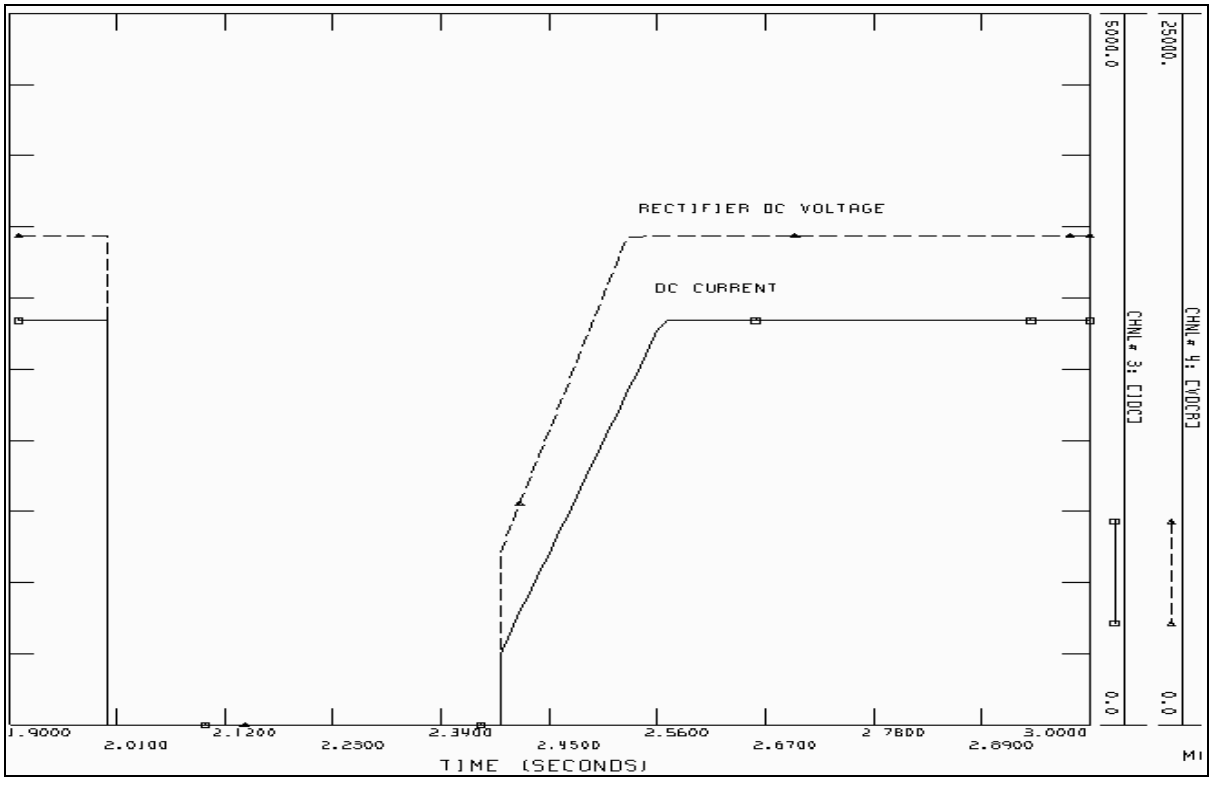

Figure 50 Reestablishment of rectifier dc voltage [V] and dc current [A] with the VDCL disabled.

Hence, the dc current reestablishment profile following a converter shutdown is dependent on the VDCL setpoints in addition to the settings of the dc current recovery ramp rates. The objective of "disabling" the VDCL, as illustrated in Figure 50, may be to maximize the recovery rate while avoiding subsequent commutation failures [7].

Figure 51 and Figure 52 show that the rectifier firing delay angle (alpha), rectifier bus voltage and the rectifier reactive power consumption fluctuates after the fault as been removed. These fluctuations are similar to the fluctuations experienced in Case D. Also in Case E, the fluctuations in alpha and reactive power are caused by variations in rectifier bus voltage. The rectifier will continuously adjust alpha to maintain scheduled dc current, and the latter causes the fluctuations experienced in Figure 52. However, the reactive power fluctuations are substantially greater in Case E compared to Case D. This is elaborated further in Section 6.4.3.

Note, the rectifier real power shown in Figure 52 does not exhibit a fluctuating profile. This is because the rectifier dc voltage and dc current reaches a constant value within 200 ms after the fault has been removed. However, in a hypothetical situation with fluctuations in dc current or dc voltage, fluctuations in active power would also be expected.

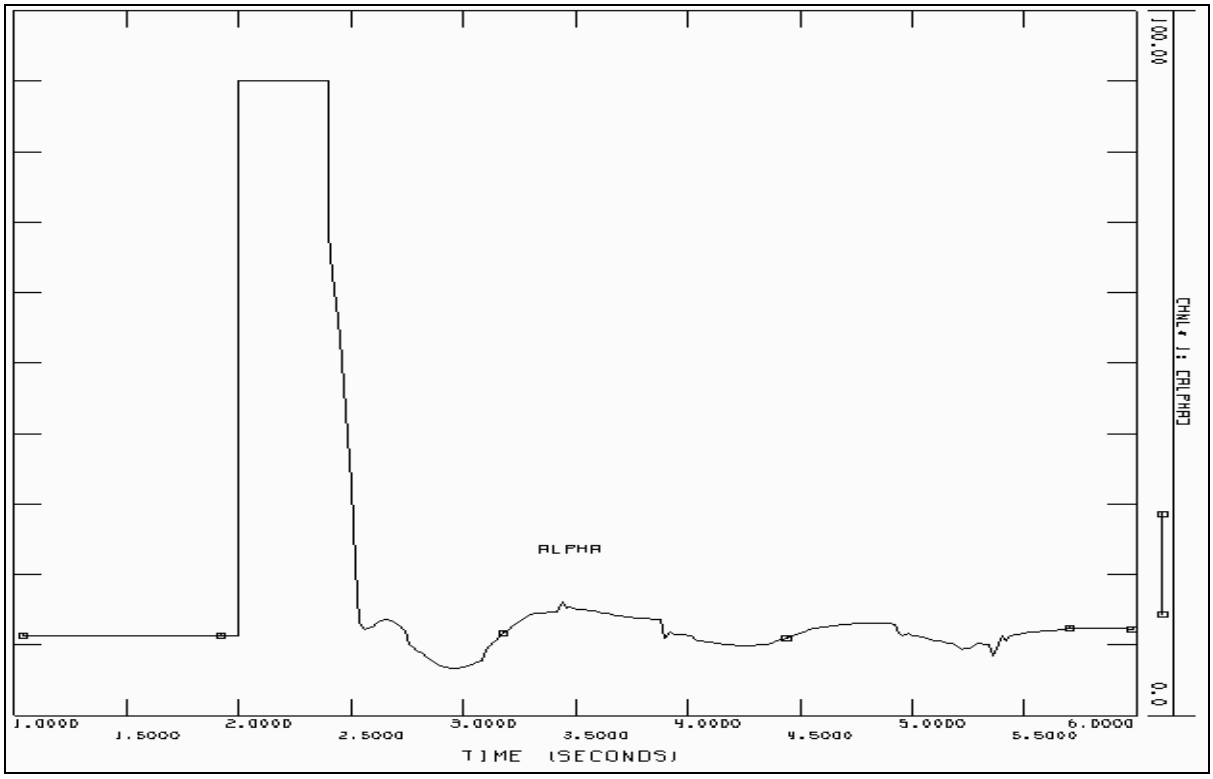

Figure 51 Rectifier firing delay angle [degrees]. The figure illustrates both the pre fault and post fault situation.

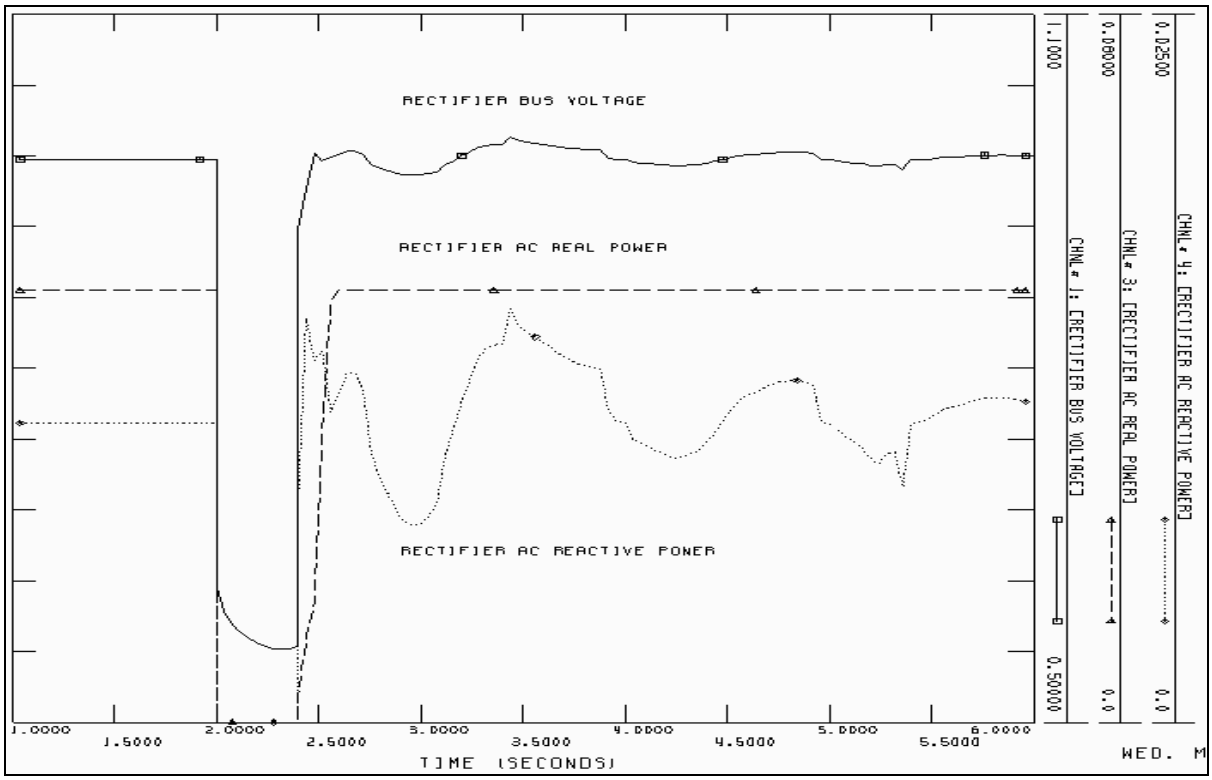

Figure 52 Rectifier bus voltage [V], rectifier ac real power [pu] and rectifer ac reactive power [pu]. The active and reactive power are based on system base (1000 MVA).

6.4.3 Case D versus Case E

This section illuminates an important aspect concerning the converters' recovery from a system disturbance. Comparing the post fault reactive power consumption of the rectifier in Case D and Case E, see Figure 53 and Figure 54, it is clear that the reactive fluctuations are substantially greater for Case E than for Case D. These will also cause fluctuations in the rectifier ac bus voltage. Consequently, the rectifier bus voltage in Case E exhibits greater voltage fluctuations than Case D. The latter can be verified by studying Figure B2 and Figure B3 in Appendix B.

Variations in reactive consumption might hinder post fault ac voltage recovery. Also, since voltage variations can be detrimental to the overall system stability, it is of great importance to acknowledge which factors and parameter setting of the converter model that influences the post fault reactive fluctuations [7].

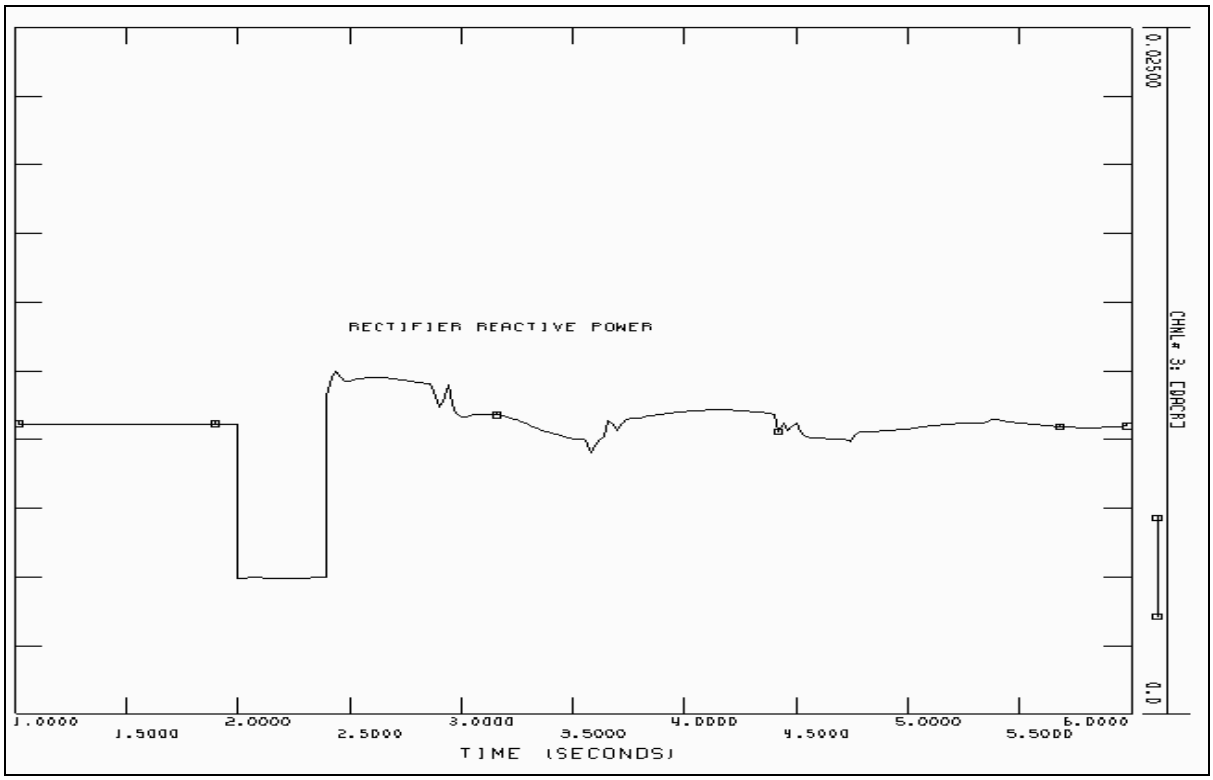

Figure 53 Rectifier ac reactive power [pu] for Case D. The power is based on system base (1000 MVA).

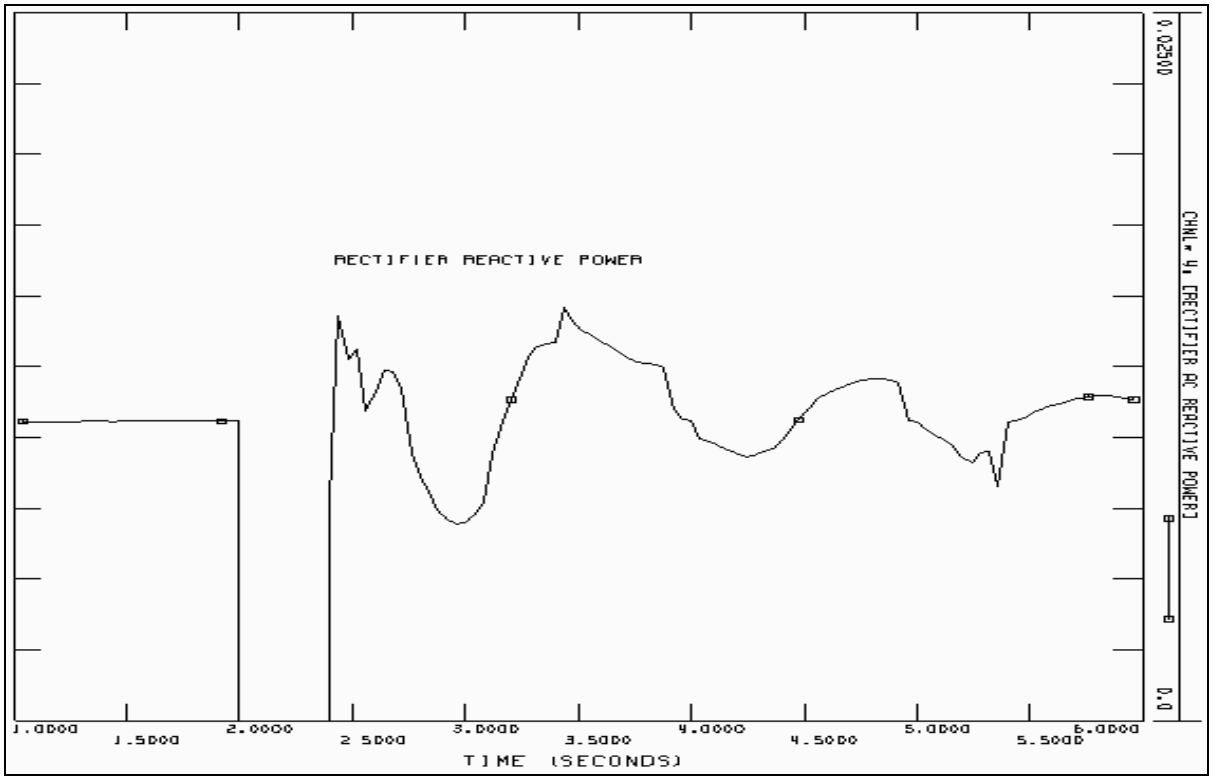

Figure 54 Rectifier ac reactive power [pu] for Case E. The power is based on system base (1000 MVA).

To understand what causes greater reactive power fluctuations in Case E compared to Case D, see Figure 55 and Figure 56. The latter figures illustrate the reestablishment of rectifier firing delay angle for respectively Case D and Case E. From Figure 55 it is clear that alpha is instantaneously raised to a value close to its pre fault value at time t = 2.4 seconds. In Figure 56, however, alpha is not instantaneously reduced to its pre fault value. At approximately 67 degrees, the reestablishment of alpha has a breaking point. This means that at time t = 2.4, alpha is reduced from 90 degrees to 67 degrees. From this point, alpha is "ramped" down and reaches a value close to its pre fault value at approximately t = 2.54 seconds.

Since the rectifier reactive consumption increases with increasing alpha, it is clear that the reactive consumption during the reestablishment of alpha is greater for Case E than Case D. Consequently, Case E exhibits greater reactive fluctuations than Case D.

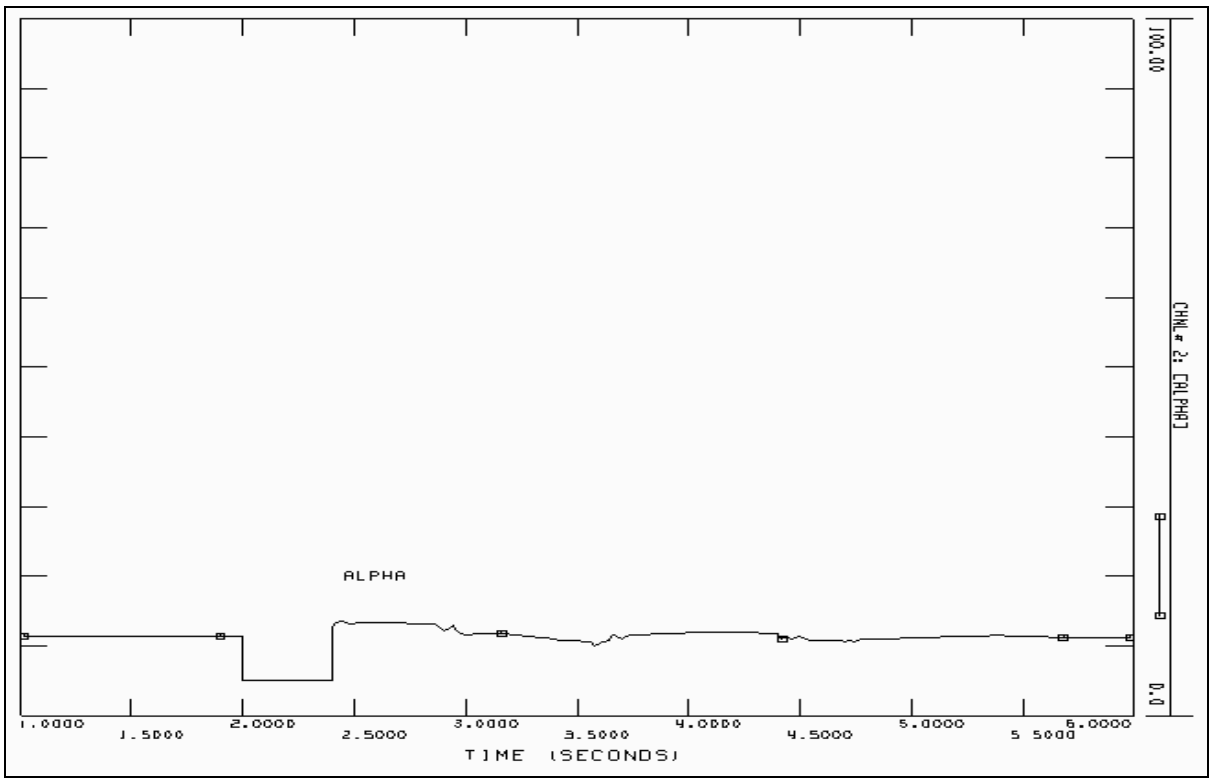

Figure 55 Reestablishment of alpha [degrees] for Case D.

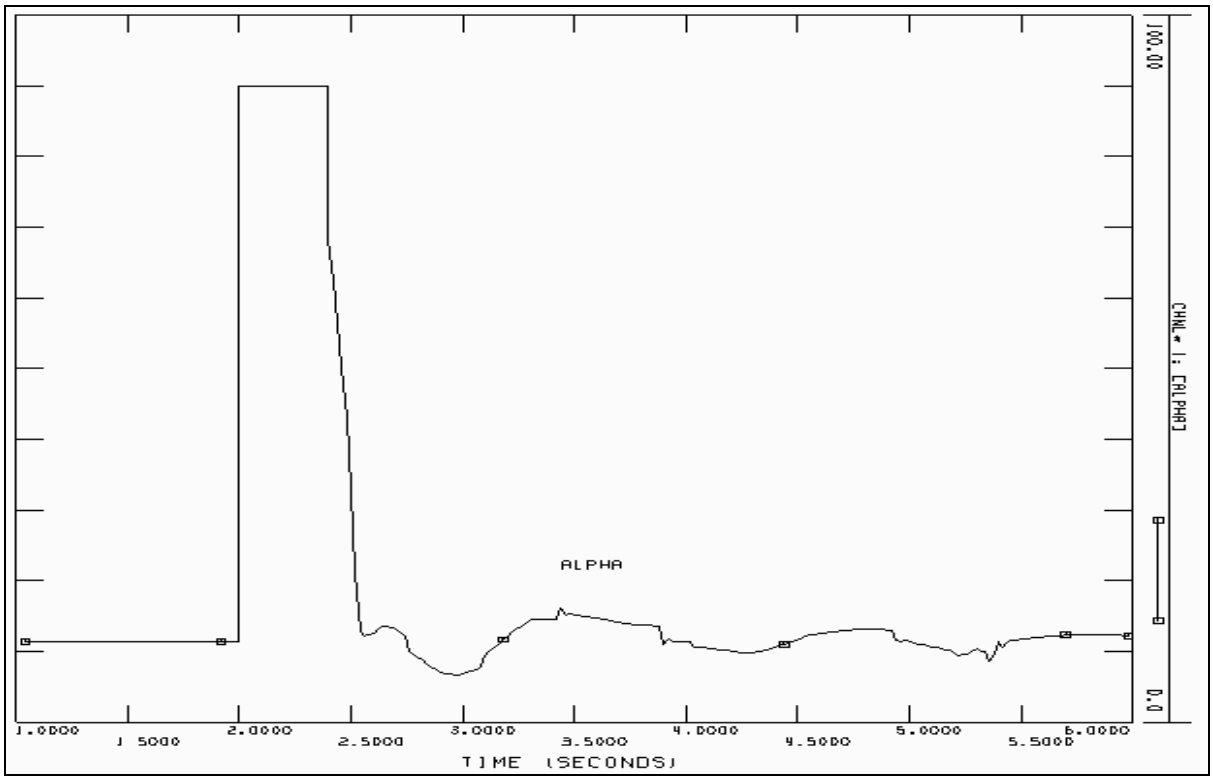

Figure 56 Reestablishment of alpha [degrees] for Case E.

The reestablishment of alpha in Case E, see Figure 56, is analogues to the reestablishment of rectifier dc voltage and dc current following the converter shutdown, described in Section 6.4.2. The breaking point at $\alpha = 67°$ in Figure 56 is hence a consequence of the values chosen for reestablishment parameters RSVOLT, RSCUR, VRAMP and CRAMP in Section 5.1.1.

It is also important to acknowledge that the VDCL function can play a significant role in determining the recovery from faults. The VDCL limits the current order as a function of dc voltage. Consequently, the VDCL can (if correctly defined) reduce the reactive power demand during periods of depressed voltage, and thus, reduce reactive power fluctuations [3].

Hence, the user defined values for the parameters defining the reestablishment profile for the dc voltage and dc current can result in substantial fluctuations in the rectifier reactive power consumption, following a converter blocking.

6.5 General considerations

The results obtained from these cases have revealed an important characteristic of the CDC4T model. After fault clearance, the rectifier bus exhibited small voltage fluctuations. The rectifiers compensated these fluctuations by adjusting their rectifier firing delay angle correspondingly. The latter resulted in fluctuations in rectifier reactive power consumption. Consequently, the ac system perceives the CDC4T model as a fluctuating reactive load following a fault clearance. The reactive power fluctuations were substantially greater for Case E. This is because Case E resulted in a shutdown of the converters, and the rectifier firing delay angle following this shutdown, is determined by the parameters defining the reestablishment of dc current and voltage.

It is worth emphasizing that many of the figures in this chapter exhibit an instantaneous response to changes in ac system voltage. This is due to the nature of the converter model used in this thesis. As described in Chapter 5, the model utilized (CDC4T) is referred to as a pseudo-steady state, dynamic HVDC model. This term is used because the model represents dynamic conditions using relationships which are technically valid only for steady state conditions. Also, the model does not include the L/R dynamics of the dc system and the high frequency firing angle controller dynamics. Consequently, the responses are instantaneous and evaluation of the high frequency control system is not feasible [15, 17].

7 Model evaluation

This chapter analyses the consequence of using a converter representation of Ormen Lange instead of a traditional PQ representation. The objective is to determine whether the response from the ac system differs when using the converter model instead of a PQ-model.

This chapter uses the term converter model to refer to the dynamic two-terminal dc line model.

7.1 Introduction

The basis for the simulations performed in this chapter is two power flow models. These two models represent Ormen Lange in two distinct ways. One of the models represents Ormen Lange as a PQ-model and the other model represent Ormen Lange as a dynamic two-terminal dc line model (CDC4T), also referred as converter model.

An illustration of the two model configurations is shown in Figure 57 and Figure 58. Figure 57 shows how the PQ-model is established in PSS/E and Figure 58 shows an analogues illustration of the converter model. The converter model used in this chapter is identical to the model analyzed in Chapter 6.

The PQ-model corresponds to the model used in the preliminary study [9], however, with a different initial loading. The initial loading of the PQ-model is chosen to correspond with the initial loading of the converter model.

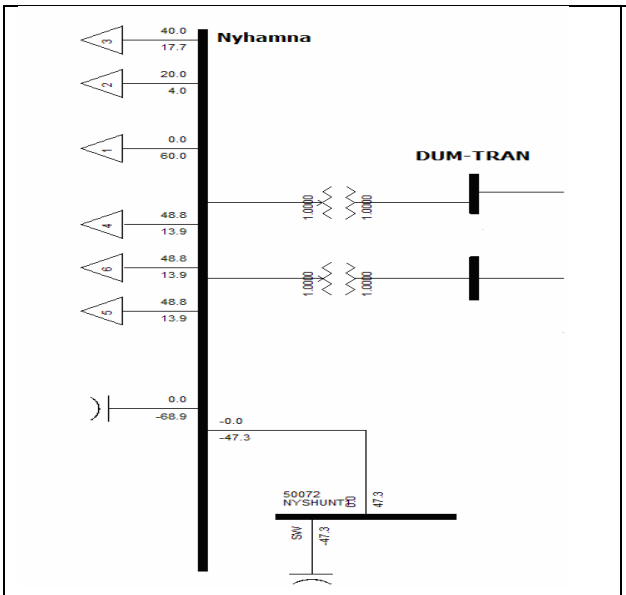

Figure 57 Ormen Lange with PQ representation.

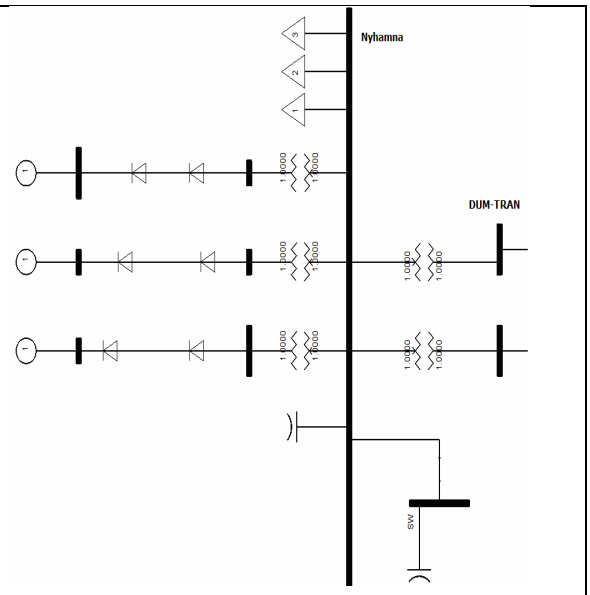

Figure 58 Ormen Lange with converter representation.

It is important to emphasize that the objective of this chapter is not to evaluate or compare stability problems associated with the PQ-model and converter model. The objective is merely to investigate to what extent the implementation of a converter model (CDC4T) causes different system responses, compared to the PQ-model.

7.2 Initial conditions and assumptions

This section presents the initial conditions and assumptions for the dynamic simulations presented in this chapter.

Since this chapter analyzes the response from two different models, it is of great importance to have two initial power flow situation that are identical, and hence, comparable. With two different initial power flow situations, it is not feasible to determine whether a different response is caused by a different load representation or by two different initial power flow situations.

Thus, the two models analyzed in this chapter are implemented with approximately identical initial conditions. This means that both the overall system generation/loading and the local Ormen Lange conditions are identical in both models. This can be verified by studying the excel files "Loads" and "Machines" given in Appendix D.

In the initial situation, the total active and reactive power drawn from Nyhamna is 206.4 MW and 123.4 MVAr for both models. This initial condition does not correspond to the loading used by Statnett in their representation of Ormen Lange. However, the latter will be of no consequence for the following simulations.

7.2.1 Power flow assumptions

The following power flow files are used in this chapter:

I. Converter model: "Converter_model_cnv.sav"
II. PQ-model: "P-Q load_cnv.sav"

The following assumptions, which differ from the default setting provided in PSS/E, were made when establishing the power flow files:

- Switched shunt adjustments locked.
- Constant MVA loads converted with the following real power distribution:
    - 40 % constant current
    - 40 % constant admittance
    - 20 % constant power
- Constant MVA loads converted with the following reactive power distribution:
    - 0 % constant current
    - 100 % constant admittance
    - 0 % constant power

The power flow files can be found in Appendix D.

7.2.2 Dynamic assumptions

The following dynamic files are used in this chapter:

I. Converter model: "NN.dyr"
II. PQ-model: "P-Q load.dyr"

Before running the dynamic simulations, the dynamic initialization activity, STRT, is invoked. After the latter activity is executed, numerous of suspect initial conditions are found. The handling of these suspect initial conditions are described in Section 6.2, and will thus not be repeated here.

As in previous dynamic simulations, all simulations are run for a period of 2 seconds before any disturbances are applied. The objective is to insure that any non steady-state variables have reached a steady-state condition.

The dynamic files can be found in Appendix D.

7.3 Application of the disturbances

This section presents the two cases which are analyzed in this chapter.

To analyze and compare the consequence of using different models to represent Ormen Lange, it is necessary to introduce a system fault which changes the initial power flow situation. Two system faults are implemented in this chapter. The first fault is the same fault as defined in Table 12 on page 76.

Table 13 describes the cases studied in this chapter.

Table 13 Case definitions.

Case	Case explanation
E	Branch fault on 130 kV line between Aura1(57013)-OSBU1(57403) with fault impedance R=2, X=2. The fault is applied for 400 ms.
F	Bus fault on the 12 kV generator bus (57024) at Aura with fault impedance R=0, X=0. The fault is applied for 200 ms.

The faults defined in Table 13 are not implemented to represent realistic fault scenarios. However, the faults function merely as a means for depressing the bus voltage at Nyhamna to a varying degree. This enables a principal evaluation of the system response when to different model representations of Ormen Lange are utilized.

Note; the fault applied are three phase faults. The value of the fault admittance is calculated based on the settings of the "Unit" toggle switch, the impedance input field and "Base kV" input field in PSS/E. When the fault is executed the line shunt at the "from" bus end of the designated branch is replaced with the per unit admittance equivalent to the value entered for R and X [11].

7.4 Simulation results

This section presents the simulation results for Case E and Case F. The discussion is given consecutive as the results are presented to increase the readability.

For each case, results are presented both locally at Nyhamna and at Viklandet. Viklandet is included because it constitutes a central junction point for power delivery to Nyhamna.

The following responses are presented in the subsequent sections:

- Bus voltage
- Bus phase angle
- Frequency deviation
- Active and reactive power flow

All simulation results are first presented for the PQ-model followed by the corresponding result for the converter model. This presentation is chosen to facilitate the evaluation of the two model responses.

It is important to emphasize that the following discussion will focus on the distinction in system response from the PQ-model and the converter model. This means that responses from a given model will be evaluated in context with the response from the other model.

Since the performance of the converter model is discussed in detail in Chapter 6, this section will not repeat the same arguments to substantiate the results obtained in this section. Hence, the reader may refer to Chapter 6 to facilitate the understanding of the converter responses obtained in this section.

Also, it's important to emphasize that the evaluations made in this section are only valid for the assumptions made introductorily.

7.4.1 Results from Case E

This section presents the simulation results at Nyhamna and Viklandet, respectively.

7.4.1.1 Response at Nyhamna

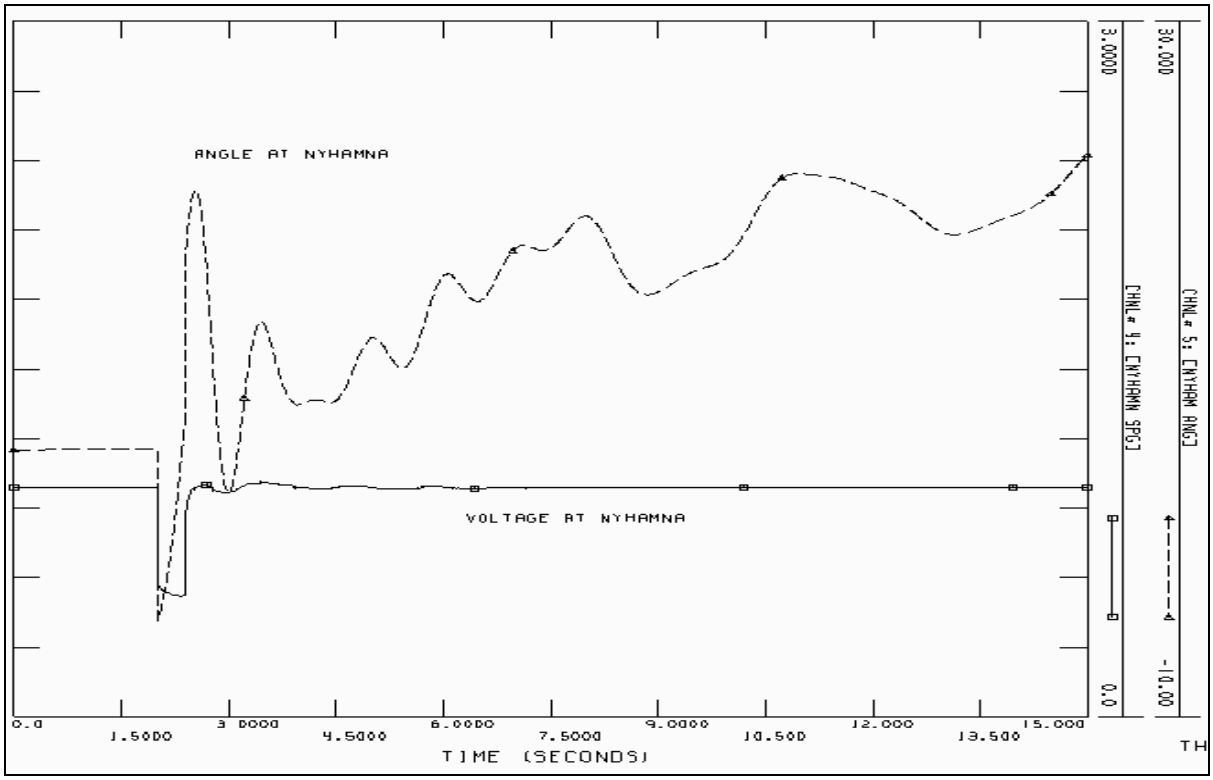

Figure 59 Bus voltage [pu] and bus phase angle [degrees] at Nyhamna with PQ representation of Ormen Lange.

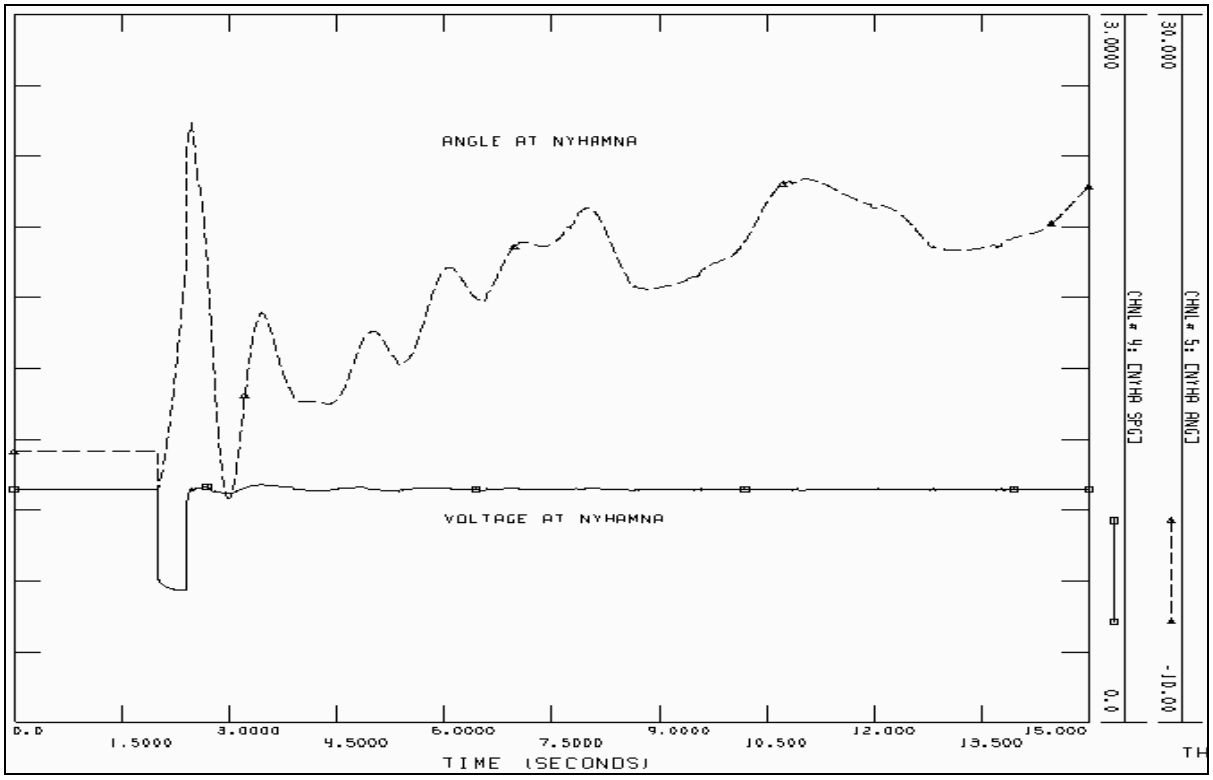

Figure 60 Bus voltage [pu] and bus phase angle [degrees] at Nyhamna with converter representation of Ormen Lange.

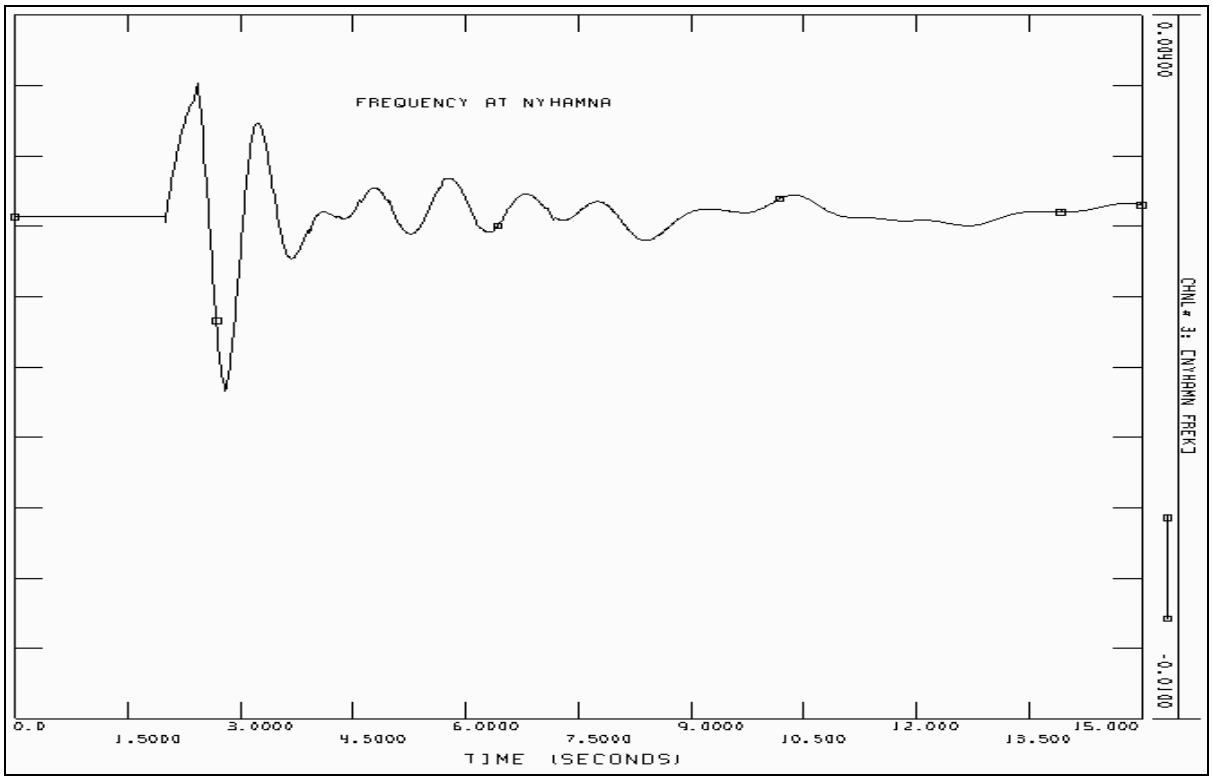

Figure 61 Frequency deviation [pu] at Nyhamna with PQ representation of Ormen Lange.

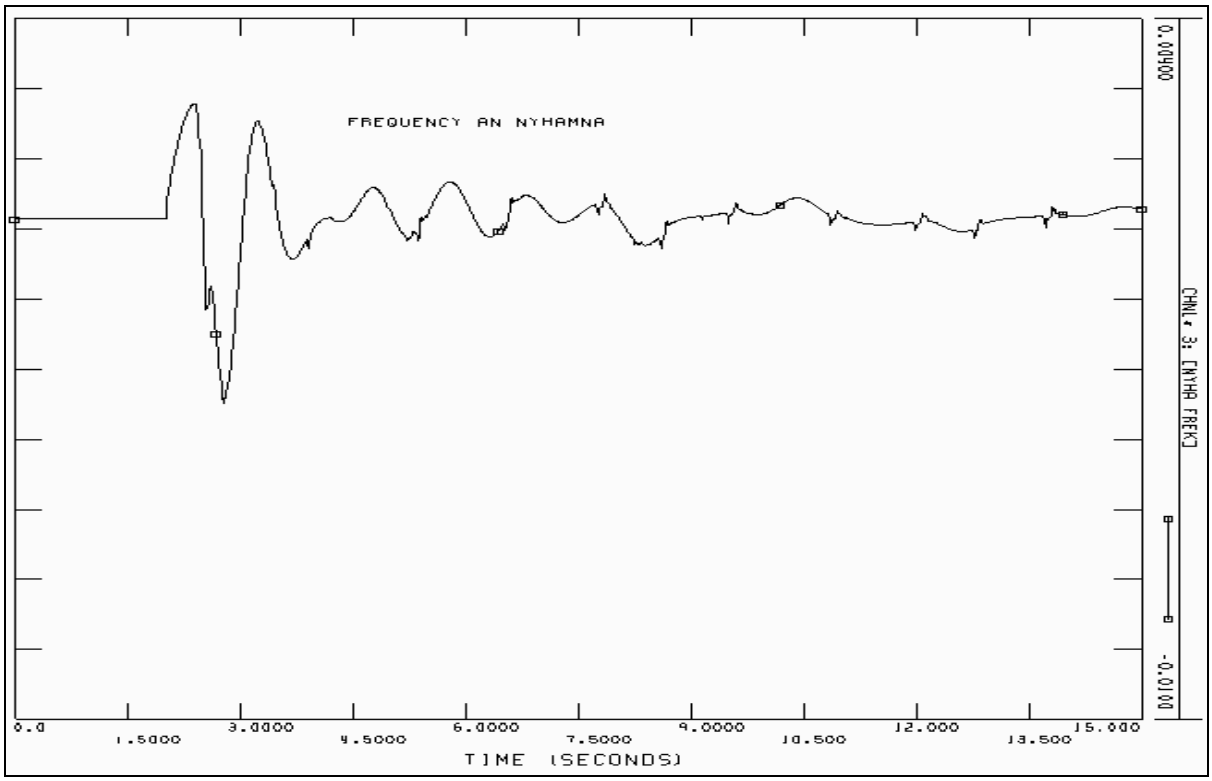

Figure 62 Frequency deviation [pu] at Nyhamna with converter representation of Ormen Lange.

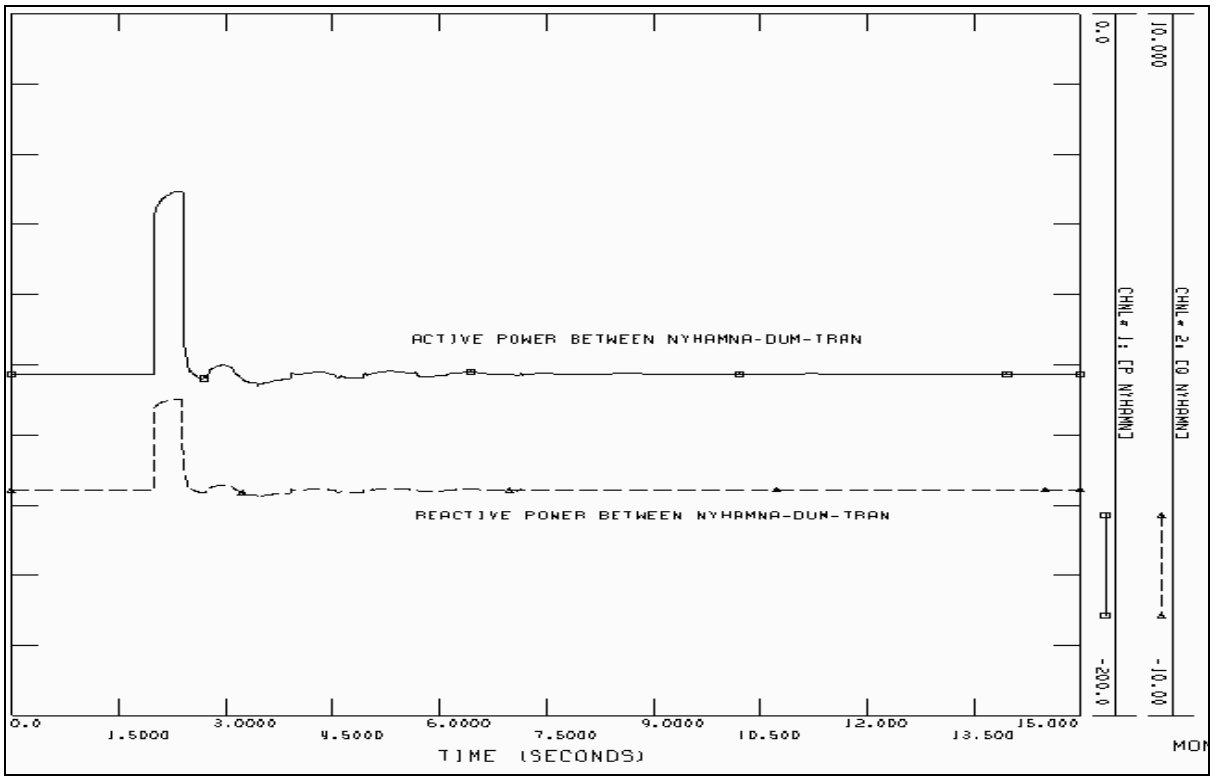

Figure 63 Active and reactive power between Nyhamna and DUM-TRAN with PQ representation of Ormen Lange. The units are [MW] and [MVAr] respectively.

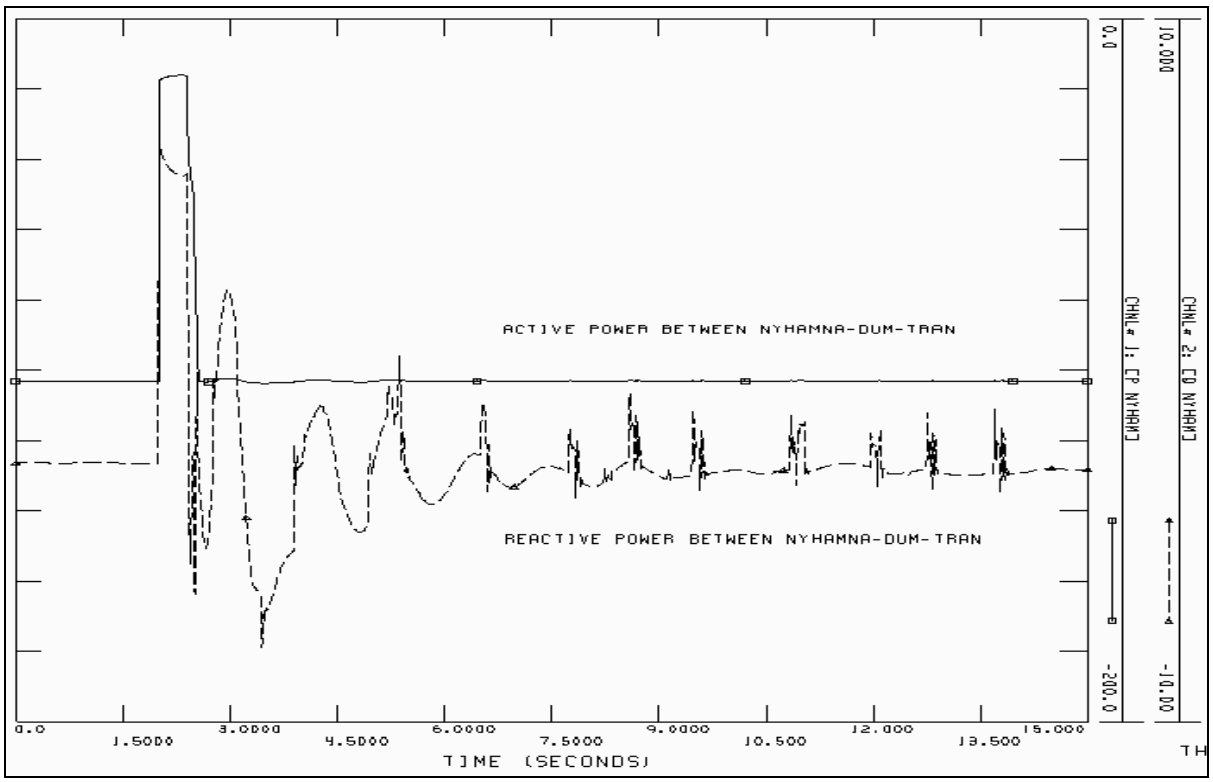

Figure 64 Active and reactive power between Nyhamna and DUM-TRAN with converter representation of Ormen Lange. The units are [MW] and [MVAr] respectively.

Comparison of the response at Nyhamna

Figure 59 and Figure 60 shows that the voltage profile at Nyhamna following the disturbance is approximately identical for the PQ-model and the converter model. The phase angle at Nyhamna also exhibits similar profiles when using the converter model and the PQ-model. The latter especially applies for $t > 3.0$ seconds. However, in the time period $2.0 < t < 3.0$, the curves differs to some extent. The PQ-model causes the phase angle at Nyhamna to drop instantaneously to a lower value than the converter model, as the fault is applied. Since the fault results in converter shutdown, and hence, a great reduction in the active power consumption, the angle reduction will be greater for the PQ-model (the PQ-model maintains active power consumption during the fault).

Figure 61 and Figure 62 illustrate the frequency deviation at Nyhamna. Except for minor fluctuations in the curve representing the converter model, both models exhibit the same profile. Since momentary change in system frequency is unphysical, the latter fluctuation could be a result of numeric calculations in PSS/E. By reducing the time step of the simulation parameter, these fluctuations are reduced.

The active and reactive power between Nyhamna and DUM-TRAN (the configuration is illustrated in Figure 58) are illustrated in Figure 63 and Figure 64. By comparing the latter figures, it becomes clear that the power going into Nyhamna differs when using the PQ-model and when using the converter model. The active power flow between Nyhamna and DUM-TRAN are approximately equal for the period $t > 2.4$ seconds. At this point the fault is removed, and the post fault power flow is close to its pre fault power flow. However, in the period where the fault is applied, i.e. $2.0 < t < 2.4$, the active power flow with the converter model is reduced to a greater extent than with the PQ- model. This is a consequence of the converter shutdown. During shutdown, no active power is transferred over the dc link and the only active power consumed at Ormen Lange is due to the small amount of PQ loads representing the auxiliary equipment, see Figure 58.

The reactive power flowing between Nyhamna and DUM-TRAN with the converter model, see Figure 64, differs greatly from the reactive flow in the PQ-model, see Figure 63. By first evaluating the period $2.0 < t < 2.4$ where the fault is applied, Figure 64 shows that the reactive power flow changes direction. This means that during the fault period, reactive power is being “supplied” from Nyhamna into the ac system. Since the converter shutdown causes a reduction in rectifier reactive consumption, a reactive power surplus emerges. This surplus emerges because reactive output from the capacitors connected to Nyhamna (see Figure 58) exceeds the reactive power demand at Ormen Lange. The latter is only true for the converter model. With the PQ-model the reduction in reactive consumption is not sufficient to cause a reactive power surplus. Hence, reactive power is flowing into Nyhamna.

After the fault is removed, i.e. $t > 2.4$, the converter model in Figure 64 exhibits large fluctuations in the reactive power flow between Nyhamna and DUM-TRAN. Figure 64 shows that the reactive power fluctuations are diminished as time approaches 15 seconds. However, the fluctuations are not reduced entirely and exhibit an amplitude of approximately 2 MVAr as time approaches 15 seconds. Considering the fact that the pre fault reactive power flow in the line is approximately 2.6 MVAr, these fluctuations can be considered substantial.

Evaluating the reactive power flow with the PQ-model in Figure 63, it becomes clear that reactive fluctuations are non-existent compared to the converter model. In the latter figure the post fault value reaches the pre fault value shortly after the fault is removed.

To facilitate the understanding of the cause of the reactive power fluctuations with the converter model, see Figure 65. This figure shows both rectifier firing delay angle and the reactive power flow between Nyhamna and DUM-TRAN. As stated in previous chapters, the rectifier reactive power consumption varies with the rectifier firing delay angle (alpha). An increased alpha results in increased rectifier reactive consumption. The latter can be confirmed by analyzing Figure 65. The peaks in the reactive power correspond to the peaks in alpha, i.e. the fluctuations are in step.

Note, the reason the reactive power seemingly is reduced when alpha is increased, is because the reactive power flow is defined negative when going into Nyhamna. Hence, the curves fluctuate in anti-phase.

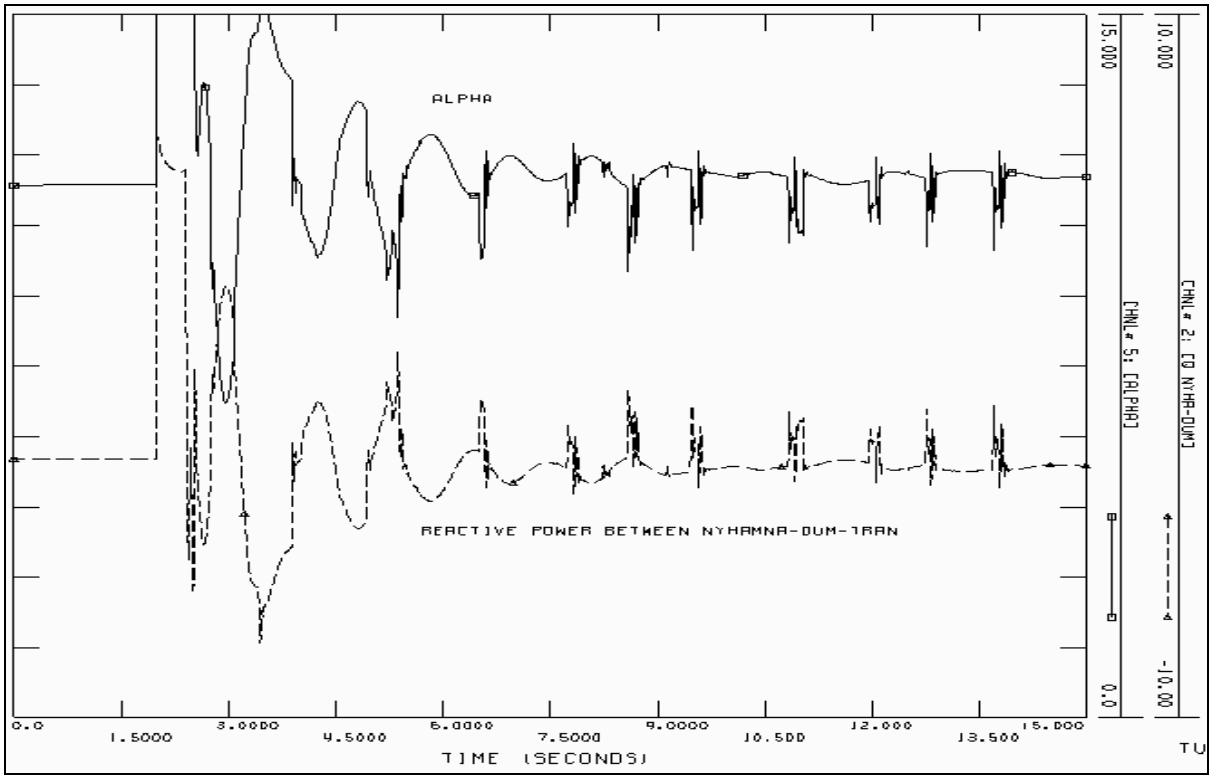

Figure 65 Rectifier firing delay angle [degrees] and reactive power flow [MVAr] between Nyhamna and DUM-TRAN with converter representation of Ormen Lange.

The results in this section illuminate an important characteristic of the converter model. As apposed to the PQ-model, the ac system will perceive the converter model as a fluctuating reactive load. The latter results in the reactive power fluctuations illustrated in the previous figures. As long as there are fluctuations in alpha, the reactive power fluctuations will persist. Since the cause of the converters' reactive fluctuations has been discussed in detail in the previous chapter, it will not be repeated here.

7.4.1.2 Response at Viklandet

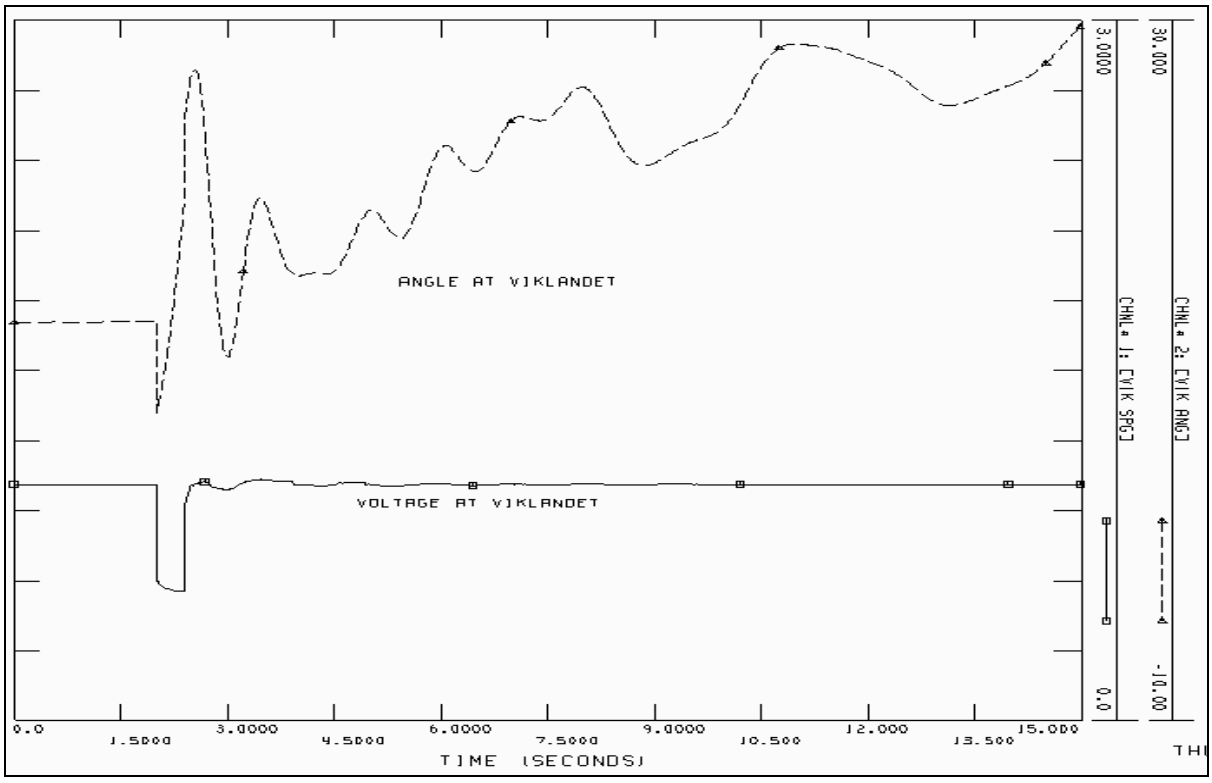

Figure 66 Bus voltage [pu] and bus phase angle [degrees] at Viklandet with PQ representation of Ormen Lange.

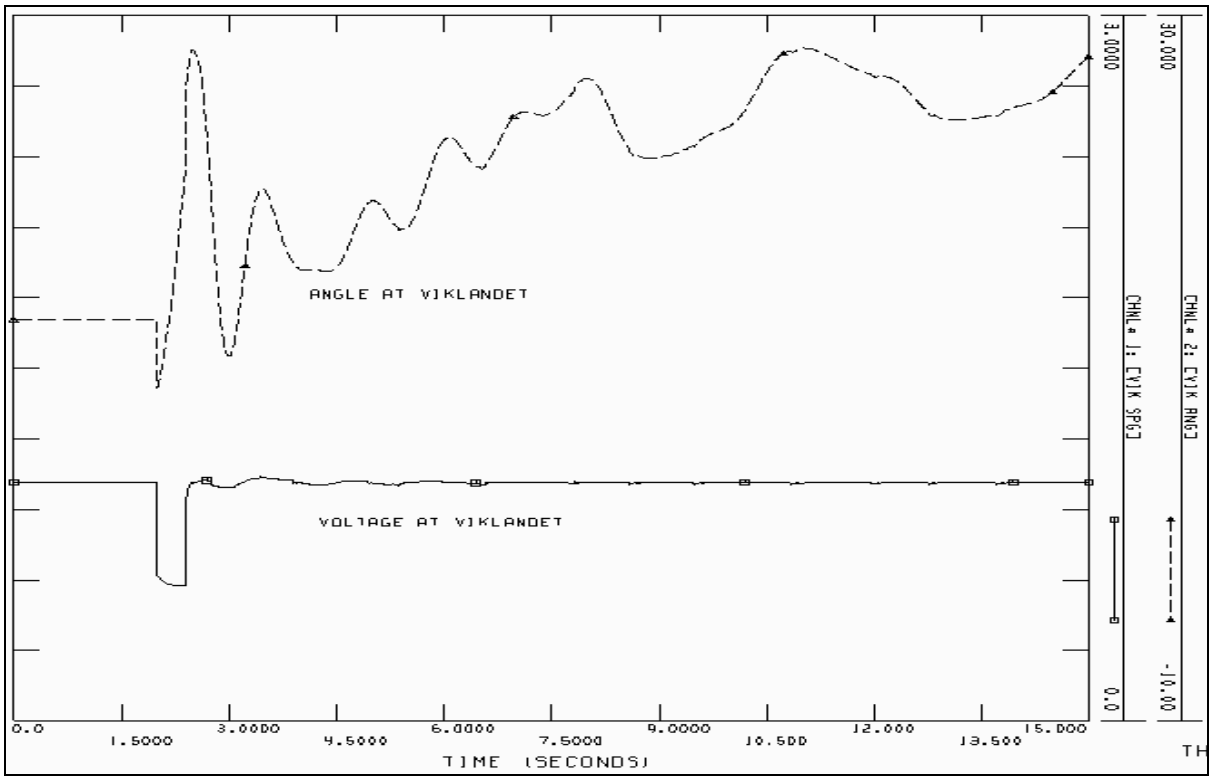

Figure 67 Bus voltage [pu] and bus phase angle [degrees] at Viklandet with converter representation of Ormen Lange.

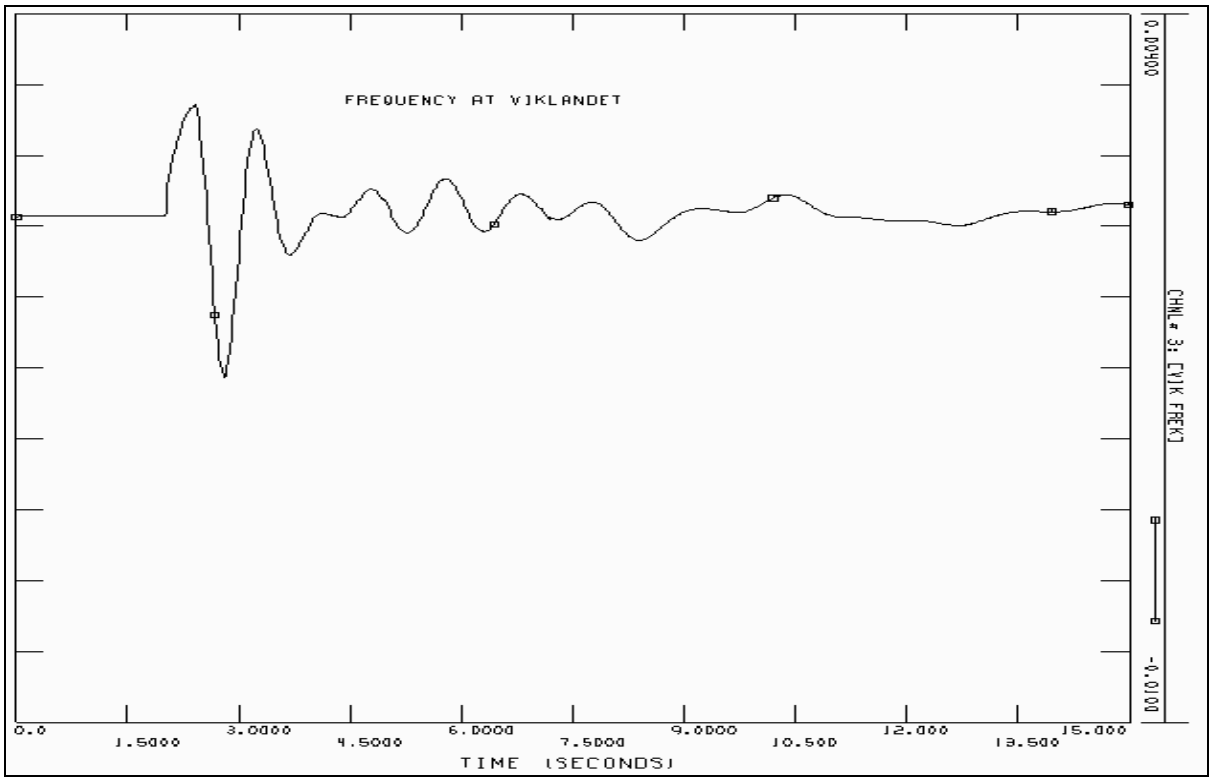

Figure 68 Frequency deviation [pu] at Viklandet with PQ representation of Ormen Lange.

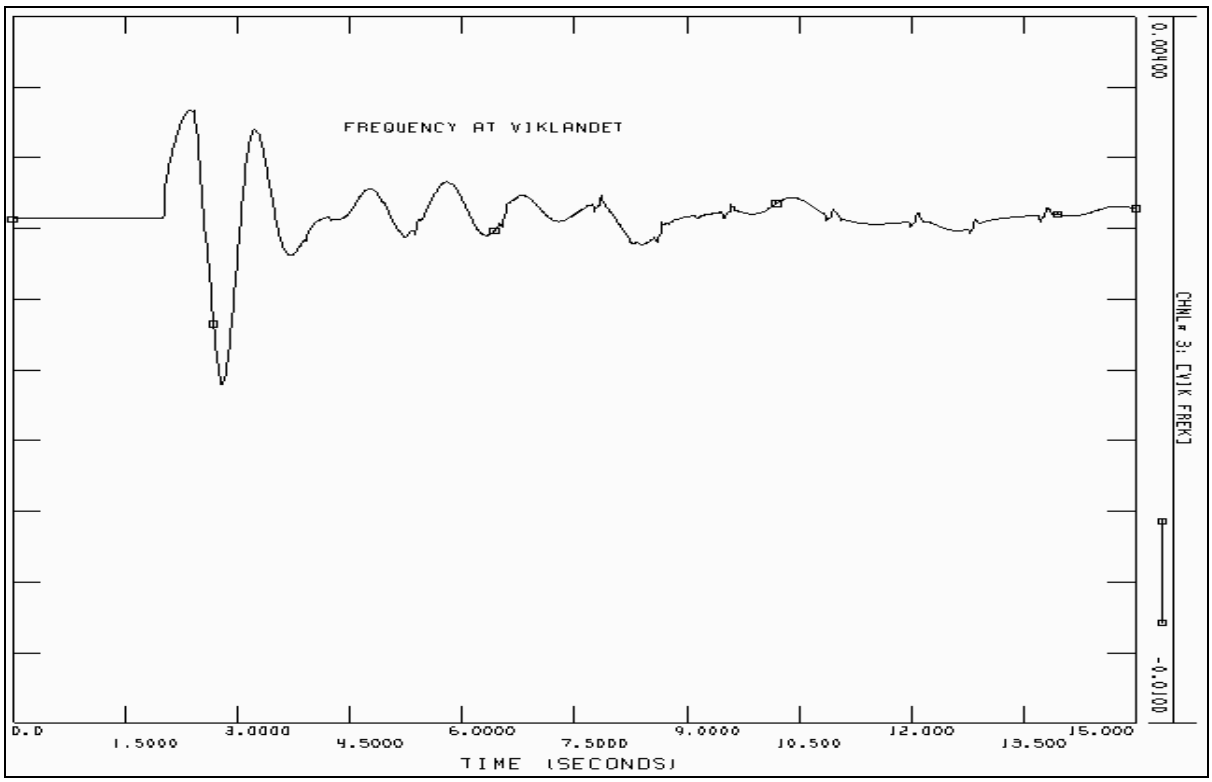

Figure 69 Frequency deviation [pu] at Viklandet with converter representation of Ormen Lange.

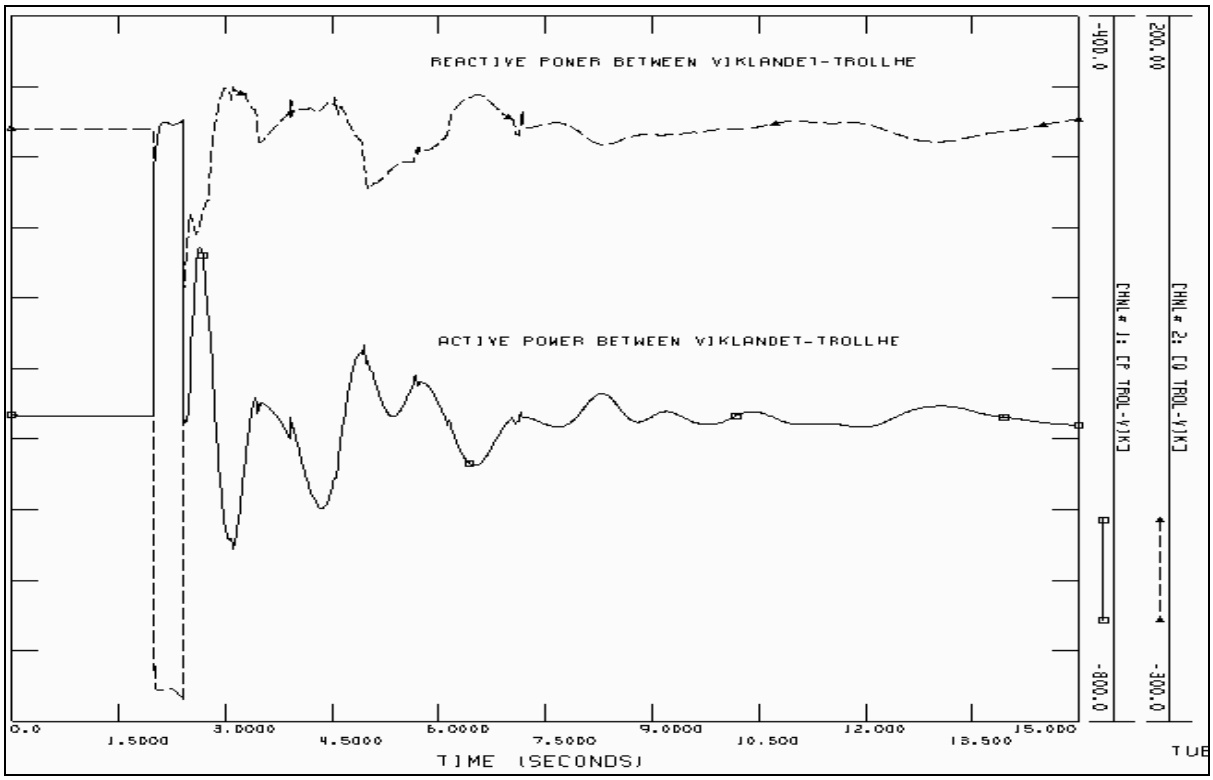

Figure 70 Active and reactive power between Viklandet and Trollhei with PQ representation of Ormen Lange. The units are [MW] and [MVAr] respectively.

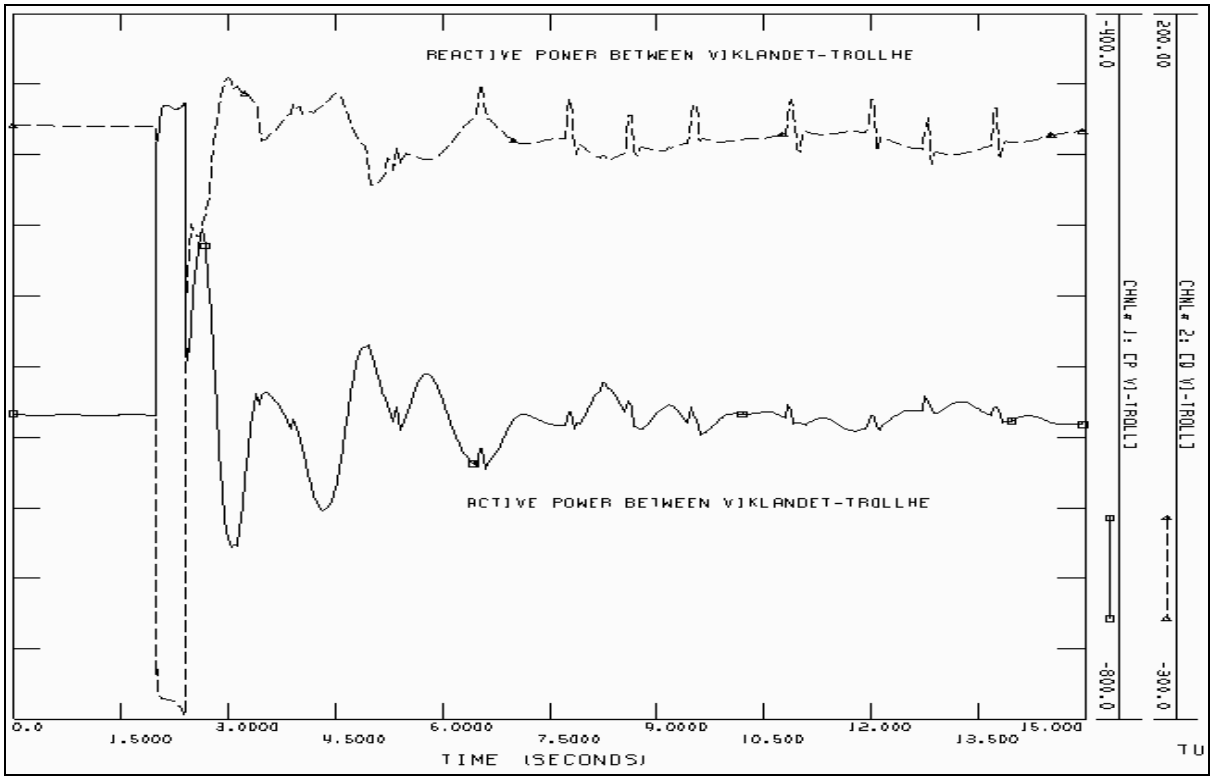

Figure 71 Active and reactive power between Viklandet-Trollhei with converter representation of Ormen Lange. The units are [MW] and [MVAr] respectively.

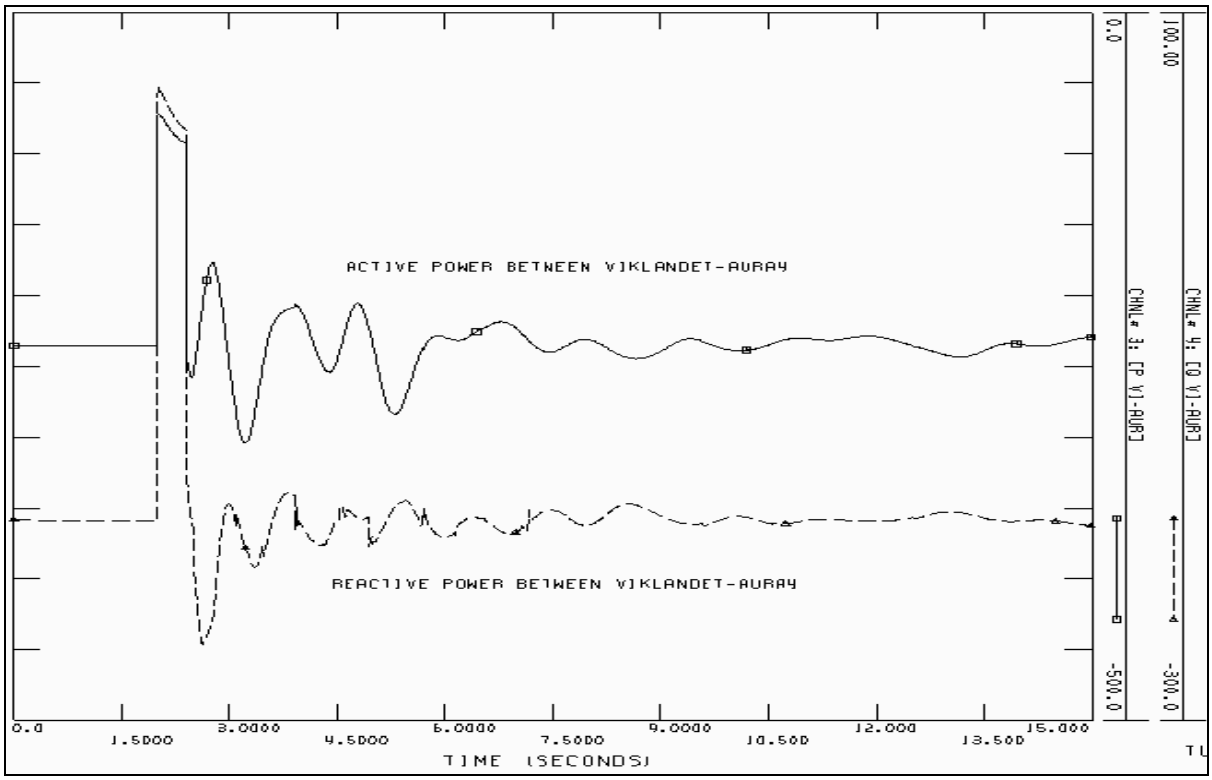

Figure 72 Active and reactive power between Viklandet-Aura4 with PQ representation of Ormen Lange. The units are [MW] and [MVAr] respectively.

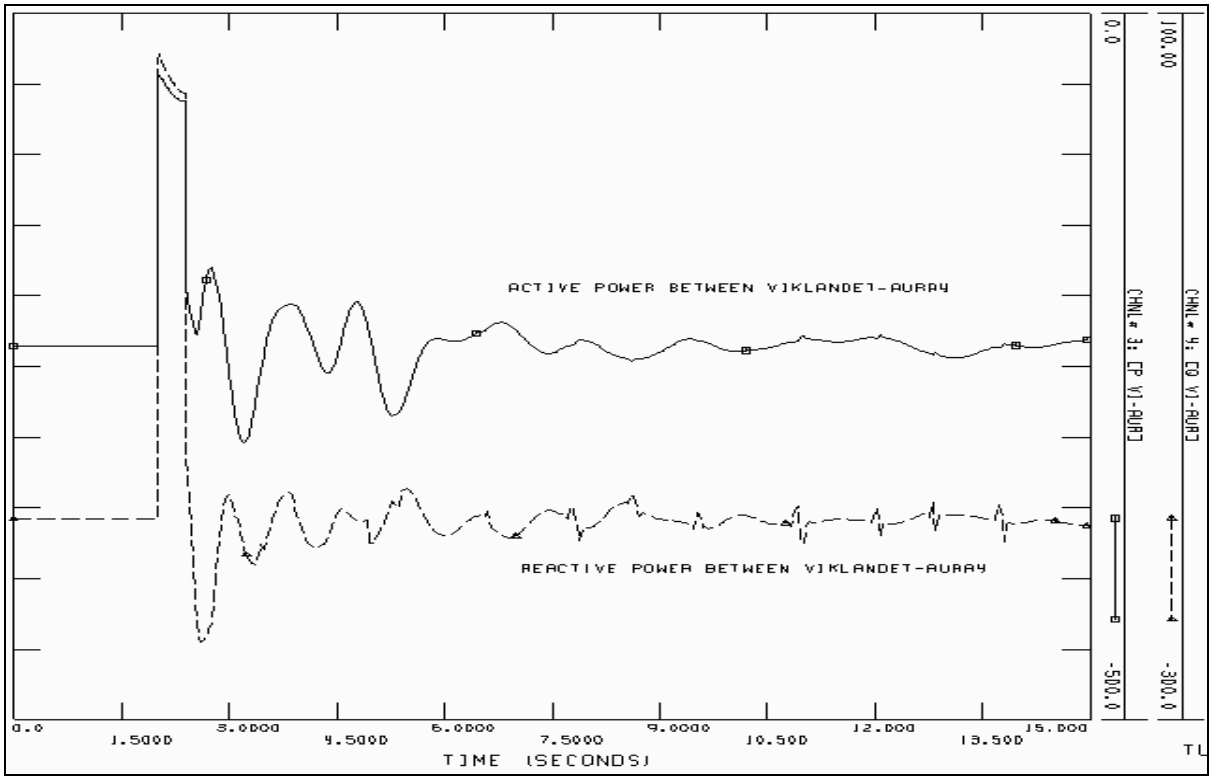

Figure 73 Active and reactive power between Viklandet-Aura4 with converter representation of Ormen Lange. The units are [MW] and [MVAr] respectively.

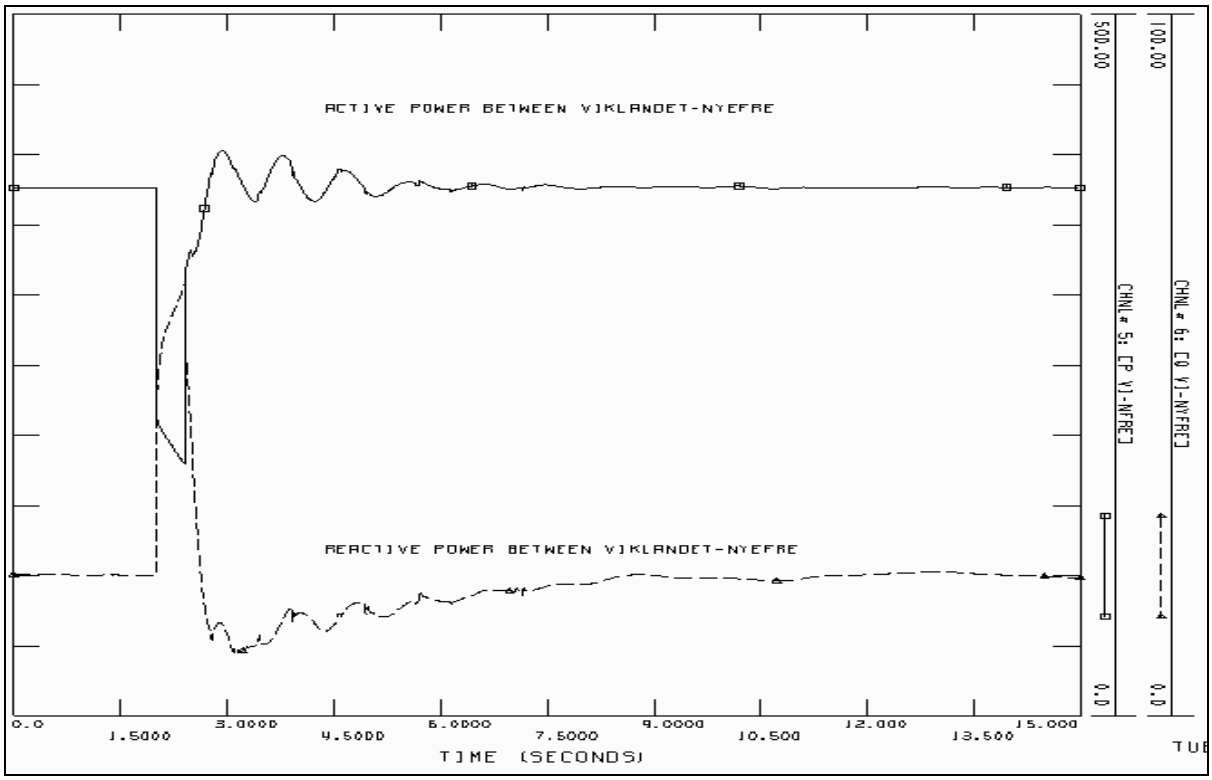

Figure 74 Active and reactive power between Viklandet-NyeFrena with PQ representation of Ormen Lange. The units are [MW] and [MVAr] respectively.

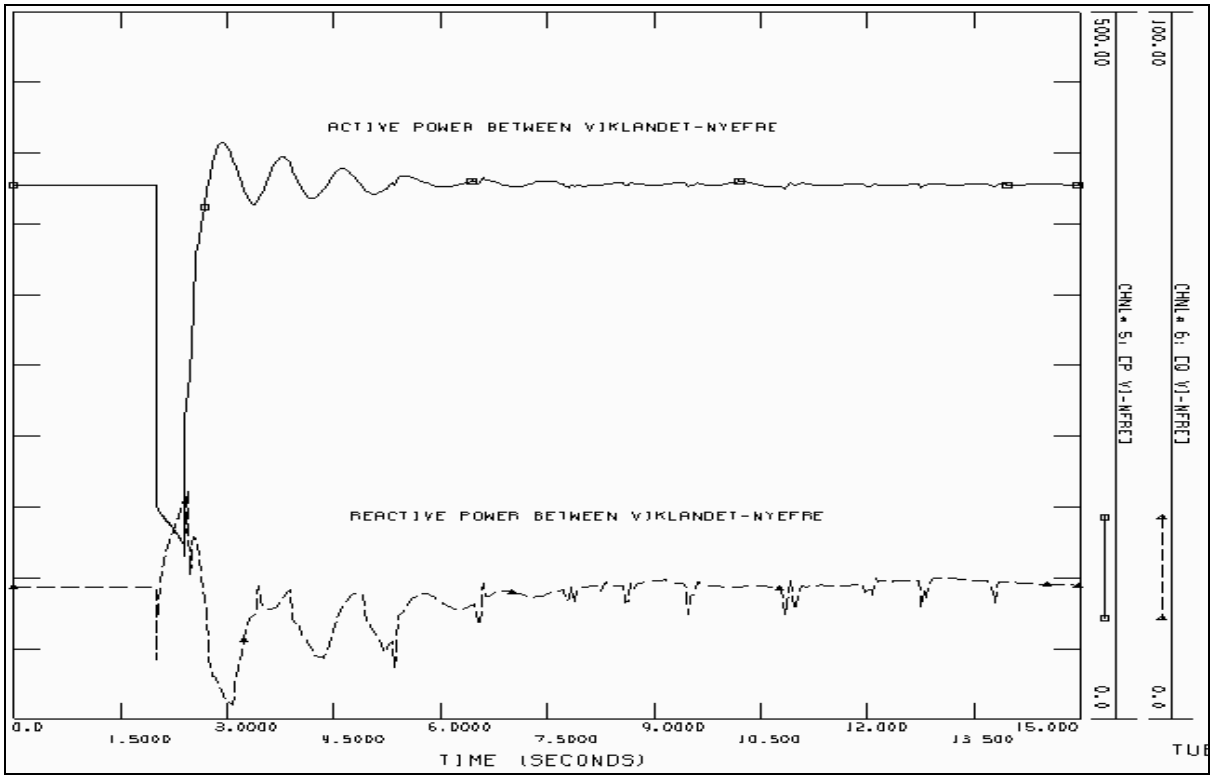

Figure 75 Active and reactive power between Viklandet-NyeFrena with converter representation of Ormen Lange. The units are [MW] and [MVAr] respectively.

Comparison of the response at Viklandet

Figure 66 to Figure 69 demonstrates how the bus voltage, bus phase angle and bus frequency deviation varies with time for both the PQ-model and the converter model. When comparing the response from these two models it becomes clear that the power system exhibits approximately the same response whether Ormen Lange is represented as a PQ-model or as a converter model. The only response which differs slightly when using a converter representation is the frequency deviation at Viklandet, see Figure 68 and Figure 69. The latter figures show that the frequency curve is "smoother" with a PQ- model. The frequency curve for the converter model has the same fundamental shape, however, the curve exhibits small irregularities analogous to the irregularities experienced at Nyhamna. Since momentary change in system frequency is unphysical, the latter fluctuation could be a result of numeric calculations in PSS/E. By reducing the time step of the simulation parameter, these fluctuations are reduced.

Figure 70 to Figure 75 illustrate the active and reactive power flow in three 400 kV lines going into Viklandet. The power flow in each line is shown for both the PQ-model and the converter model. The line between Viklandet-Trollhei is initially transmitting the greatest amount of active power into Viklandet. The active and reactive power flow in the latter line is illustrated in Figure 70 and Figure 71. By comparing the reactive power flow in the PQ-model and converter model, it becomes clear that the converter model exhibits substantial fluctuations in the reactive power flow. The amplitude of these fluctuations are approximately 40 MVAr and can not be found in the PQ-model. Hence, similar reactive power fluctuations found in the line between Nyhamn and DUM-TRAN are now reveled in the line between Viklandet-Trollhei. This result is expected since the line between Viklandet and Trollhei delivers a substantial amount of power to Ormen Lange. As previous stated, also these reactive fluctuations are a result of the varying rectifier firing delay angle, and consequently, the varying reactive consumption of the rectifiers at Ormen Lange.

When analyzing the active power flow between Viklandet and Trollhei in Figure 70 and Figure 71, fluctuations with the converter model can be observed. These fluctuations are a result of the relatively large reactive power fluctuations. When the reactive power flow increases, this causes increased losses and reduction in bus voltages. Consequently, active power fluctuations are experienced in the same transmission line.

Also the line between Viklandet-Aura4, see Figure 72 and Figure 73, contain reactive power fluctuations with the converter model. Due to less initial loading, the amplitude of the latter fluctuations are smaller than for Viklandet-Trollhei.

When analyzing the power flow between Viklandet-NyeFrena in Figure 74 and Figure 75, it becomes clear that both the active and reactive power differs in the period when the fault is applied. Due to shutdown of the converters, the drop in active power transfer is greater for the converter model than for the PQ-model. The shutdown also results in a greater deflection in reactive power during the fault period, i.e. $2.0 < t < 2.4$, for the PQ- model. The period after the fault is removed, the converter model exhibits greater reactive power fluctuations than the PQ-model. As described earlier, these fluctuations are a direct consequence of the fluctuations in rectifier firing delay angle, illustrated in Figure 65.

7.4.2 Results from Case F

This section presents the simulation results at Nyhamna and Viklandet, respectively.

7.4.2.1 Response at Nyhamna

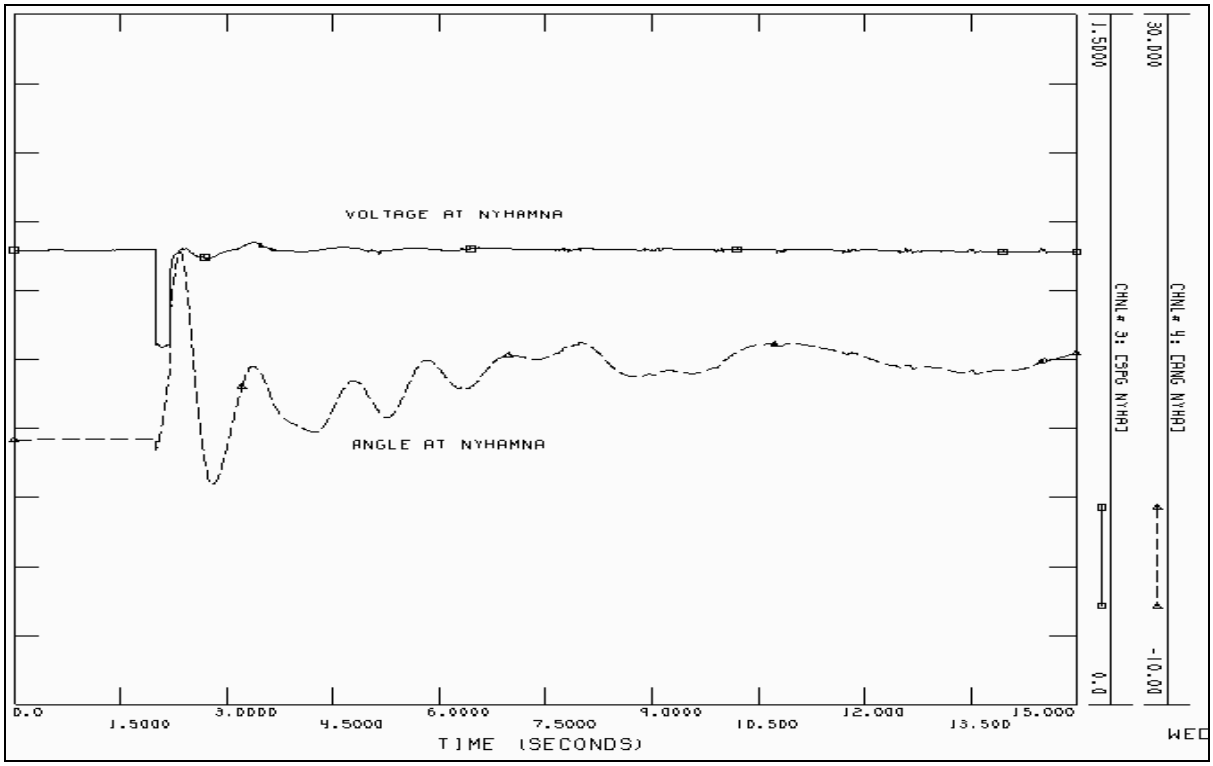

Figure 76 Bus voltage [pu] and bus phase angle [degrees] at Nyhamna with PQ representation of Ormen Lange.

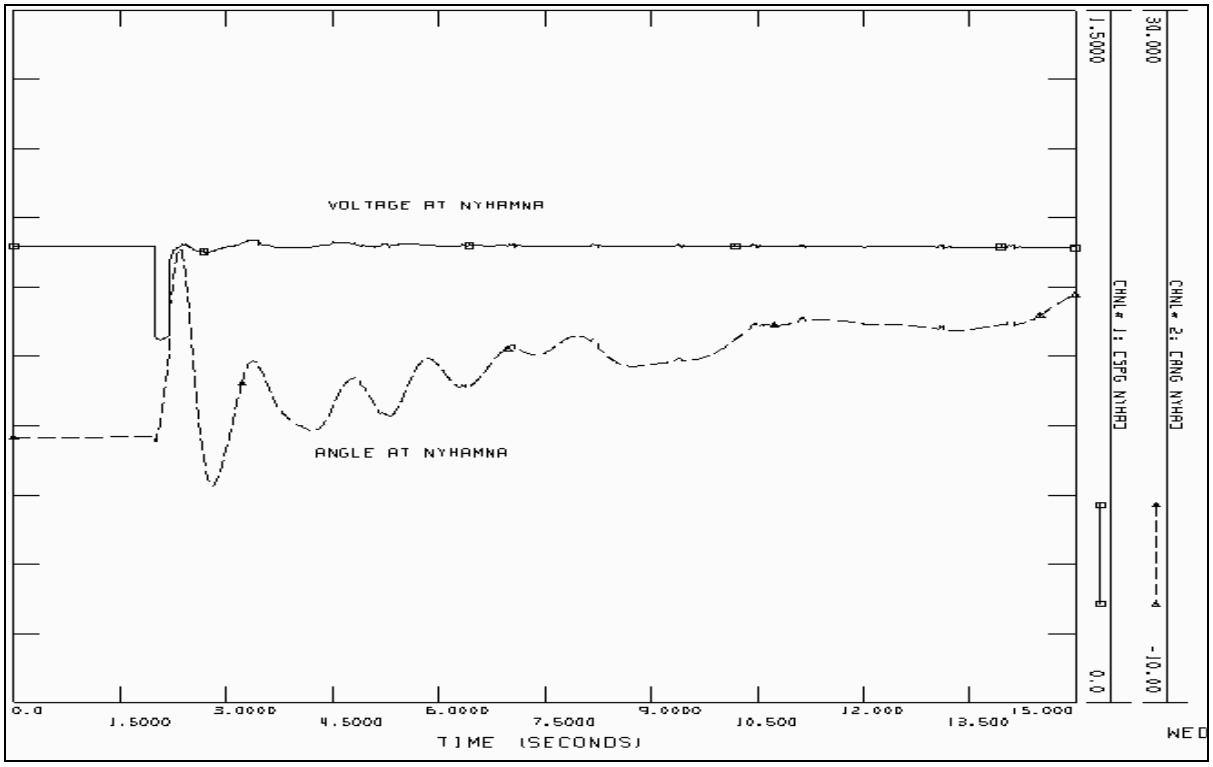

Figure 77 Bus voltage [pu] and bus phase angle [degrees] at Nyhamna with converter representation of Ormen Lange.

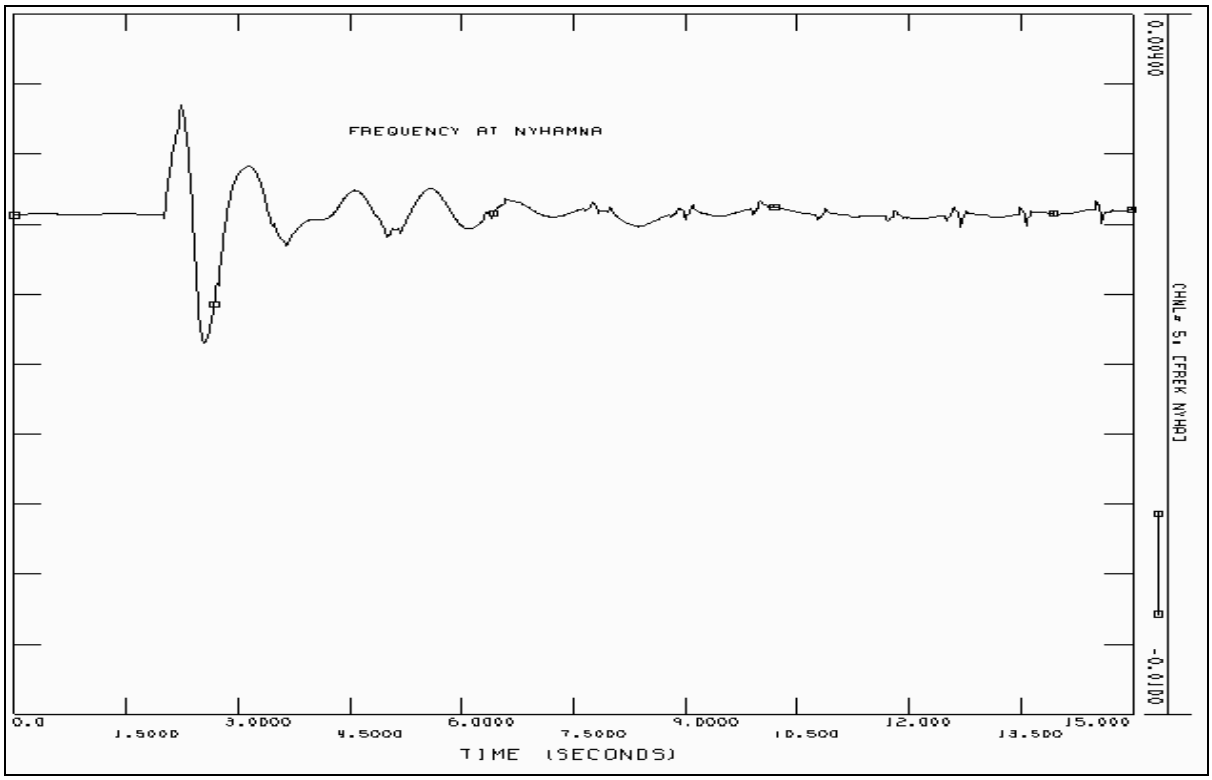

Figure 78 Frequency deviation [pu] at Nyhamna with PQ representation of Ormen Lange.

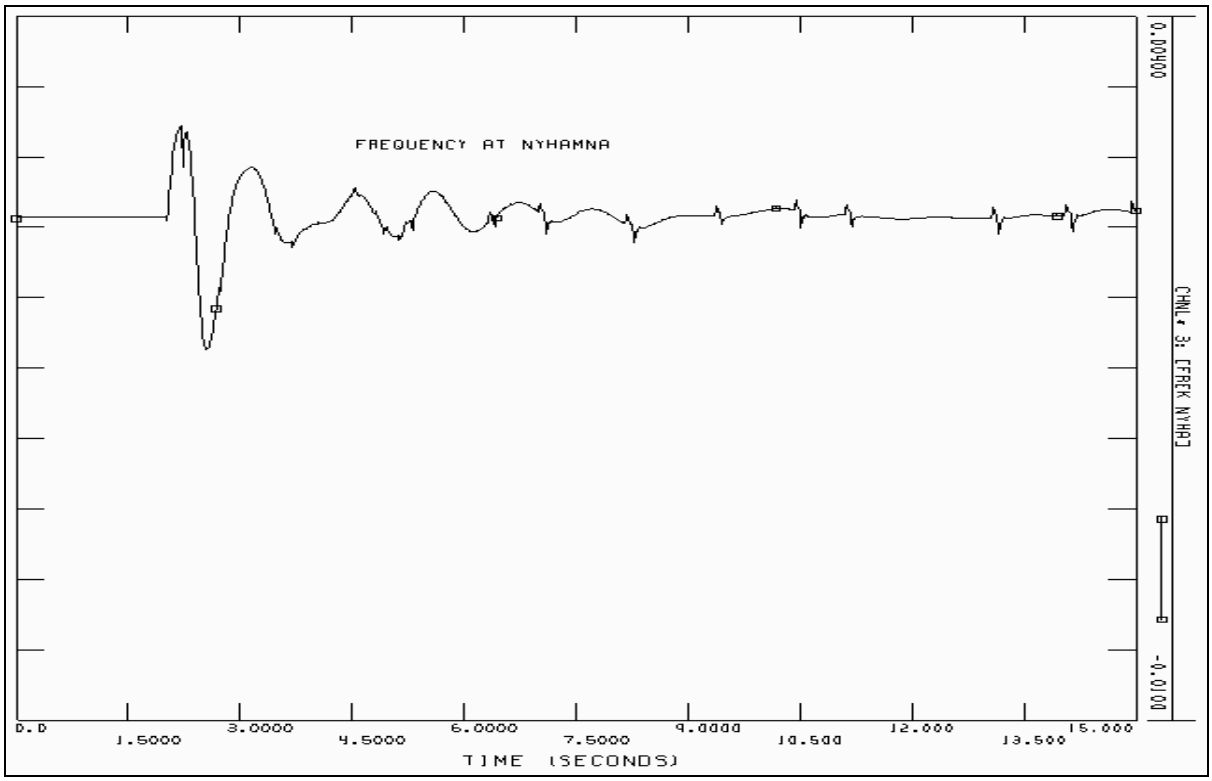

Figure 79 Frequency deviation [pu] at Nyhamna with converter representation of Ormen Lange.

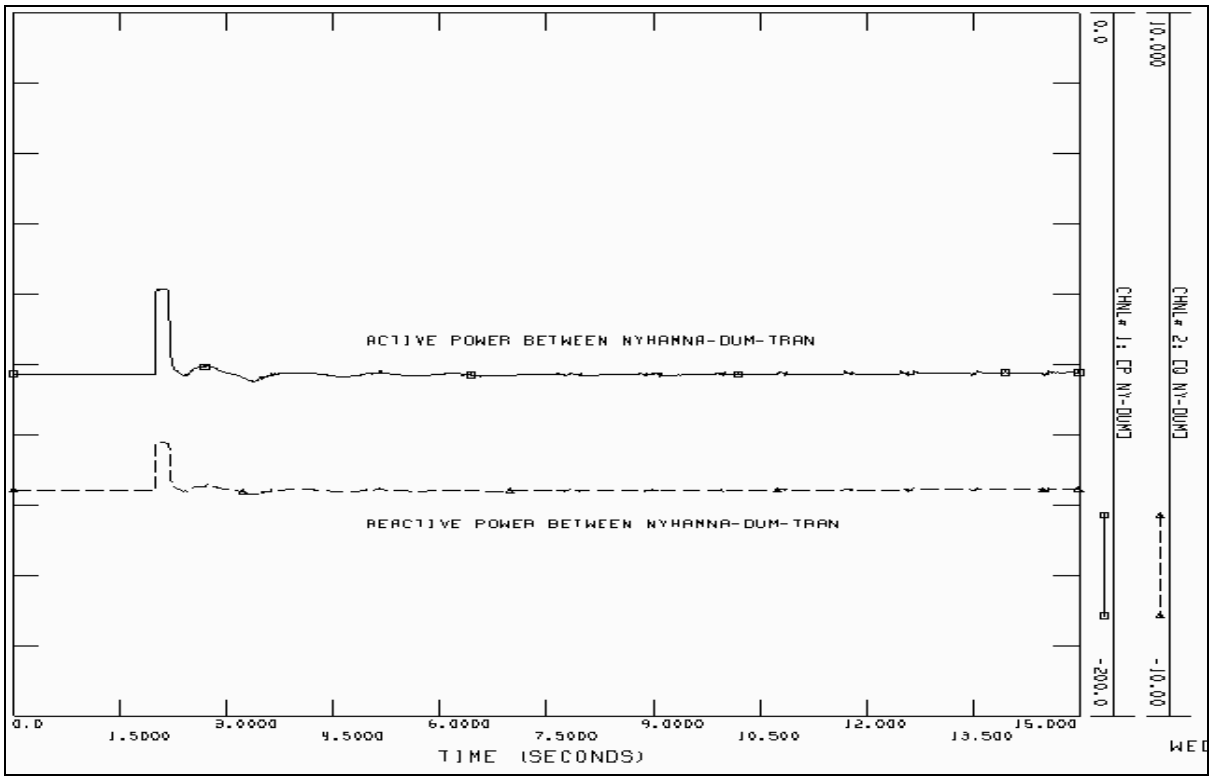

Figure 80 Active and reactive power between Nyhamna and DUM-TRAN with PQ representation of Ormen Lange. The units are [MW] and [MVAr] respectively.

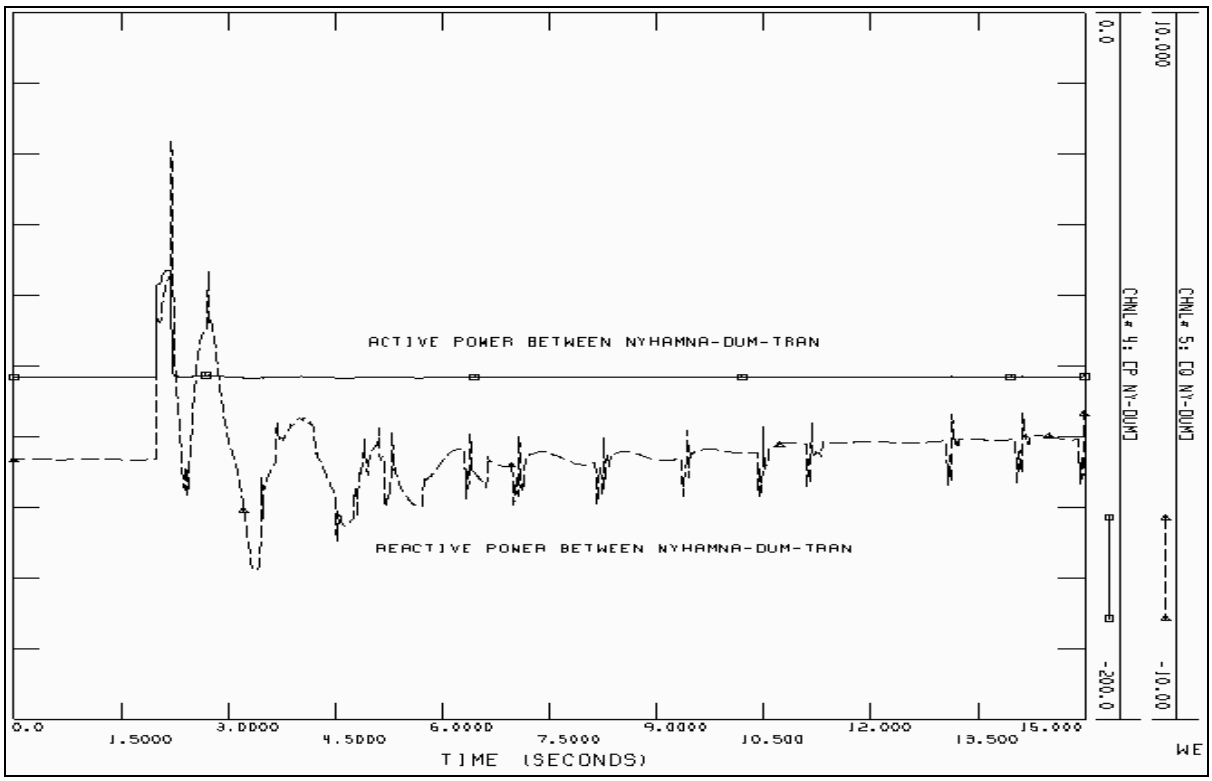

Figure 81 Active and reactive power between Nyhamna and DUM-TRAN with converter representation of Ormen Lange. The units are [MW] and [MVAr] respectively.

Comparison of the response at Nyhamna

Case F, apposed to Case E, does not cause sufficient voltage depression at Nyhamna to result in a shutdown of the converters. However, the fault introduced in Case F forces the rectifiers to lose control of the dc current. As the fault is removed, the rectifiers regain control of the dc current.

The results given in Figure 76 and Figure 77 illustrate that the bus voltage and bus phase angle at Nyhamna exhibits approximately identical responses with the PQ-model and with the converter model. This is analogue to the corresponding response in Case E. However, apposed to Case E, the phase angle at Nyhamna also exhibits the same profile during fault in both PQ-model and converter model. This is because the converters do not shutdown in Case F. Hence, the active power consumption at Ormen Lange is not reduced to the same extent as in Case E. Consequently, Figure 76 and Figure 77 have similar phase angle profiles, also during the fault period.

As in Case E, the frequency deviation at Nyhamna is similar for the PQ- model and the converter model. The latter can be seen in Figure 78 and Figure 79. Note, in Case F both models exhibit irregularities in the frequency deviation curve. This implies that the irregularities in not a result of the converter model, but rather a result of numeric calculations in PSS/E.

Figure 80 and Figure 81 illustrate the active and reactive power between Nyhamna and DUM-TRAN for the PQ-model and the converter model, respectively. By first evaluating the active power flow in the latter two models, it becomes clear that the power exhibits similar profiles for both models. However, the amplitude of the "fault-peak" is somewhat larger in the converter model. This is a direct result of the rectifier's loss of current control during the fault. Hence, the reduction in dc current causes a reduction in transferred power through the dc link.

As in Case E, the reactive power flowing between Nyhamna and DUM-TRAN differs greatly when using the PQ-model and the converter model, see Figure 80 and Figure 81. By first evaluating the period $2.0 < t < 2.2$ when the fault is applied, Figure 81 shows that the reactive power flow changes direction. Reactive power is now being delivered from Ormen Lange to the ac system. This is analogue to the situation that occurred in Case E. As the rectifiers loses control of the dc current, the rectifier firing delay angle is reduced to its minimum, and consequently, the reactive consumption of the rectifiers are reduced. This causes a reactive power surplus at Nyhamna, which explains the change in power flow direction. Evidently, the latter is only valid for the converter model.

After fault clearance, i.e. $t > 2.2$ seconds, the converter model in Figure 81 exhibits large fluctuations in reactive power flow between Nyhamna and DUM-TRAN. Similar fluctuations are not experienced with the PQ-model, see Figure 80. The amplitude of the fluctuations are relatively large compared to the pre fault power flow.

As in Case E, the understanding of these reactive fluctuations can be facilitated through Figure 82. The figure shows the rectifier firing delay angle (alpha) and the reactive power between Nyhamna and DUM-TRAN. Also in this case, the fluctuations in reactive power

flow correspond to the fluctuations in alpha. The greatest deflections in alpha can be observed in the period $2.0 < t < 3.4$, which corresponds to the period where the reactive fluctuations are greatest. A reduction in alpha causes a reduction in reactive power consumption. This can be verified by studying Figure 82 in the time period $2.0 < t < 2.2$.

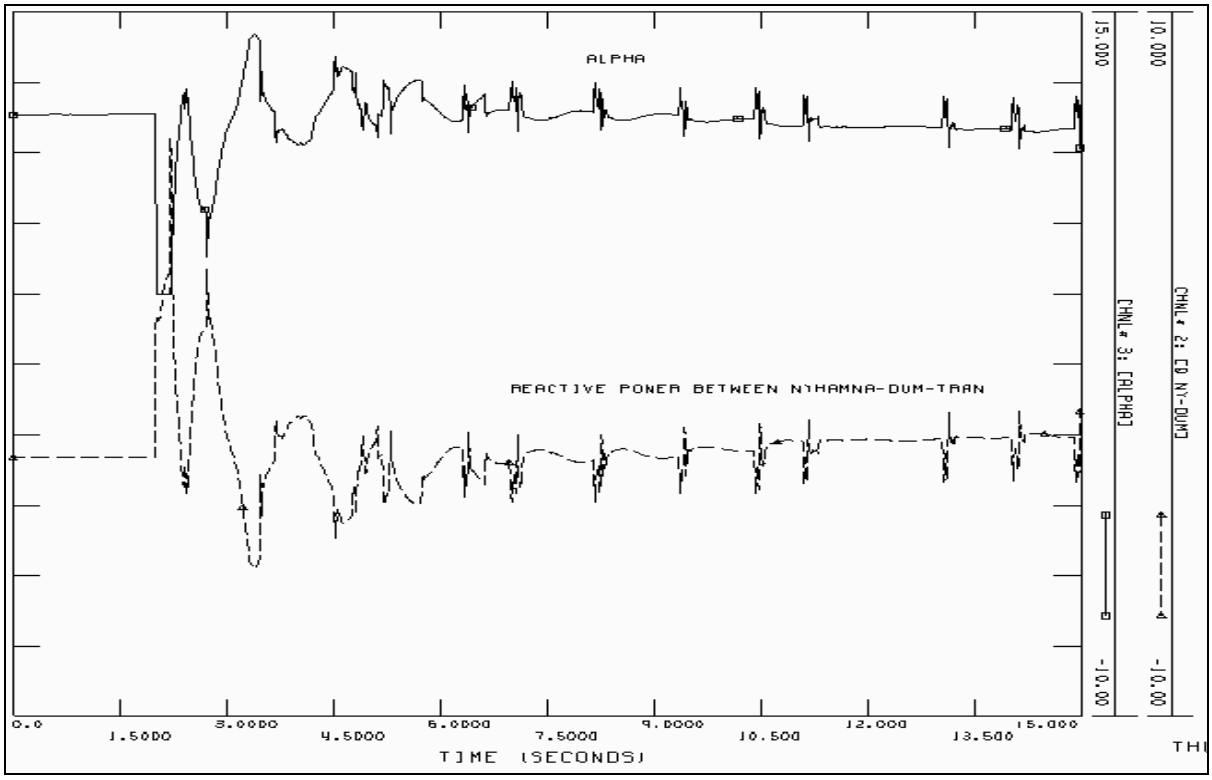

Figure 82 Rectifier firing delay angle [degrees] and reactive power [MVAr] between Nyhamna and DUM-TRAN with the converter model.

7.4.2.2 Response at Viklandet

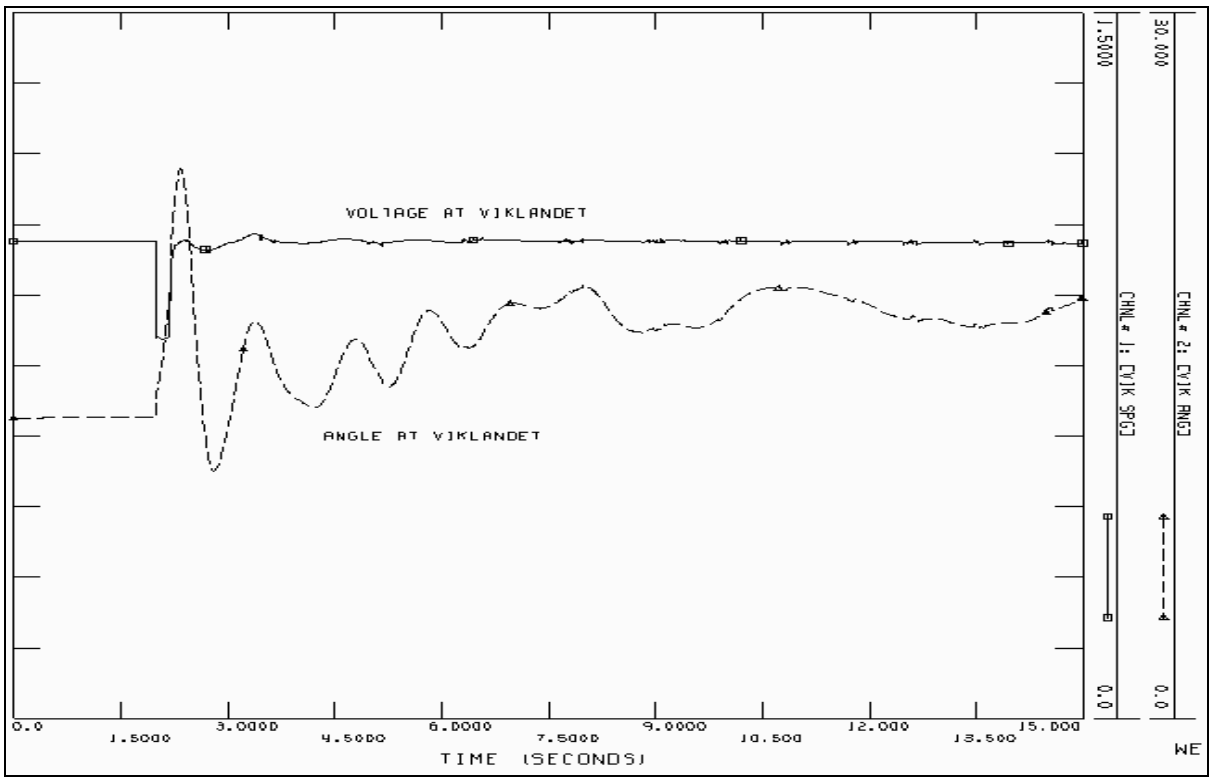

Figure 83 Bus voltage [pu] and bus phase angle [degrees] at Viklandet with PQ representation of Ormen Lange.

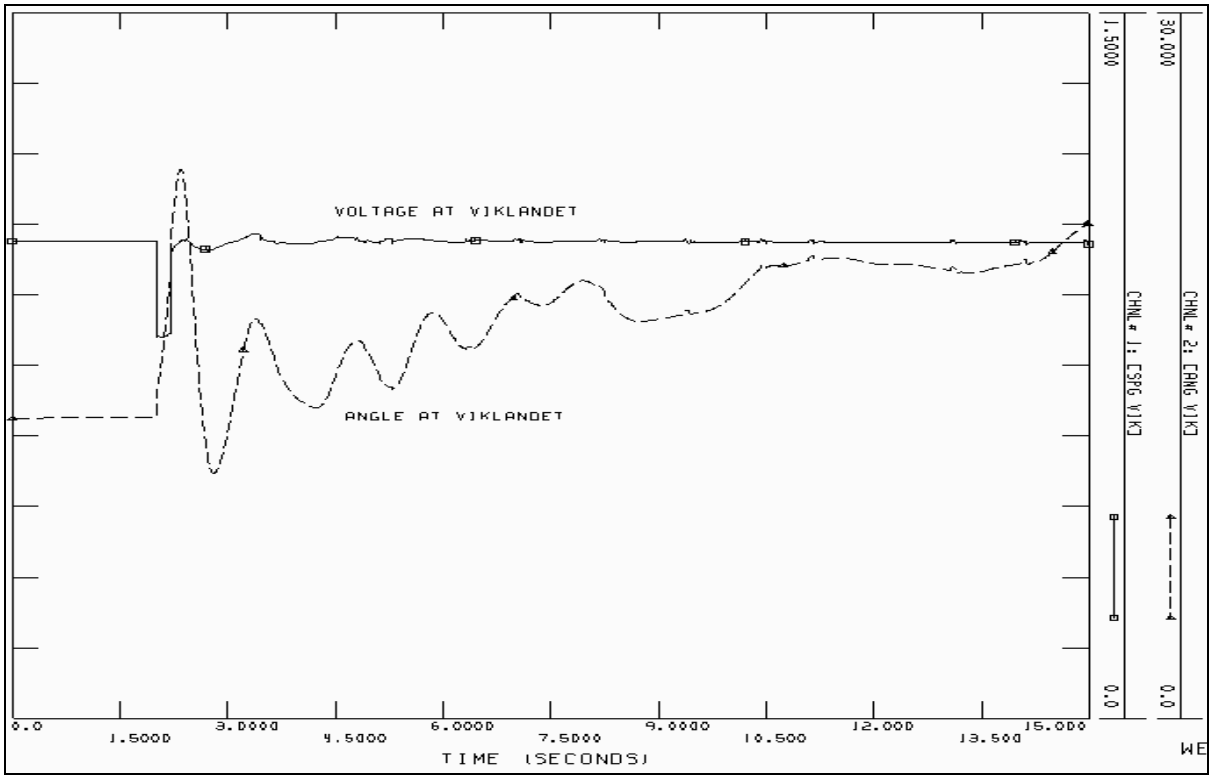

Figure 84 Bus voltage [pu] and bus phase angle [degrees] at Viklandet with converter representation of Ormen Lange.

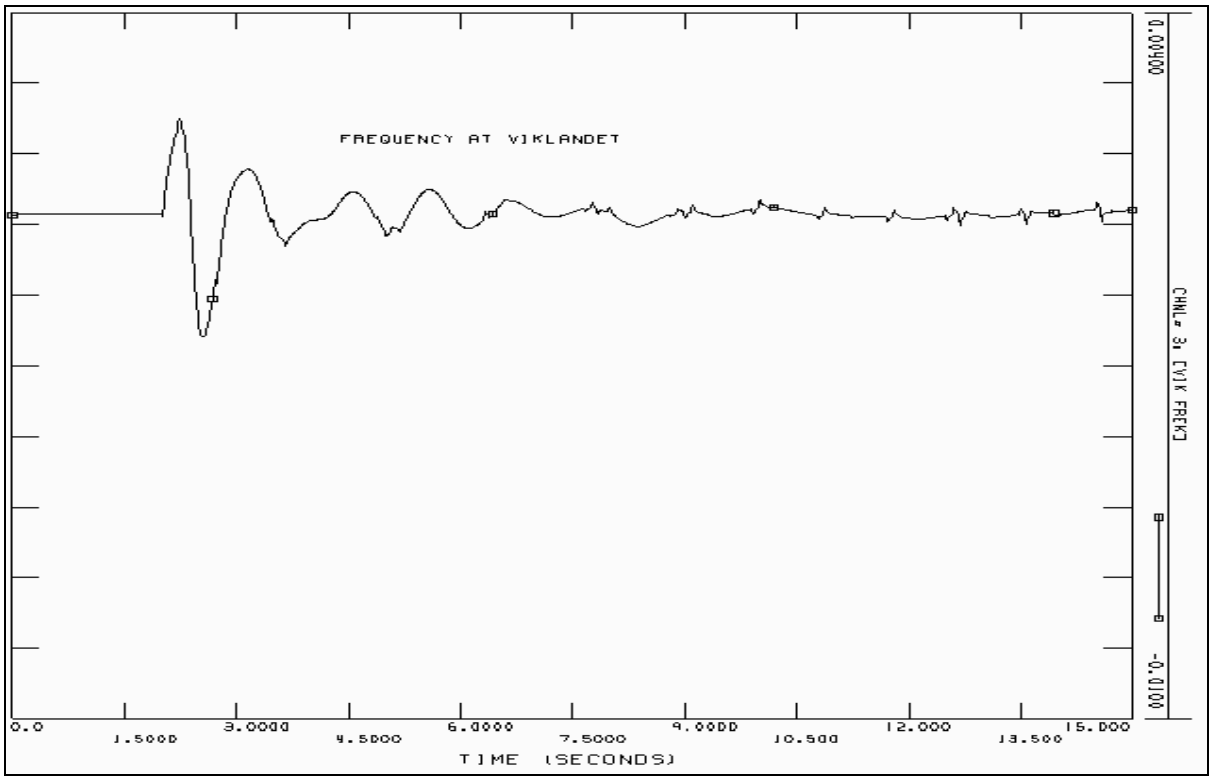

Figure 85 Frequency deviation [pu] at Viklandet with PQ representation of Ormen Lange.

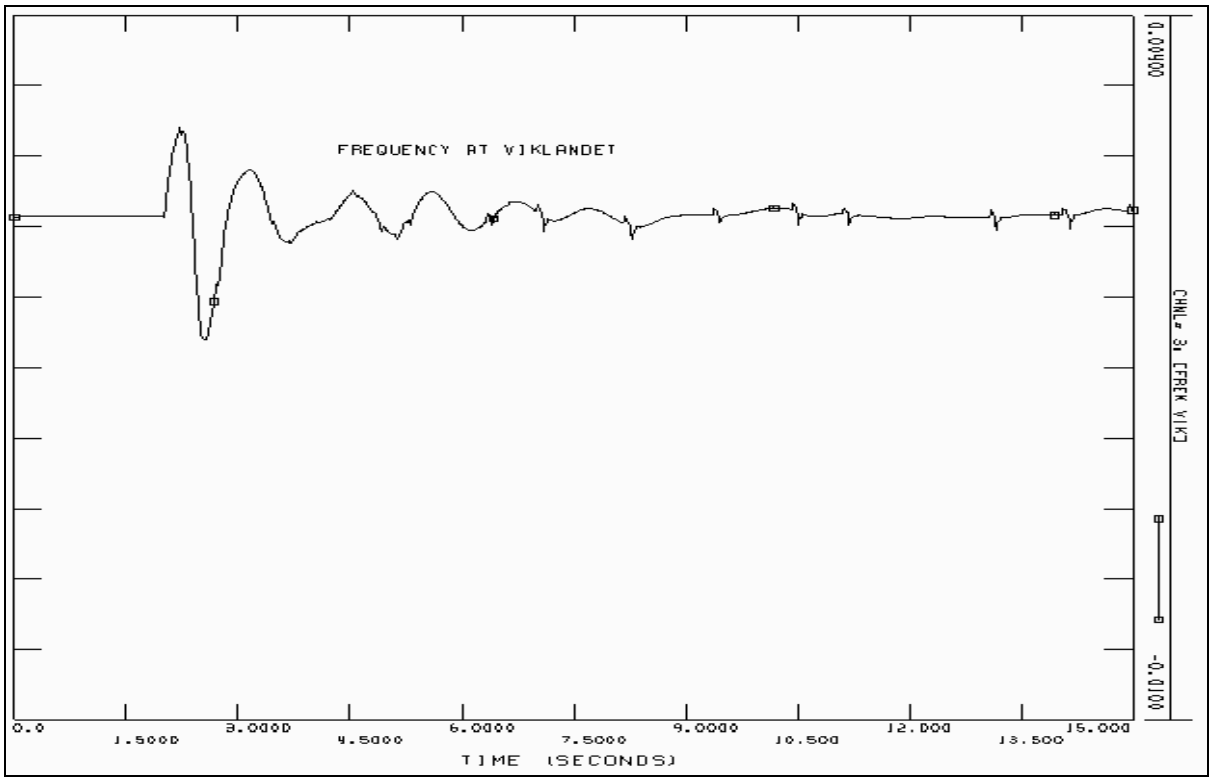

Figure 86 Frequency deviation [pu] at Viklandet with converter representation of Ormen Lange.

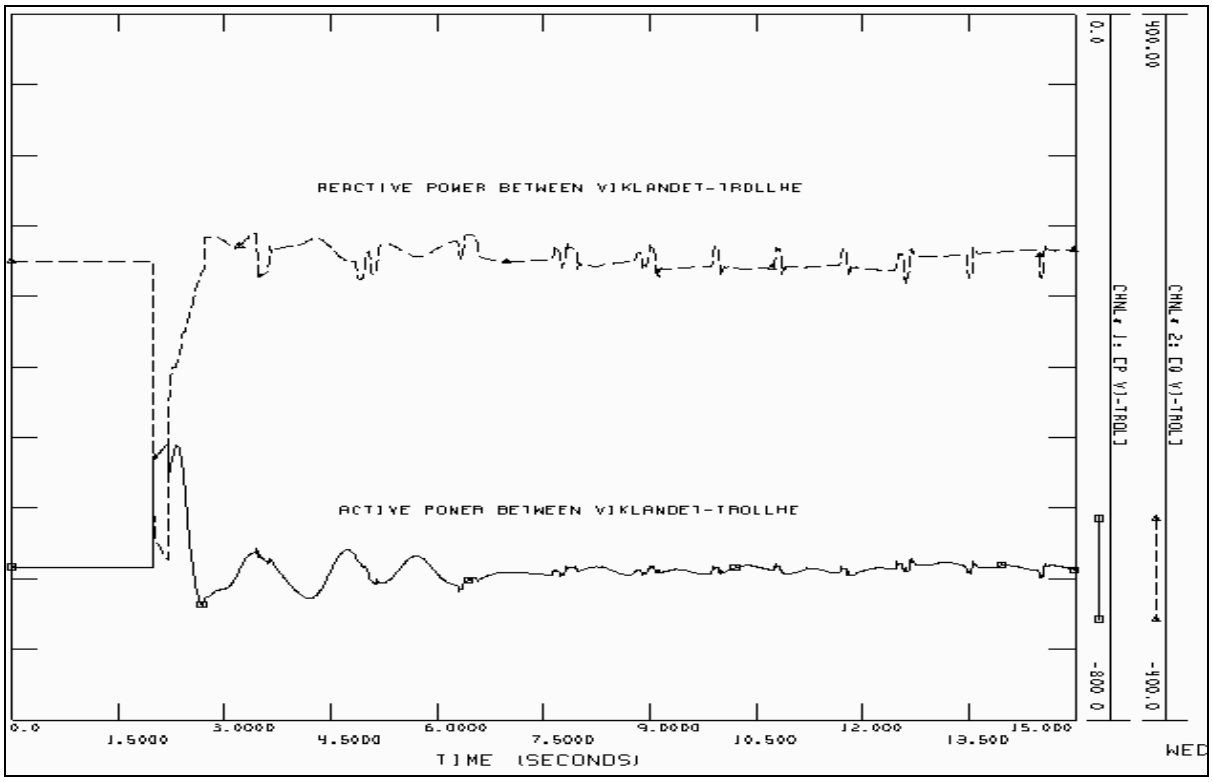

Figure 87 Active and reactive power between Viklandet and Trollhei with PQ representation of Ormen Lange. The units are [MW] and [MVAr] respectively.

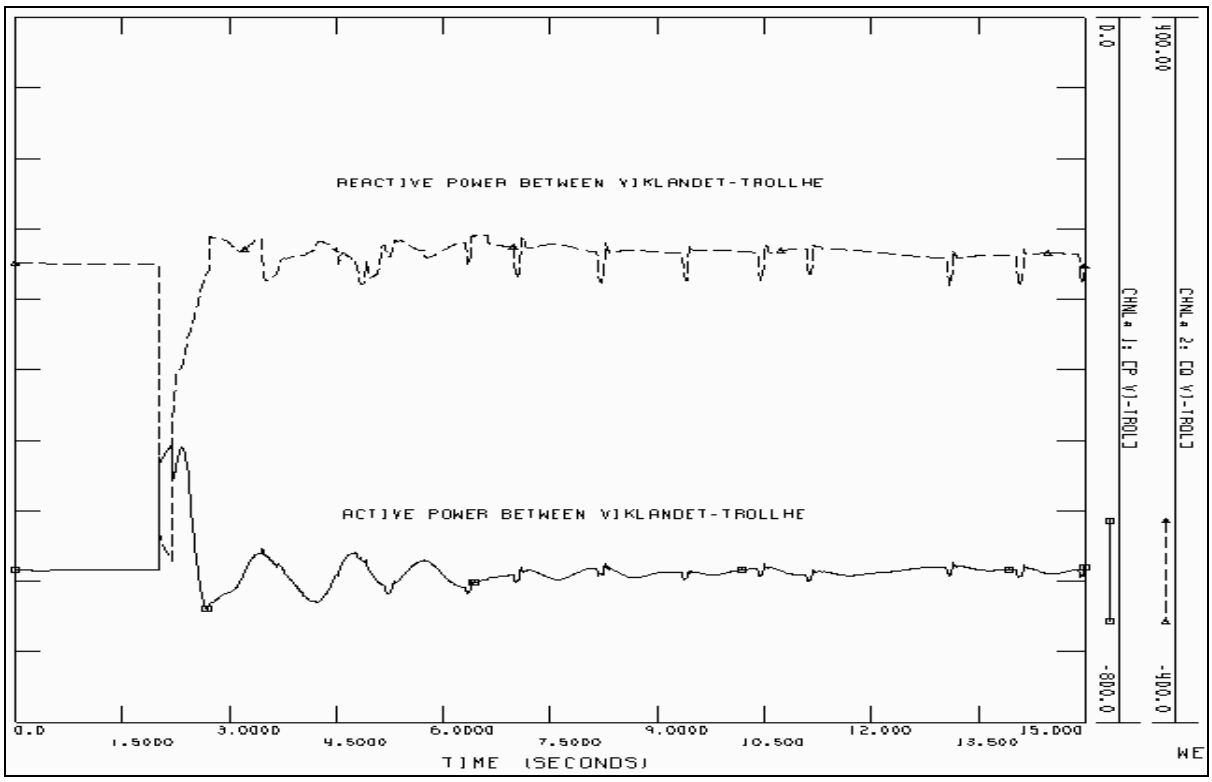

Figure 88 Active and reactive power between Viklandet and Trollhei with converter representaion of Ormen Lange. The units are [MW] and [MVAr] respectively.

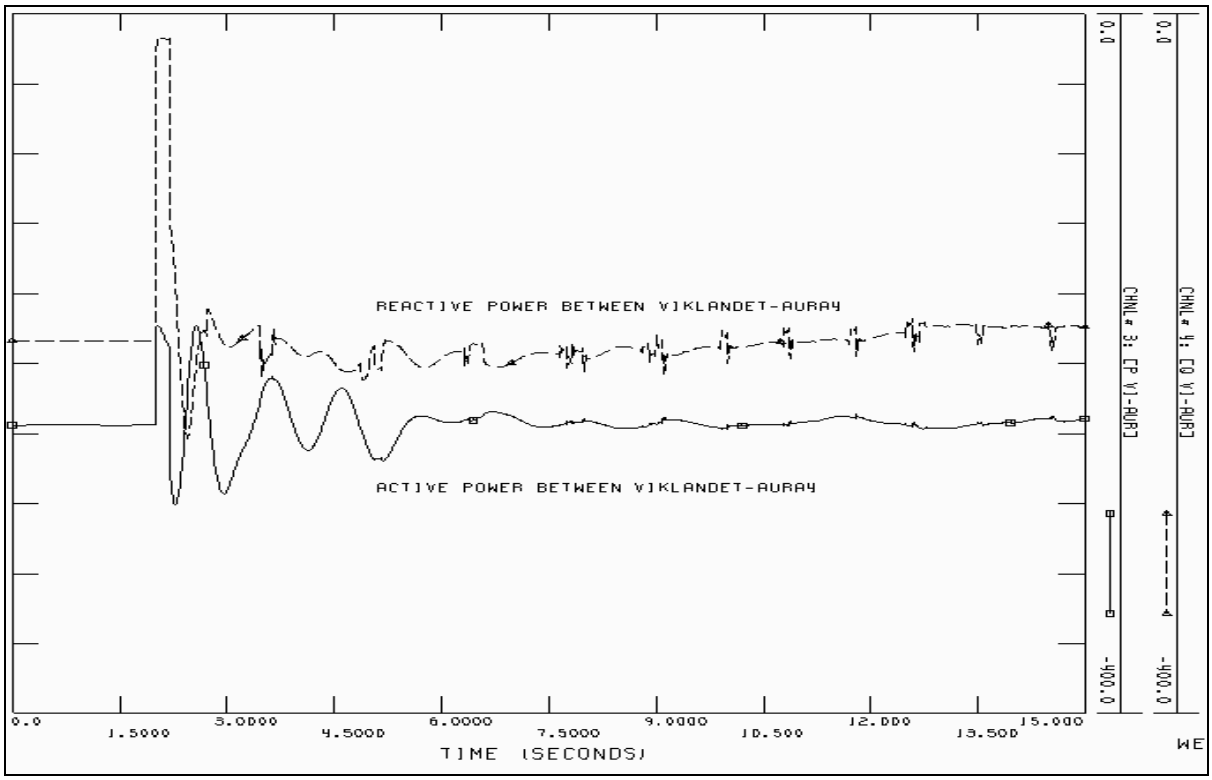

Figure 89 Active and reactive power between Viklandet and Aura4 with PQ representation of Ormen Lange. The units are [MW] and [MVAr] respectively.

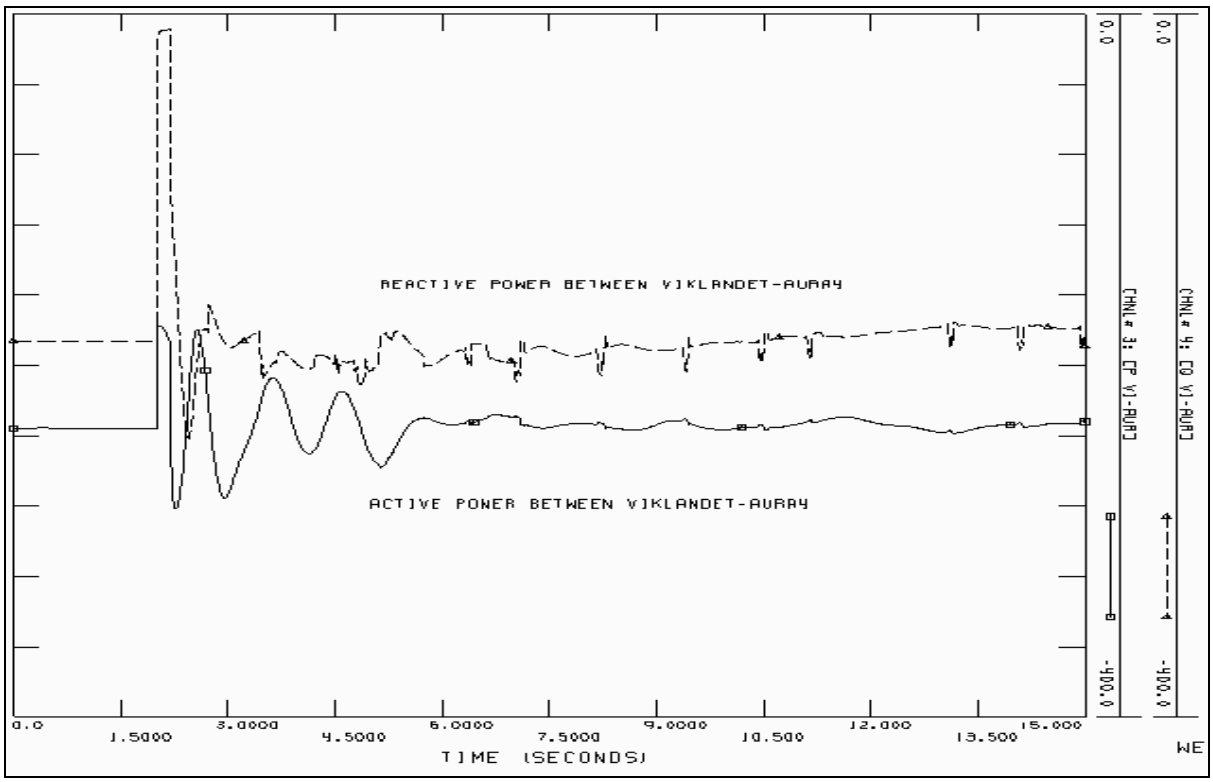

Figure 90 Active and reactive power between Viklandet and Aura4 with converter representation of Ormen Lange. The units are [MW] and [MVAr] respectively.

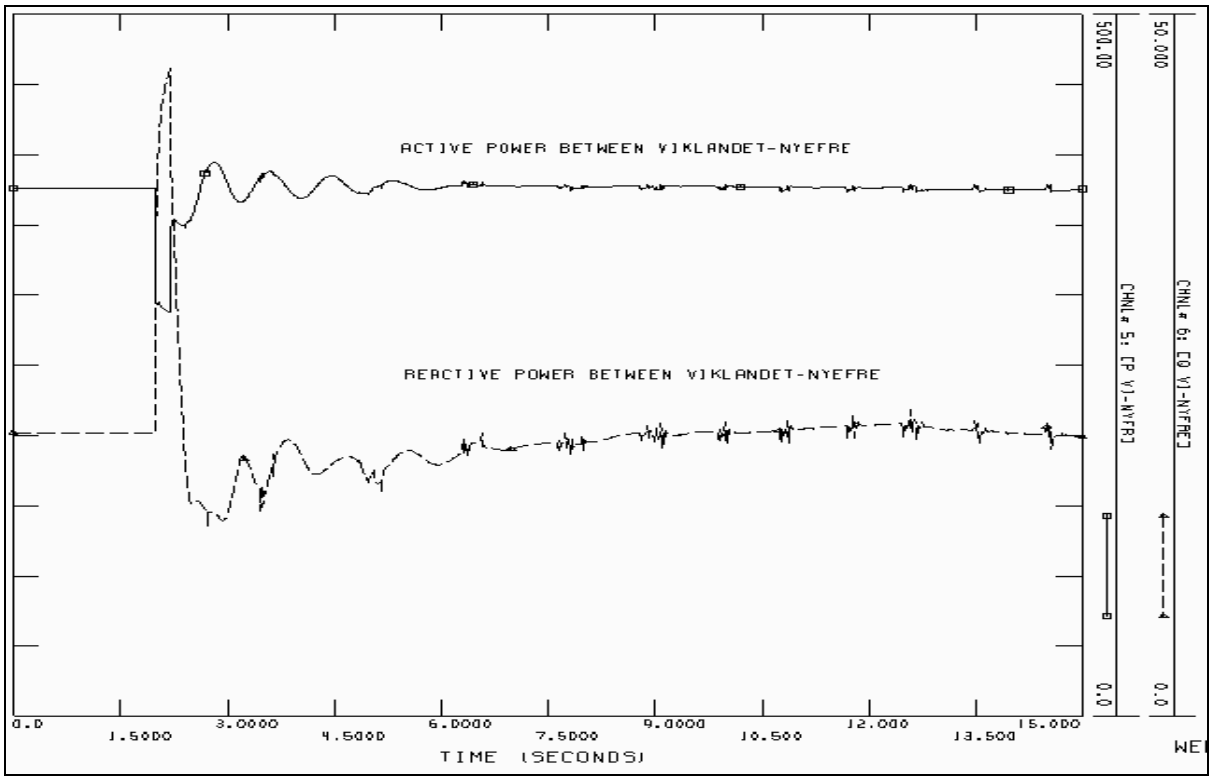

Figure 91 Active and reactive power between Viklandet and NyeFrena with PQ representation of Ormen Lange. The units are [MW] and [MVAr] respectively.

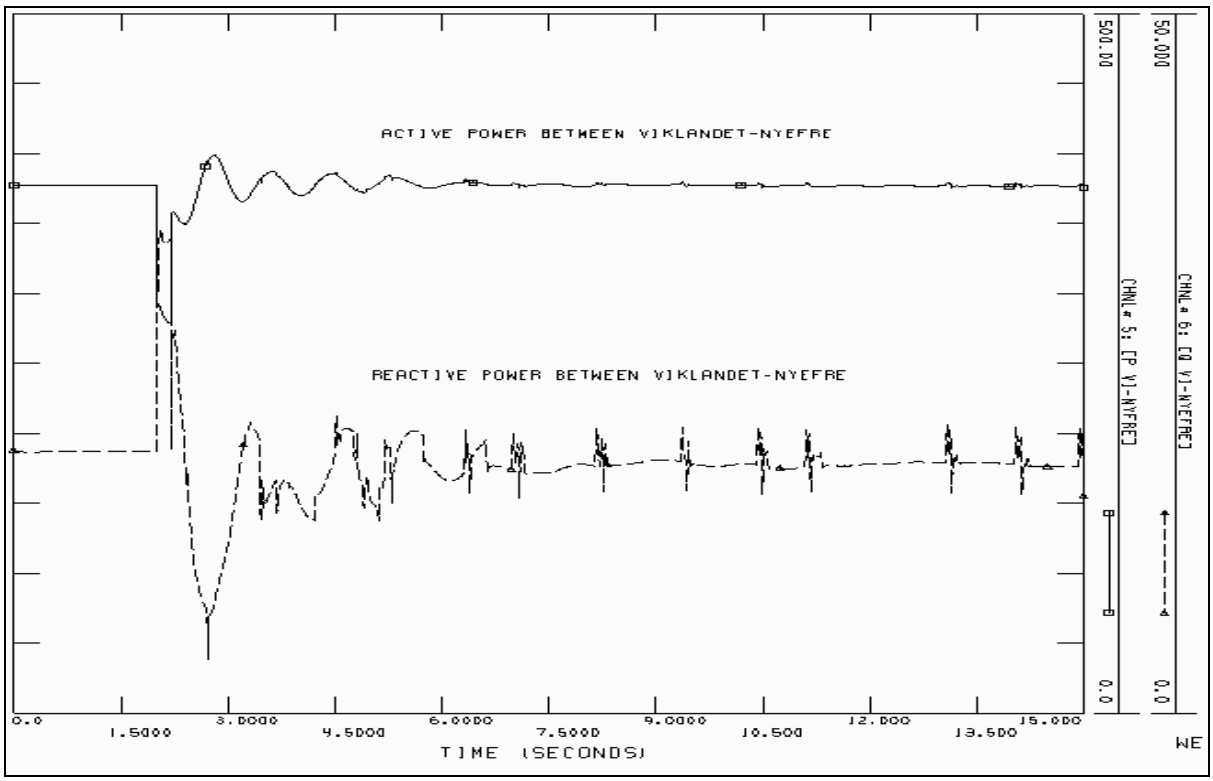

Figure 92 Active and reactive power between Viklandet and NyeFrena with converter representation of Ormen Lange. The units are [MW] and [MVAr] respectively.

Comparison of the response at Viklandet

Figure 83 to Figure 86 illustrate how the bus voltage, phase voltage and bus frequency deviation varies with time for the PQ-model and the converter model at Viklandet. By evaluating the response from these models, it becomes clear that the power system exhibits approximately the same response whether a PQ-model or a converter model is utilized.

Figure 87 to Figure 92 illustrate the active and reactive power flow in three 400 kV lines going into Viklandet. The power flow in each line is shown for the PQ-model and the converter model. The line between Viklandet and Trollhei is initially transmitting the greatest amount of power into Viklandet. The active and reactive power flow in the latter line is shown in Figure 87 and Figure 88. These figures show that the PQ-model and the converter model exhibit similar behavior after the fault is applied and cleared. Both the PQ-model and converter model contains power fluctuations after fault clearance. The latter is especially true for the reactive power flow. However, it is worth noticing that the fluctuations in reactive power for the converter model, see Figure 88, corresponds in time with the fluctuations between Nyhamna and DUM-TRAN, see Figure 81.

Also the line between Viklandet-Aura4 exhibits the same principal behavior as described for Vikland-Trollhei, see Figure 89 and Figure 90. Hence, the PQ-model and the converter model exhibit similar behavior. Both models have fluctuations in reactive power, however, at different point in time.

The active and reactive power between Viklandet-NyeFrena differs when using the converter model, see Figure 91 and Figure 92. This is analogue to the situation described in Case E. Even though Case F does not cause shutdown for the converters, the rectifiers loss of current control causes similar response as in Case E. The reactive fluctuations in Figure 92 are also a consequence of the rectifier firing delay angle illustrated in Figure 82.

7.5 General Considerations

The previous sections have analyzed the principal system response when a PQ-model and converter model is used to represent Ormen Lange. The results obtained from these analyses have shown that the main difference between these two models is the generation of reactive power fluctuations. As far as the ac system is concerned, the converter model is perceived as a varying reactive load, which again causes the reactive fluctuations exhibited in the previous sections. To illuminate why the response from the converter model only differs from the PQ-model in terms of reactive fluctuations, consider the subsequent sections.

The strength of ac/dc junction at Nyhamna

In Section 2.6 the term short circuit ratio (SCR) was introduced as a fundamental indication of the strength of the ac/dc connection. The latter section also presented a classification of the strength based on the numerical value of SCR, with the problems associated with a weak ac/dc connection. The reader may refer to Section 2.6 for a detailed description.

In order to obtain an indication of the strength of the ac/dc connection at Nyhamna, Appendix C contains a simplified calculation of the short circuit capacity and SCR at Nyhamna. These

calculations are simplified and only intended to give an indication of the ac/dc strength. With reference to Appendix C, the SCR was calculated to be 11.15. According to Section 2.6, a system with SCR=11.15 is characterized as strong.

The results from the SCR calculation cannot, and will not, be solely used as an explanation for why the ac system exhibits similar response whether a PQ-model or a converter model are utilized. At best, this SCR evaluation can be used to substantiate the results obtained in this chapter.

The complexity of the converter model used in PSS/E

The dynamic converter model used in this thesis is called CDC4T. As described in Chapter 5 and Section 6.5, CDC4T is based upon pseudo-steady state relationships. This means that the model represents dynamic conditions using relationships which are technically valid only for steady-state conditions. Also, the model does not represent the L/R dynamics of the dc line and smoothing reactors as well as the high frequency firing angel controller dynamics. Strictly speaking, this means that the only dynamic behavior the model exhibits is a varying active and reactive power loading [15, 17].

In order to obtain a more dynamic behavior from the converter model implemented in PSS/E, one possibility is to use the dc line model CDCRL. This model includes the L/R dynamics of the dc system and high-speed controller dynamics, and will thus influence the ac system to a greater extent than CDC4T. However, this is not investigated in this thesis. [15].

8 Conclusion

This chapter includes the main conclusions which can be drawn from the results presented in this thesis. Also, a recommendation for further work is included at the end of this chapter.

8.1 Background

This thesis was initiated to establish and evaluate an alternative model representation of the facility at Ormen Lange. Traditionally, a PQ-model has been used to represent Ormen Lange. This thesis, however, has implemented three two-terminal dc line models (converter models) to represent the facility. The main results from the power flow and dynamic simulations are presented in the subsequent sections.

8.2 Power flow

Two cases were studied to simulate the action of the converter control system when exposed to a depression in rectifier bus voltage. In the first case the rectifier transformer tap settings were adjustable. In the second case the rectifier transformer tap setting were locked to its initial value. The latter case represents a transient situation where the tap changer action is too slow and hence not considered.

The results from the first case showed that a depression in rectifier bus voltage caused the control logic to reduce the rectifier transformer tap position and firing delay angle. This increased the voltage on the valve side of the rectifier transformer and enabled the rectifier to maintain dc current control. Consequently, the scheduled dc values were unaffected by the depression in rectifier bus voltage.

The results from the second case showed that with the rectifier tap setting locked, the transformer did not boost the voltage on the valve side of the rectifier transformer. Consequently, the control logic reduced the rectifier firing delay angle to its minimum, and the inverter assumed control of the dc current. With the inverter in control of the current, the scheduled dc current was reduced by a fraction equal to the current margin along with the remainder dc values.

Hence, the presence of an adequate rectifier transformer tap setting is essential for the two-terminal dc line model to maintain scheduled dc values during voltage depression.

All simulations showed that a voltage depression at the rectifier bus lead to a reduction in rectifier reactive power consumption. This is due to the action from the control logic which reduced the rectifier firing delay angle to “counteract” the voltage depression. The greatest reduction in reactive power was experienced when the rectifier firing delay angle was reduced to its minimum value.

Hence in a situation with depressed bus voltage, the latter operation of the converter control logic causes the two-terminal dc line model to exhibit less stress to the ac system than the PQ-model, in terms of reactive power consumption.

In power flow simulations, the inverter bus must be defined as a swing bus. This means that the generator connected to the swing bus will adjust its power output to maintain a specified bus voltage and phase angle. Hence, a voltage depression at the valve side of the inverter transformer will never take place and there will be no tap adjustment on the inverter transformer. The inverter is decoupled from the remaining ac system and all changes in operation condition for the inverter is handled by the swing bus.

8.3 Dynamic

The results from the dynamic simulations showed that the dynamic two-terminal dc line model (CDC4T) exhibited an instantaneous response to changes in rectifier ac system voltage. This is because CDC4T is a pseudo steady-state dynamic model which does not include the L/R dynamics of the dc system and the high frequency firing angle controller dynamics. Consequently, evaluation of the high frequency controller action is not feasible.

Two cases were utilized to simulate the control action of the CDC4T model. The first case introduced a fault which depressed the rectifier bus voltage to an extent that the control action remained in normal regulation. The second case introduced a fault which depressed the rectifier bus voltage to an extent that caused shutdown of the converters.

The results obtained from these simulations revealed an important characteristic of the CDC4T model. After fault clearance, the rectifier bus voltage exhibited small voltage fluctuations. The rectifiers compensated these fluctuations by adjusting their rectifier firing delay angles correspondingly. Consequently, the latter resulted in fluctuations in rectifier reactive power consumption. This means that the ac system will perceive the CDC4T model as a varying reactive load following fault clearance.

The reactive power fluctuations were substantially greater for the case representing shutdown of the converters. This is because the rectifier firing delay angle following the converter shutdown, is determined by the parameters defining the reestablishment of dc voltage and dc current. Hence, the user defined values for the latter parameters can result in substantial reactive power fluctuations from the rectifiers, and must be evaluated carefully. However, it is important to acknowledge that the voltage dependant current limit (VDCL) can, if correctly defined, reduce the reactive power demand during periods of depressed voltage, and thus, reduce the reactive power fluctuations.

The consequence of representing Ormen Lange with the dynamic CDC4T model was analyzed by comparing the ac system response when using the CDC4T model and when using the PQ-model. The results obtained from these analyses showed that the main difference between the latter two models was CDC4T's generation of reactive power fluctuations in the transmission line into Nyhamna and Viklandet. These fluctuations were substantial compared

to the initial loading of the transmission line, and are a direct consequence of fluctuations in rectifier firing delay angle.

Two arguments were presented to substantiate why the repose from the CDC4T model only differed from the PQ-model in terms of reactive power fluctuations.

I. The calculated value of the short circuit ratio at Nyhamna indicated a strong interconnected ac/dc system.
II. The dynamic behavior of the pseudo-steady state model, CDC4T, is limited. Both the L/R dynamic of the dc line, smoothing reactors and high frequency controller dynamics are omitted.

To obtain a more dynamic behavior from the model implemented in PSS/E, one could use the more complex dc line model CDCRL. This model includes the L/R dynamics of the dc system and high-speed controller dynamics, and will thus influence the ac system to a greater extent than CDC4T.

8.4 Further work

This thesis has established and evaluated the implementation of the dynamic two-terminal dc line model, CDC4T. CDC4T is a pseudo steady-state dynamic model which represents dynamic relationships which are technically valid only for steady-state conditions. This means that the dynamic behavior of the model is limited.

In further studies of the implementation of converter models at Ormen Lange, models that offer more dynamic behavior should be utilized. The models should represent both the L/R dynamic of the dc system and the high frequency firing angle controller dynamics. Further, the model establishment should focus on achieving a sufficiently realistic load representation of Ormen Lange. In this manner, the converters' influence on system stability can be investigated.

References

[1] K. R. Padiyar, *HVDC Power Transmission Systems – Technology and System Interactions,* John Wiley & Sons., 1990.

[2] J. Arrillaga, *High Voltage Direct Current Transmission,* IEE Power Engineering Series 6, Peter Peregrinus Ltd., 1983.

[3] P. Kundur, *Power System Stability and Control,* McGraw-Hill, New York, 1994.

[4] J. O. Gjerde, K. Uhlen, M. Hernes, "HVDC-FACTS State of the art – power system harmonics", Sintef, 1996.

[5] W. Long, S. Nilsson, HVDC Transmission: Yesterday and Today, *IEEE power & energy magazine,* Volume 5, Number 2, March/April 2007.

[6] I. Norheim, *Suggested Methods for Preventing Core Saturation Instability in HVDC Transmission Systems*. Doctoral dissertation, Norwegian University of Science and Technology, 2002.

[7] IEEE Std 1204-1997, "IEEE Guide for Planning DC Links Terminating at AC Locations Having Low Short-Circuit Capacities". (Result of CIGRÈ Working Group 14.07 and IEEE Working Group 15.05.05).

[8] R. S. Thallam, "Review of the Design and Performance Features of HVDC Systems Connected to Low Short Circuit Ratio AC Systems", *IEEE Trans.,* Volume 7, No. 4, October 1992.

[9] T. Skånøy, "Voltage instability – Impact of load modelling", Norwegian University of Science and Technology, 2006.

[10] Power Technologies International, PSS/E 30.2, "Users Manual", November 2005.

[11] Power Technologies International, PSS/E 30.2, "Program Operation Manual", Volume I, November 2005.

[12] D. A. Woodford, "HVDC Transmission", Manitoba HVDC Research Center, Canada, Mach 1998.

[13] Power Technologies International, PSS/E 30.2, "Program Application Guide", Volume I, November 2005.

[14] Power Technologies International, PSS/E 30.2, "Program Operation Manual", Volume II, November 2005.

[15] Power Technologies International, PSS/E 30.2, “Program Application Guide”, Volume II, November 2005.

[16] Statnett. “Veiledende krav til vern i regionalnettet (KtVr)”, Statnett SF Nettstyringsdivisjonen Avdeling Vern og Feilanalyse, 2006. (Written in Norwegian).

[17] B. K. Johnson, ”HVDC models used in stability studies”, *IEEE Trans.,* Volume 4*,* No. 4, April 1989.

[18] H. H. Faanes, K. J. Olsen, “TET4115 Elektriske Kraftsystemer”, Institutt for elkraftteknikk, NTNU, 2005. (Written in Norwegian).

Appendix index

Appendix A Power flow simulations

This appendix shows the results obtained from the power flow simulations in Chapter 4. These results are identical to the results presented in Chapter 4, however, the results are illustrated with single line diagrams.

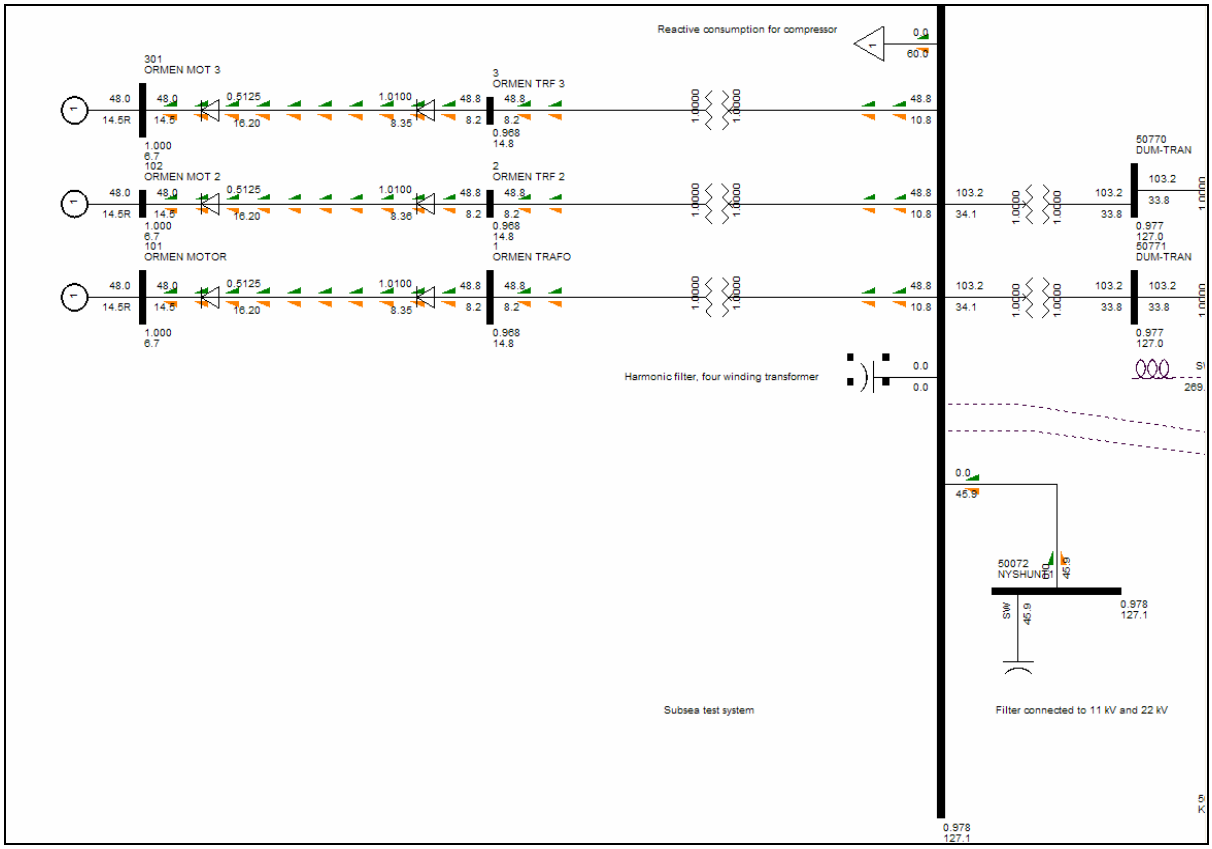

Figure A1 Single line diagram for case A_1.

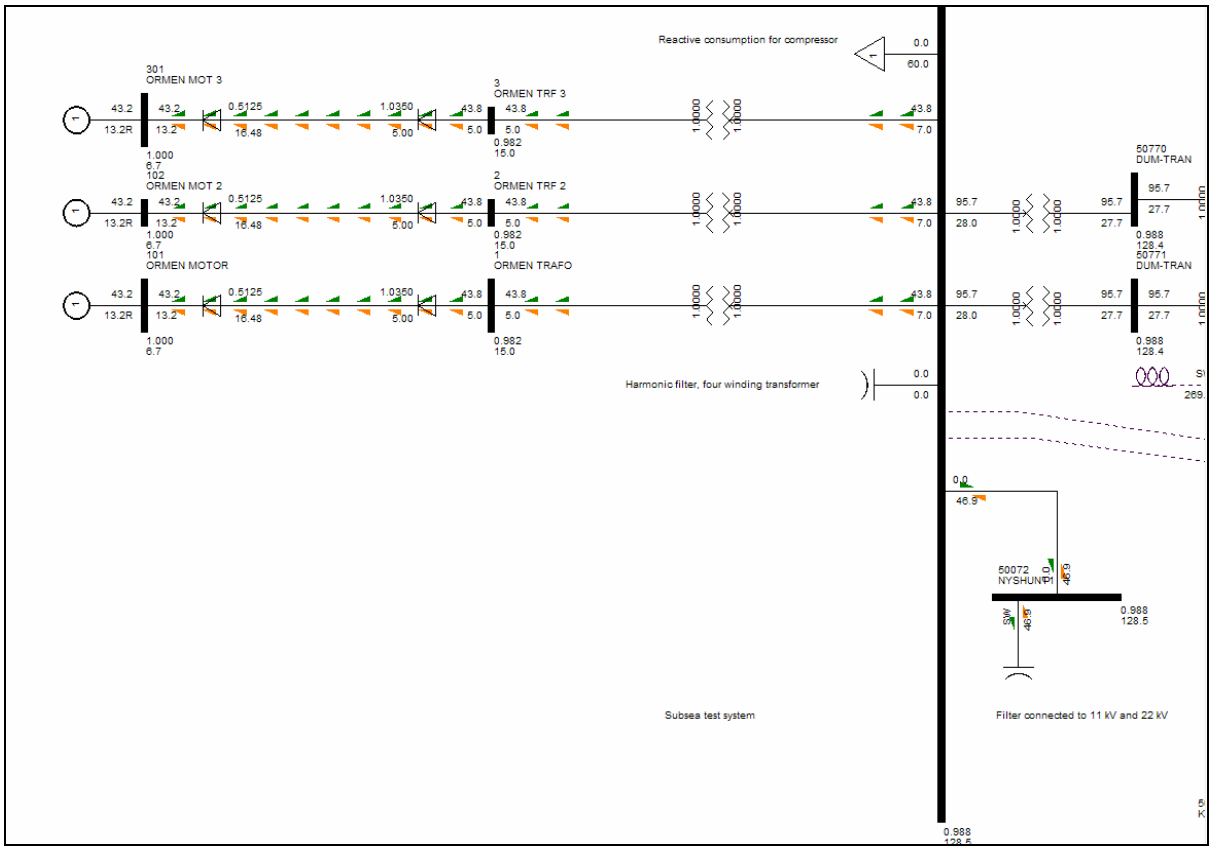

Figure A2 Single line diagram for Case B_1.

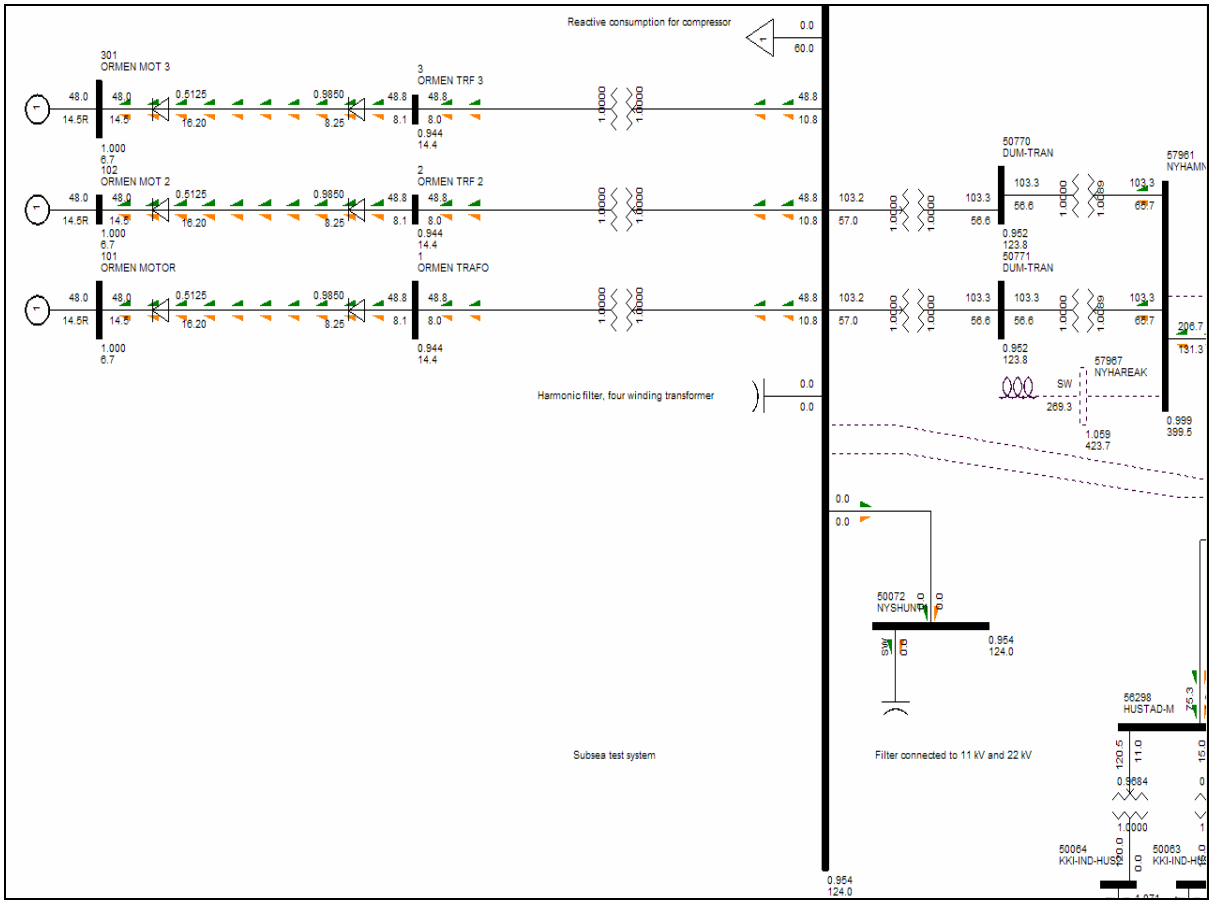

Figure A3 Single line diagram for Case A_2.

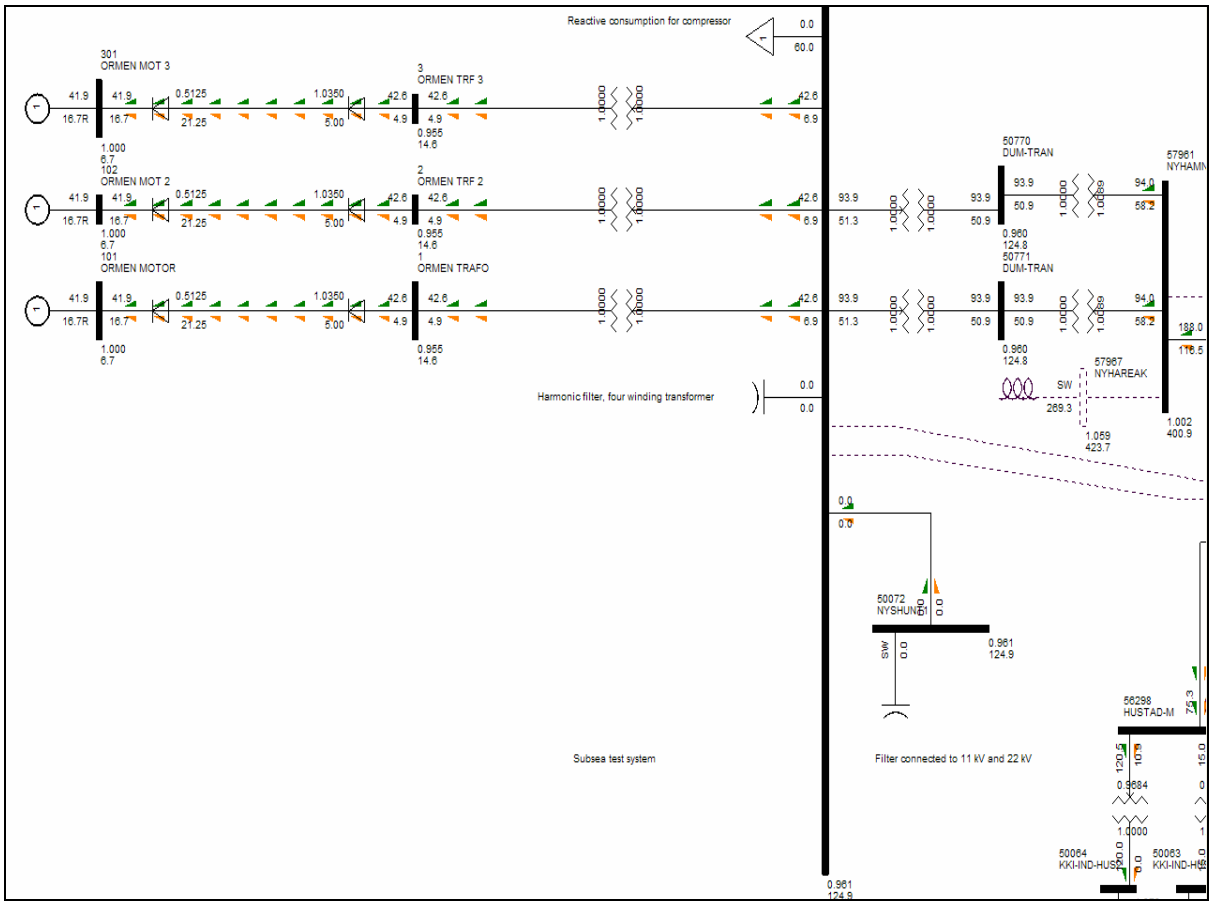

Figure A4 Single line diagram for Case B_2.

Appendix B Dynamic simulations

This appendix presents some of the results obtained from the simulations performed in Chapter 6.

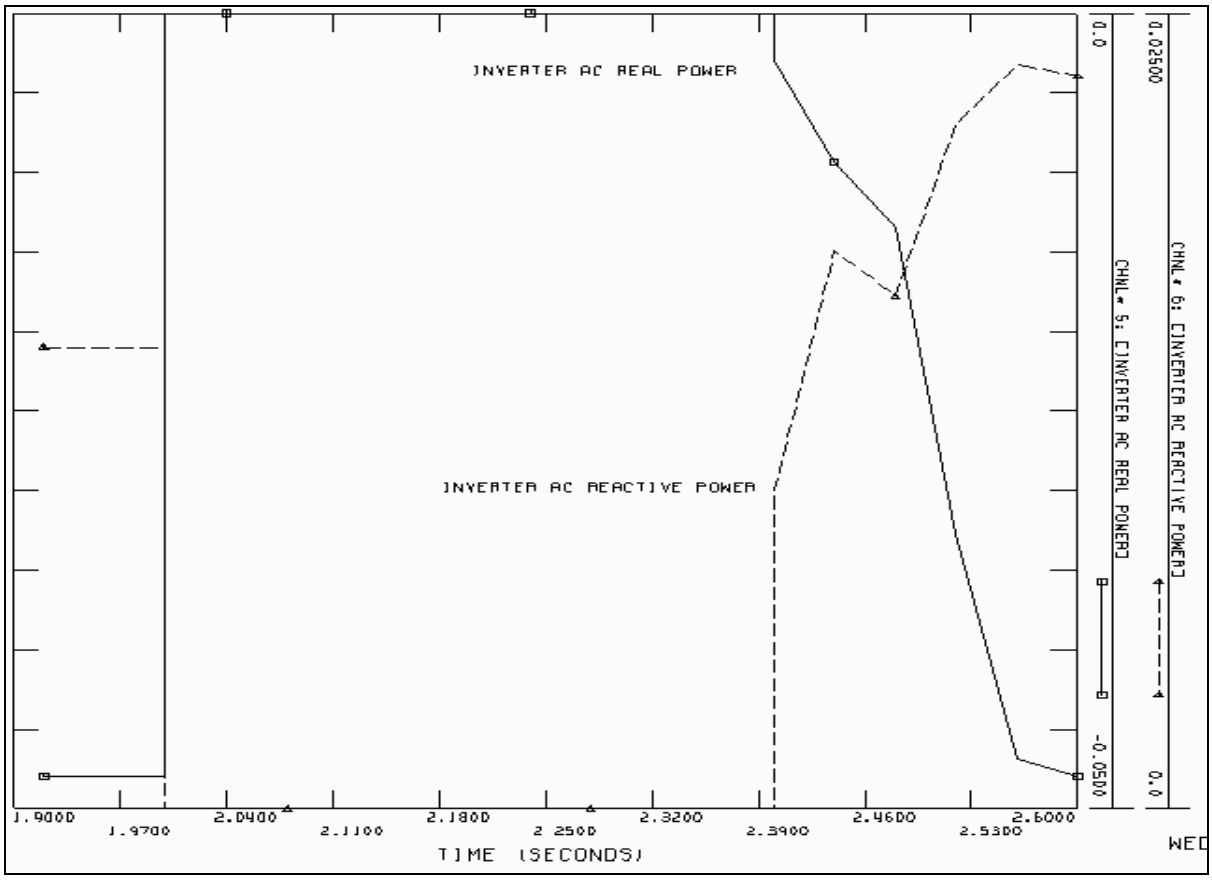

Figure B1 Inverter ac real power [pu] and inverter ac reactive power [pu] during fault. The active and reactive power are based on system base (1000 MVA).

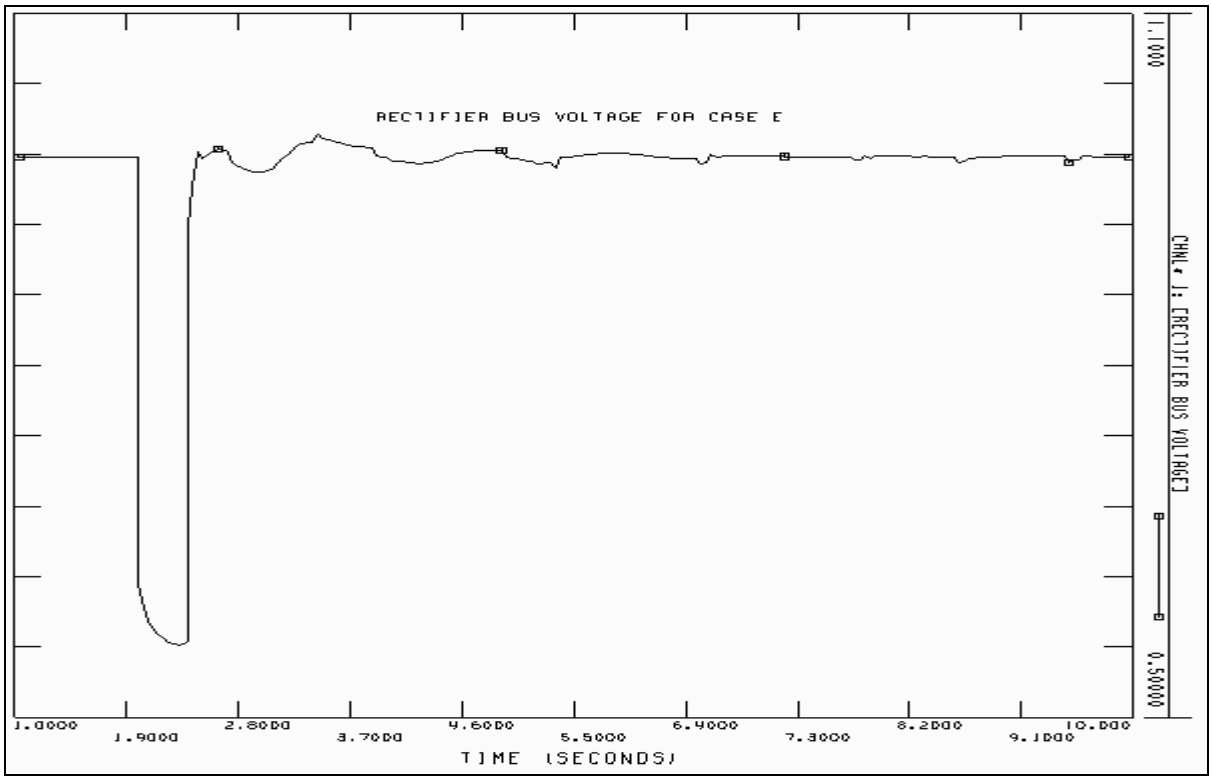

Figure B2 Rectifier bus voltage [pu] for Case E.

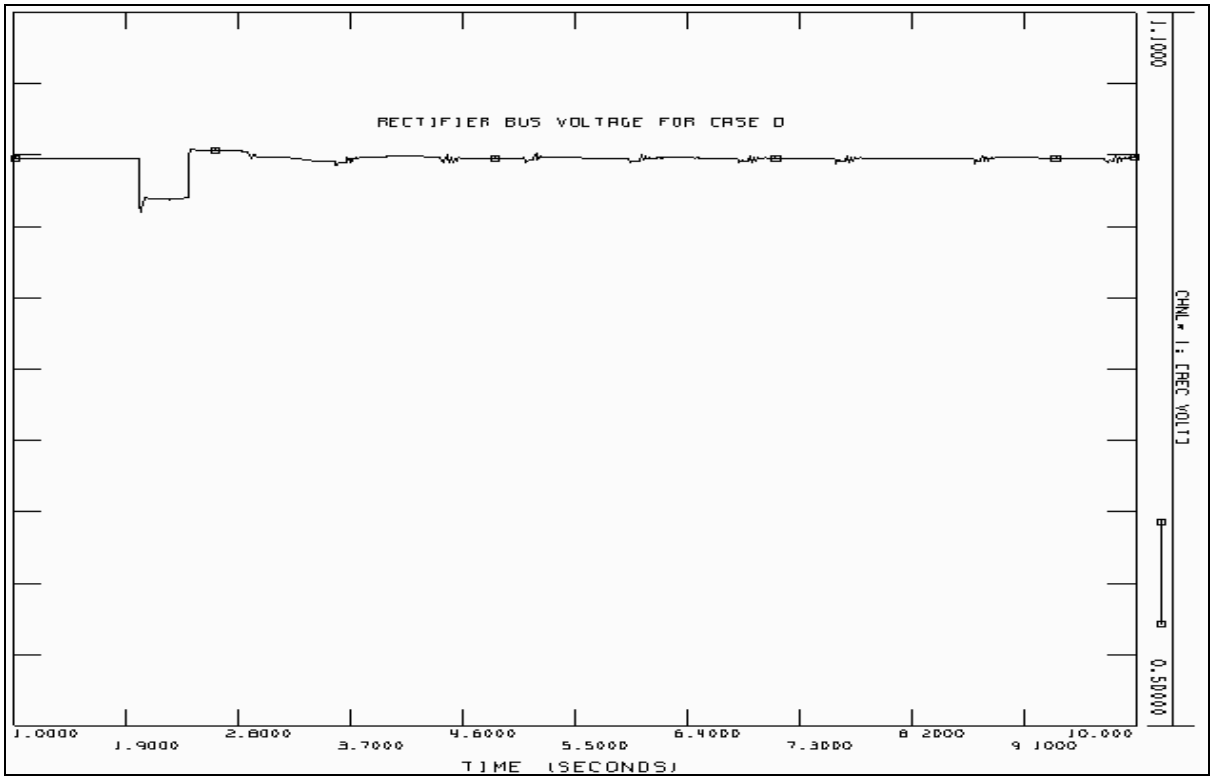

Figure B3 Rectifier bus voltage [pu] for Case D.

Appendix C Calculation of the SCR at Nyhamna

This section describes how the short circuit capacity (SCC) and the short circuit ratio (SCR) at Nyhamna are calculated in PSS/E. The calculations are simplified and do not represent a correct value of the SCC or SCR. However, the objective of these calculations is to give an indication of the strength of the ac/dc junction at Nyhamna.

Configuration implemented in PSS/E

This section describes the configuration used in PSS/E when calculating the SCC. Figure C1 shows a schematic illustration of the configuration used in PSS/E. The figure only shows one of the three converters at Nyhamna.

A dummy bus is connected to the 130 kV bus at Nyhamna through a zero impedance transmission line. A three-phase bus fault with zero fault impedance is implemented at the dummy bus to calculate the short circuit current.

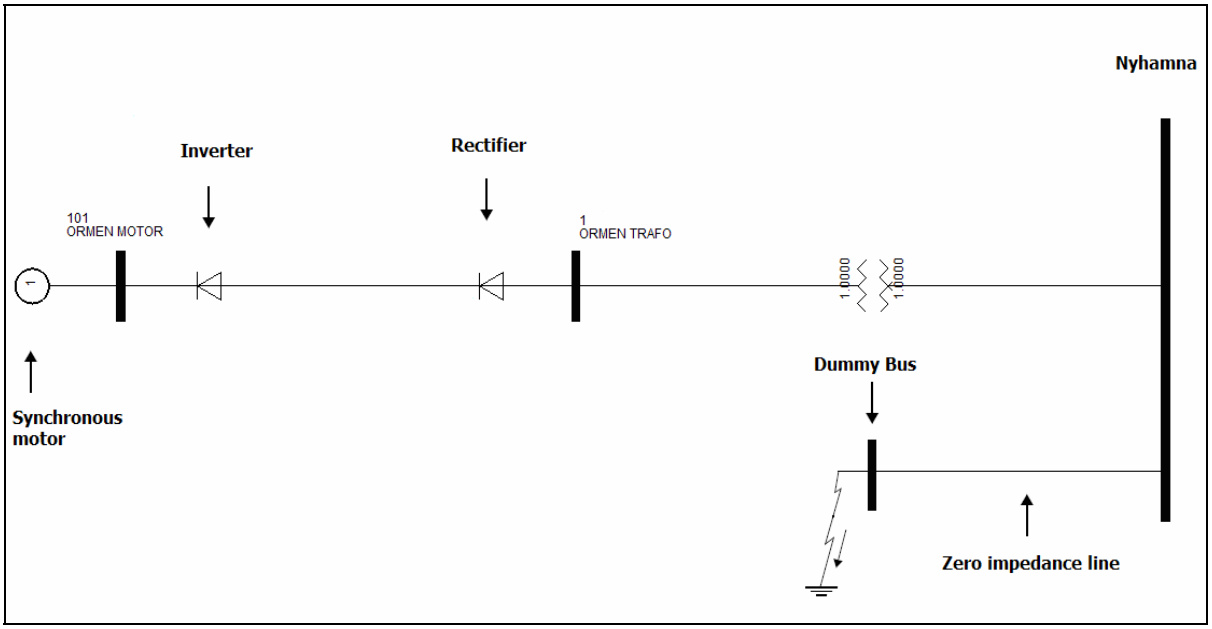

Figure C1 Configuration used in PSS/E for calculating the SCC at Nyhamna.

The following events are implemented:

t = 0 Simulations start

t = 1.0 sec. Three-phase bus fault with zero impedance fault at the dummy bus

t = 2.0 sec. End of simulations

Since the current cannot be obtained directly in PSS/E, the MVA flow is plotted along with the bus voltage at both Nyhamna and the dummy bus. The latter values are then implemented in a excel sheet where the short circuit current is calculated from the following equations [18]:

$$S_{N,MVA} = 1000MVA \tag{C.1}$$

$$U_{N,Nyhamna} = 130kV \tag{C.2}$$

$$I_N = \frac{S_{N,MVA}}{\sqrt{3}U_{N,Nyhamna}} = \frac{1000MVA}{\sqrt{3}\cdot 130kV} = 4.441kA \tag{C.3}$$

$$I_{SC,pu} = \frac{S_{SC,MVA}}{S_{N,MVA}} \cdot \frac{1}{U_{SC,pu}} \tag{C.4}$$

$$I_{SC} = I_{SC,pu} \cdot I_N \tag{C.5}$$

Table 14 shows the results obtained from the simulation in PSS/E. The variable "S [MVA]" listed in the second column corresponds the variable $S_{SC,MVA}$ given in the equations above. The variable "Isc [pu]" listed in the last column correspond to the variable $I_{SC,pu}$, and is calculated manually from Equation (C.4).

Calculated short circuit ratio

The maximum short circuit capacity can be obtained by evaluating the last column in Table 14. The maximum short circuit current (shown in red) is 1.6719 per unit. The latter short circuit current corresponds to:

$$I_{SC} = I_{SC,pu} \cdot I_N = 1.6719 \cdot 4.441kA = 7.425kA \tag{C.6}$$

The short circuit capacity can be obtained from the following equation [18]:

$$S_{SC} = \sqrt{3} \cdot U_{N,Nyhamna} \cdot I_{SC} = \sqrt{3} \cdot 130kV \cdot 7.425kA = 1671.9MVA \tag{C.7}$$

The short circuit ratio can be obtained from the equation given in Section 2.6.1:

$$SCR = \frac{S_{SC}}{P_{d1}} = \frac{1671.9MVA}{150MW} = 11.15 \tag{C.8}$$

In Equation (C.8) it is assumed that the rated dc terminal power equals 150 MW. In the latter value, the ratings of each of the three converters are added up.

With Section 2.6.1 as basis, a SCR of 11.15 indicates that the ac/dc connection at Nyhamna is strong.

In Equation (C.8) the effect of filter and shunt capacitors is omitted. The effective short circuit ratio can be calculated from the following equation (see Section 2.6.1):

$$ESCR = \frac{S_{SC} - Q_c}{P_{d1}} = \frac{1671.9MVA - 120MVAr}{150MW} = 10.35 \qquad \text{(C.9)}$$

In Equation (C.9) it is assumed that the total reactive output from the filter and shunt capacitor is 120 MVAr.

It is important to emphasize that the calculations in this section are simplified and the objective is merely to give an indication of the strength of the ac system connected to Nyhamna.

Synchronous machines connected at, or near a converter station, should be represented by the subtransient reactance when calculating the SCR. The subtransient reactance is not used for all synchronous machines in the model analyzed in Chapter 7. Those machines which are modeled as subtransient level machines have an impedance equal to the subtransient impedance. However, the latter is not valid for the machines modeled as classical (GENCLS) or transient (GENTRA) level machines. To what extent this will influence the SCR calculations, is not considered in this thesis [11].

Table 14 Results from PSS/E.

TIME	S [MVA]	Spg Nyhamna [pu]	Spg Dum [pu]	Isc [pu]
-0,0200	2,5418E-06	9,8806E-01	9,8806E-01	2,5725E-09
-0,0100	2,8721E-06	9,8793E-01	9,8793E-01	2,9072E-09
0,0000	3,8850E-06	9,8887E-01	9,8887E-01	3,9287E-09
0,0000	1,5061E-06	9,8891E-01	9,8891E-01	1,5230E-09
0,0100	2,8780E-06	9,8894E-01	9,8894E-01	2,9102E-09
0,0200	2,4851E-06	9,8868E-01	9,8868E-01	2,5135E-09
0,0300	3,3087E-06	9,8887E-01	9,8887E-01	3,3459E-09
0,0400	4,9048E-06	9,8888E-01	9,8888E-01	4,9600E-09
0,0500	3,1098E-06	9,8880E-01	9,8880E-01	3,1450E-09
0,0600	1,0316E-06	9,8879E-01	9,8879E-01	1,0432E-09
0,0700	3,1460E-06	9,8879E-01	9,8879E-01	3,1817E-09
0,0800	2,5846E-06	9,8877E-01	9,8877E-01	2,6139E-09
0,0900	2,2815E-06	9,8876E-01	9,8876E-01	2,3075E-09
0,1000	2,8792E-06	9,8876E-01	9,8876E-01	2,9119E-09
0,1100	2,6288E-06	9,8875E-01	9,8875E-01	2,6587E-09
0,1200	1,1133E-06	9,8875E-01	9,8875E-01	1,1259E-09
0,1300	1,3116E-06	9,8874E-01	9,8874E-01	1,3266E-09
0,1400	6,5547E-06	9,8874E-01	9,8874E-01	6,6293E-09
0,1500	4,2432E-06	9,8874E-01	9,8874E-01	4,2915E-09
0,1600	1,5913E-06	9,8874E-01	9,8874E-01	1,6094E-09
0,1700	3,1521E-06	9,8873E-01	9,8873E-01	3,1881E-09
0,1800	2,8443E-06	9,8873E-01	9,8873E-01	2,8767E-09
0,1900	1,9164E-06	9,8873E-01	9,8873E-01	1,9383E-09
0,2000	4,2280E-06	9,8873E-01	9,8873E-01	4,2762E-09
0,2100	3,2390E-06	9,8873E-01	9,8873E-01	3,2759E-09
0,2200	2,5953E-06	9,8873E-01	9,8873E-01	2,6249E-09
0,2300	1,5486E-06	9,8873E-01	9,8873E-01	1,5662E-09
0,2400	2,0092E-06	9,8873E-01	9,8873E-01	2,0321E-09
0,2500	3,2131E-06	9,8868E-01	9,8868E-01	3,2499E-09
0,2600	1,8942E-06	9,8870E-01	9,8870E-01	1,9159E-09
0,2700	8,0599E-07	9,8872E-01	9,8872E-01	8,1518E-10
0,2800	2,4991E-06	9,8868E-01	9,8868E-01	2,5277E-09
0,2900	4,7435E-07	9,8870E-01	9,8870E-01	4,7977E-10
0,3000	2,1508E-06	9,8869E-01	9,8869E-01	2,1754E-09
0,3100	6,3644E-07	9,8871E-01	9,8871E-01	6,4371E-10
0,3200	2,0033E-06	9,8869E-01	9,8869E-01	2,0262E-09
0,3300	3,5691E-06	9,8872E-01	9,8872E-01	3,6098E-09
0,3400	2,9674E-06	9,8874E-01	9,8874E-01	3,0012E-09
0,3500	8,8913E-07	9,8869E-01	9,8869E-01	8,9930E-10
0,3600	3,7108E-06	9,8872E-01	9,8872E-01	3,7531E-09
0,3700	2,6166E-06	9,8875E-01	9,8875E-01	2,6463E-09
0,3800	4,2837E-06	9,8875E-01	9,8875E-01	4,3324E-09
0,3900	2,4302E-06	9,8870E-01	9,8870E-01	2,4579E-09
0,4000	3,3169E-06	9,8874E-01	9,8874E-01	3,3547E-09
0,4200	2,7508E-06	9,8877E-01	9,8877E-01	2,7820E-09
0,4300	3,1764E-06	9,8877E-01	9,8877E-01	3,2125E-09
0,4400	2,3647E-06	9,8878E-01	9,8878E-01	2,3915E-09
0,4500	2,6500E-06	9,8878E-01	9,8878E-01	2,6801E-09

TIME	S [MVA]	Spg Nyhamna [pu]	Spg Dum [pu]	Isc [pu]
0,4500	2,6500E-06	9,8878E-01	9,8878E-01	2,6801E-09
0,4600	3,2656E-06	9,8879E-01	9,8879E-01	3,3026E-09
0,4700	4,6144E-07	9,8875E-01	9,8875E-01	4,6669E-10
0,4800	4,4839E-08	9,8879E-01	9,8879E-01	4,5347E-11
0,4900	2,4835E-06	9,8882E-01	9,8882E-01	2,5116E-09
0,5000	4,2119E-06	9,8882E-01	9,8882E-01	4,2595E-09
0,5100	2,4907E-06	9,8882E-01	9,8882E-01	2,5189E-09
0,5200	1,4089E-06	9,8878E-01	9,8878E-01	1,4249E-09
0,5300	1,2537E-07	9,8882E-01	9,8882E-01	1,2679E-10
0,5400	4,2464E-06	9,8885E-01	9,8885E-01	4,2942E-09
0,5500	3,1709E-06	9,8885E-01	9,8885E-01	3,2067E-09
0,5600	3,7943E-06	9,8881E-01	9,8881E-01	3,8372E-09
0,5700	4,0513E-06	9,8884E-01	9,8884E-01	4,0970E-09
0,5800	2,9702E-06	9,8887E-01	9,8887E-01	3,0036E-09
0,5900	4,2946E-06	9,8883E-01	9,8883E-01	4,3431E-09
0,6000	2,6403E-06	9,8886E-01	9,8886E-01	2,6701E-09
0,6100	4,4950E-06	9,8888E-01	9,8888E-01	4,5455E-09
0,6200	1,0367E-06	9,8890E-01	9,8890E-01	1,0483E-09
0,6300	1,2524E-06	9,8885E-01	9,8885E-01	1,2666E-09
0,6400	8,0327E-07	9,8888E-01	9,8888E-01	8,1230E-10
0,6500	2,4852E-06	9,8890E-01	9,8890E-01	2,5131E-09
0,6600	2,3397E-06	9,8891E-01	9,8891E-01	2,3659E-09
0,6700	2,1569E-07	9,8891E-01	9,8891E-01	2,1811E-10
0,6800	2,9318E-07	9,8892E-01	9,8892E-01	2,9647E-10
0,6900	8,2122E-07	9,8892E-01	9,8892E-01	8,3042E-10
0,7000	7,3051E-08	9,8892E-01	9,8892E-01	7,3869E-11
0,7100	5,5097E-06	9,8892E-01	9,8892E-01	5,5715E-09
0,7200	3,0772E-06	9,8892E-01	9,8892E-01	3,1117E-09
0,7300	4,5462E-06	9,8892E-01	9,8892E-01	4,5971E-09
0,7400	3,0447E-06	9,8892E-01	9,8892E-01	3,0788E-09
0,7400	4,2912E-06	9,8889E-01	9,8889E-01	4,3394E-09
0,7500	2,9948E-06	9,8889E-01	9,8889E-01	3,0284E-09
0,7600	3,8449E-06	9,8890E-01	9,8890E-01	3,8880E-09
0,7700	3,0102E-06	9,8892E-01	9,8892E-01	3,0439E-09
0,7800	6,8115E-07	9,8891E-01	9,8891E-01	6,8879E-10
0,7900	1,6486E-06	9,8891E-01	9,8891E-01	1,6671E-09
0,8000	3,9679E-06	9,8891E-01	9,8891E-01	4,0124E-09
0,8100	6,3422E-07	9,8890E-01	9,8890E-01	6,4134E-10
0,8200	1,0777E-06	9,8890E-01	9,8890E-01	1,0898E-09
0,8300	1,5232E-06	9,8890E-01	9,8890E-01	1,5403E-09
0,8400	3,3459E-06	9,8889E-01	9,8889E-01	3,3835E-09
0,8500	4,1256E-06	9,8889E-01	9,8889E-01	4,1719E-09
0,8600	2,5079E-06	9,8888E-01	9,8888E-01	2,5361E-09
0,8700	2,5295E-06	9,8888E-01	9,8888E-01	2,5580E-09
0,8800	2,7819E-06	9,8887E-01	9,8887E-01	2,8132E-09
0,8900	2,7848E-06	9,8886E-01	9,8886E-01	2,8162E-09
0,9000	1,4393E-06	9,8886E-01	9,8886E-01	1,4555E-09
0,9100	1,8624E-06	9,8885E-01	9,8885E-01	1,8834E-09

TIME	S [MVA]	Spg Nyhamna [pu]	Spg Dum [pu]	Isc [pu]
0,9200	1,7019E-06	9,8884E-01	9,8884E-01	1,7211E-09
0,9300	1,7906E-06	9,8883E-01	9,8883E-01	1,8108E-09
0,9400	3,5091E-06	9,8882E-01	9,8882E-01	3,5487E-09
0,9500	2,5772E-06	9,8882E-01	9,8882E-01	2,6063E-09
0,9600	6,8377E-07	9,8881E-01	9,8881E-01	6,9151E-10
0,9700	2,6639E-06	9,8880E-01	9,8880E-01	2,6940E-09
0,9800	2,4917E-06	9,8879E-01	9,8879E-01	2,5200E-09
0,9900	3,1644E-06	9,8878E-01	9,8878E-01	3,2003E-09
1,0000	1,3293E-06	9,8877E-01	9,8877E-01	1,3444E-09
1,0000	1,2707E-05	7,9708E-09	7,9708E-09	1,5942E+00
1,0100	1,2570E-05	7,9276E-09	7,9276E-09	1,5855E+00
1,0200	1,2527E-05	7,9142E-09	7,9142E-09	1,5828E+00
1,0300	1,2525E-05	7,9135E-09	7,9135E-09	1,5827E+00
1,0400	1,2457E-05	7,8919E-09	7,8919E-09	1,5784E+00
1,0500	1,2406E-05	7,8760E-09	7,8760E-09	1,5752E+00
1,0600	1,2373E-05	7,8655E-09	7,8655E-09	1,5731E+00
1,0700	1,2357E-05	7,8604E-09	7,8604E-09	1,5721E+00
1,0800	1,2352E-05	7,8588E-09	7,8588E-09	1,5718E+00
1,0900	1,2354E-05	7,8594E-09	7,8594E-09	1,5719E+00
1,1000	1,2363E-05	7,8622E-09	7,8622E-09	1,5724E+00
1,1100	1,2378E-05	7,8671E-09	7,8671E-09	1,5734E+00
1,1200	1,2399E-05	7,8735E-09	7,8735E-09	1,5747E+00
1,1300	1,2423E-05	7,8814E-09	7,8814E-09	1,5763E+00
1,1400	1,2452E-05	7,8904E-09	7,8904E-09	1,5781E+00
1,1500	1,2483E-05	7,9003E-09	7,9003E-09	1,5801E+00
1,1600	1,2517E-05	7,9111E-09	7,9111E-09	1,5822E+00
1,1700	1,2553E-05	7,9224E-09	7,9224E-09	1,5845E+00
1,1800	1,2591E-05	7,9343E-09	7,9343E-09	1,5869E+00
1,1900	1,2630E-05	7,9466E-09	7,9466E-09	1,5893E+00
1,2000	1,2670E-05	7,9591E-09	7,9591E-09	1,5918E+00
1,2100	1,2710E-05	7,9719E-09	7,9719E-09	1,5944E+00
1,2200	1,2752E-05	7,9849E-09	7,9849E-09	1,5970E+00
1,2300	1,2793E-05	7,9979E-09	7,9979E-09	1,5996E+00
1,2400	1,2835E-05	8,0110E-09	8,0110E-09	1,6022E+00
1,2500	1,2877E-05	8,0241E-09	8,0241E-09	1,6048E+00
1,2600	1,2919E-05	8,0372E-09	8,0372E-09	1,6074E+00
1,2700	1,2961E-05	8,0501E-09	8,0501E-09	1,6100E+00
1,2800	1,3002E-05	8,0630E-09	8,0630E-09	1,6126E+00
1,2900	1,3044E-05	8,0757E-09	8,0757E-09	1,6151E+00
1,3000	1,3084E-05	8,0883E-09	8,0883E-09	1,6177E+00
1,3100	1,3124E-05	8,1006E-09	8,1006E-09	1,6201E+00
1,3200	1,3163E-05	8,1127E-09	8,1127E-09	1,6225E+00
1,3300	1,3202E-05	8,1246E-09	8,1246E-09	1,6249E+00
1,3400	1,3240E-05	8,1362E-09	8,1362E-09	1,6272E+00
1,3500	1,3276E-05	8,1475E-09	8,1475E-09	1,6295E+00
1,3600	1,3312E-05	8,1585E-09	8,1585E-09	1,6317E+00
1,3700	1,3347E-05	8,1692E-09	8,1692E-09	1,6338E+00
1,3800	1,3381E-05	8,1795E-09	8,1795E-09	1,6359E+00

TIME	S [MVA]	Spg Nyhamna [pu]	Spg Dum [pu]	Isc [pu]
1,3900	1,3414E-05	8,1895E-09	8,1895E-09	1,6379E+00
1,4000	1,3439E-05	8,1971E-09	8,1971E-09	1,6394E+00
1,4100	1,3465E-05	8,2050E-09	8,2050E-09	1,6410E+00
1,4200	1,3493E-05	8,2136E-09	8,2136E-09	1,6427E+00
1,4300	1,3519E-05	8,2215E-09	8,2215E-09	1,6443E+00
1,4400	1,3544E-05	8,2292E-09	8,2292E-09	1,6458E+00
1,4500	1,3569E-05	8,2368E-09	8,2368E-09	1,6474E+00
1,4600	1,3593E-05	8,2441E-09	8,2441E-09	1,6488E+00
1,4700	1,3617E-05	8,2512E-09	8,2512E-09	1,6502E+00
1,4800	1,3639E-05	8,2581E-09	8,2581E-09	1,6516E+00
1,4900	1,3662E-05	8,2648E-09	8,2648E-09	1,6530E+00
1,5000	1,3683E-05	8,2713E-09	8,2713E-09	1,6543E+00
1,5100	1,3704E-05	8,2776E-09	8,2776E-09	1,6555E+00
1,5200	1,3724E-05	8,2837E-09	8,2837E-09	1,6567E+00
1,5300	1,3744E-05	8,2897E-09	8,2897E-09	1,6579E+00
1,5400	1,3763E-05	8,2956E-09	8,2956E-09	1,6591E+00
1,5500	1,3782E-05	8,3012E-09	8,3012E-09	1,6602E+00
1,5600	1,3800E-05	8,3065E-09	8,3065E-09	1,6613E+00
1,5700	1,3817E-05	8,3118E-09	8,3118E-09	1,6623E+00
1,5800	1,3834E-05	8,3167E-09	8,3167E-09	1,6633E+00
1,5900	1,3850E-05	8,3215E-09	8,3215E-09	1,6643E+00
1,6000	1,3863E-05	8,3257E-09	8,3257E-09	1,6651E+00
1,6100	1,3876E-05	8,3294E-09	8,3294E-09	1,6659E+00
1,6200	1,3887E-05	8,3328E-09	8,3328E-09	1,6666E+00
1,6300	1,3898E-05	8,3360E-09	8,3360E-09	1,6672E+00
1,6400	1,3908E-05	8,3390E-09	8,3390E-09	1,6678E+00
1,6500	1,3917E-05	8,3417E-09	8,3417E-09	1,6683E+00
1,6600	1,3925E-05	8,3443E-09	8,3443E-09	1,6688E+00
1,6700	1,3933E-05	8,3466E-09	8,3466E-09	1,6693E+00
1,6800	1,3940E-05	8,3488E-09	8,3488E-09	1,6698E+00
1,6900	1,3947E-05	8,3508E-09	8,3508E-09	1,6701E+00
1,7000	1,3953E-05	8,3526E-09	8,3526E-09	1,6705E+00
1,7100	1,3959E-05	8,3542E-09	8,3542E-09	1,6708E+00
1,7200	1,3963E-05	8,3556E-09	8,3556E-09	1,6711E+00
1,7300	1,3967E-05	8,3568E-09	8,3568E-09	1,6714E+00
1,7400	1,3971E-05	8,3578E-09	8,3578E-09	1,6716E+00
1,7500	1,3973E-05	8,3585E-09	8,3585E-09	1,6717E+00
1,7600	1,3975E-05	8,3591E-09	8,3591E-09	1,6718E+00
1,7700	1,3976E-05	8,3594E-09	8,3594E-09	**1,6719E+00**
1,7800	1,3976E-05	8,3595E-09	8,3595E-09	1,6719E+00
1,7900	1,3976E-05	8,3594E-09	8,3594E-09	1,6719E+00
1,8000	1,3975E-05	8,3591E-09	8,3591E-09	1,6718E+00
1,8100	1,3973E-05	8,3585E-09	8,3585E-09	1,6717E+00
1,8200	1,3970E-05	8,3578E-09	8,3578E-09	1,6716E+00
1,8300	1,3967E-05	8,3568E-09	8,3568E-09	1,6714E+00
1,8400	1,3963E-05	8,3556E-09	8,3556E-09	1,6711E+00
1,8500	1,3959E-05	8,3542E-09	8,3542E-09	1,6708E+00
1,8600	1,3953E-05	8,3526E-09	8,3526E-09	1,6705E+00

TIME	S [MVA]	Spg Nyhamna [pu]	Spg Dum [pu]	Isc [pu]
1,8700	1,3947E-05	8,3507E-09	8,3507E-09	1,6701E+00
1,8800	1,3940E-05	8,3486E-09	8,3486E-09	1,6697E+00
1,8900	1,3932E-05	8,3463E-09	8,3463E-09	1,6693E+00
1,9000	1,3924E-05	8,3438E-09	8,3438E-09	1,6688E+00
1,9100	1,3915E-05	8,3411E-09	8,3411E-09	1,6682E+00
1,9200	1,3905E-05	8,3383E-09	8,3383E-09	1,6677E+00
1,9300	1,3896E-05	8,3353E-09	8,3353E-09	1,6671E+00
1,9400	1,3885E-05	8,3322E-09	8,3322E-09	1,6664E+00
1,9500	1,3875E-05	8,3291E-09	8,3291E-09	1,6658E+00
1,9600	1,3864E-05	8,3258E-09	8,3258E-09	1,6652E+00
1,9700	1,3853E-05	8,3226E-09	8,3226E-09	1,6645E+00
1,9800	1,3842E-05	8,3193E-09	8,3193E-09	1,6639E+00
1,9900	1,3832E-05	8,3161E-09	8,3161E-09	1,6632E+00
2,0000	1,3821E-05	8,3130E-09	8,3130E-09	1,6626E+00